Soft Solar X-Ray Burst Characteristics*

by

Jerry F. Drake**

Department of Physics and Astronomy
THE UNIVERSITY OF IOWA
Iowa City, Iowa

Soft Solar X-Ray Burst Characteristics*

by

Jerry F. Drake**

A thesis submitted in partial fulfillment of the
requirements for the degree of Doctor of Philosophy
in the Department of Physics and Astronomy
in the Graduate College of
The University of Iowa

January 1970

Thesis supervisor: Professor James A. Van Allen

*Research supported in part by Goddard Space Flight Center under contract NAS5-9076, by the National Aeronautics and Space Administration grant NGL 16-001-002, and by the Office of Naval Research under contract Nonr 1509(06).

**Part of the work was done while the author was a NASA trainee and part while a U. S. Steel Fellow.

ACKNOWLEDGEMENTS

The author wishes to thank Professor James A. Van Allen for making Explorer 33 and Explorer 35 data available to him and for guidance and suggestions during the course of the work with which this thesis is concerned. Dr. J. Neff is thanked for helpful discussions and interest in this topic. Dr. J. Gibson, O.S.B., is thanked for help rendered in the development and execution of the data reduction method. Assistance of E. Sarris with the data analysis is appreciated, as is the assistance of P. Dylhoff with the computer program.

The author is indebted to Drs. H. S. Hudson, L. E. Peterson, and D. A. Schwartz of the University of California at San Diego for the use of their 7.7 - 12.5 keV x-ray burst data in Section VII-B of this thesis.

Thanks are due also to the staff of the satellite analysis department and to the drafting department of the University of Iowa for their assistance in the preparation of this thesis. The typing of this thesis was done by Miss Sally Hanson.

The author would like to thank his wife, Connie, and son, Jordy, for their support and sacrifices during the course of this work.

Support for this work has been provided at various stages by contract NAS5-9076 with the Goddard Space Flight Center, by National Aeronautics and Space Administration grant NGL 16-001-002, and by contract Nonr 1509(06) with the Office of Naval Research. During the various phases of this work, the author was the recipient of a National Aeronautics and Space Administration Traineeship and of a U. S. Steel Graduate Research Fellowship.

ABSTRACT

The burst component of the solar x-ray flux in the soft wavelength range 2 Å $< \lambda <$ 12 Å observed from Explorer 33 and Explorer 35 from July 1966 to September 1968 were analyzed. In this period 4028 burst peaks were observed.

The differential distributions of the temporal and intensity parameters of the bursts revealed no separation into more than one class of bursts. The most frequently observed value for rise time was 4 minutes and for decay time was 12 minutes. The distribution of the ratio of rise-to-decay time can be represented by an exponential with exponent -2.31 from a ratio of 0.3 to 2.7; the maximum in this distribution occurred at a ratio of 0.3. The values of the total observed flux, divided by the background flux, at burst maximum, can be represented by a power law with exponent -2.62 for ratios between 1.5 and 32. The distribution of peak burst fluxes can be represented by a power law with exponent -1.75 over the range 1 - 100 milli-erg $(cm^2\ sec)^{-1}$. The flux time integral values are given by a power law with exponent -1.44 over the range 1 - 50 erg cm^{-2}.

The distribution of peak burst flux as a function of Hα importance revealed a general trend for larger peak x-ray fluxes to occur

with both larger Hα flare areas and with brighter Hα flares. The heliographic longitude dependence of soft x-ray bursts indicated no significant dependence of x-ray burst occurrence on heliographic longitude; the emission thus lacks directivity.

The theory of free-free emission by a thermal electron distribution was applied to a quantitative explanation of both hard x-ray fluxes (data from Arnoldy, Kane, and Winckler [1968]; Kane and Winckler [1969]; and Hudson, Peterson, and Schwartz [1969]) and soft x-ray fluxes during solar x-ray bursts. Using bursts in three different energy intervals, covering a total range of 1 - 50 keV, temperatures of 12 - 39 x 10^6 °K and emission measures of 3.6 x 10^{47} to 2.1 x 10^{50} cm^{-3} were derived. The emission measure was found to vary from event to event. The peak time of hard x-ray events was found to occur an average of 3 minutes before the peak time of the corresponding soft x-ray bursts. Thus a changing emission measure during the event is also required. A free-free emission process with temperatures of 12 - 39 x 10^6 °K and with an emission measure in the range 3.6 x 10^{47} to 2.1 x 10^{50} cm^{-3} which varies both from event to event and within an individual event is required by the data examined.

TABLE OF CONTENTS

TABLE OF CONTENTS (CONT.)

TABLE OF CONTENTS (CONT.)

FOREWORD

The results of this thesis were obtained from a study of the burst component of the soft x-ray flux observed from July 1966 to September 1968 by Explorer 33 and Explorer 35. The raw data were first converted into reliable absolute flux values. The study of the burst component utilized the reduced absolute flux values. The data reduction method to convert the raw data into absolute values has been published in Solar Physics under the title "Iowa Catalog of Solar X-Ray Flux (2 - 12 Å)" by J. F. Drake, Sr. J. Gibson, O.S.B., and J. A. Van Allen, and is essentially the same as Chapters II and III of this thesis. Data reduced as described therein has been placed in the

National Space Science Data Center
National Aeronautics and Space Administration
Goddard Space Flight Center
Greenbelt, Maryland 20771, U.S.A.

for the following periods

From Explorer 33: 2 July 1966 to 27 July 1967

From Explorer 35: 26 July 1967 to 18 September 1968

and are made available to interested workers through that agency.

I. INTRODUCTION

A background of solar x-ray physics will be presented to provide a perspective for the discussion of the present observations of solar x-ray bursts. The physical system from which the x-ray emission originates, the current state of observational knowledge of solar x rays, x-ray emission theory and flare theory, and the objectives of this study will be discussed.

A. Solar Atmosphere

The solar atmosphere is comprised of three different layers: the photosphere, the chromosphere, and the corona.

The photosphere is a layer about 300 km thick in which most of the visible solar continuum radiation originates. This layer delineates the edge of the solar disk at a radius of 6.96×10^{10} cm. The total radiation from the photosphere is the same in magnitude as would be emitted from a blackbody with a temperature of 5785 °K. This region has the lowest ionization and the highest density (about 10^{16} H atoms cm^{-3}) in the solar atmosphere [Kundu, 1965].

Sunspots occur in the photosphere as a result of strong magnetic fields (several thousand gauss) which locally impede the flow of heat upward, causing a cooler, therefore darker, region

in the photosphere. The cooler region corresponds to temperatures of about 4500 °K. The scale size of sunspots is 1 - 2 x 10^4 km. Sunspots tend to form in bipolar groups whose number and latitude vary with the 11-year solar cycle period.

The chromosphere is an inhomogeneous region about 10^4 km thick located directly above the photosphere. The temperature rises in this region from about 5800 °K near the photosphere to about 10^6 °K at an altitude of 10^4 km. The density drops from 10^{16} H atoms cm^{-3} to 10^9 cm^{-3} from the base to the top of the chromosphere. Chromospheric faculae, or plages, appear in the lines of Hα (6563 Å) or calcium K (3934 Å) as bright mottled patches near sunspots. They are closely associated with the magnetic fields existing near and above sunspots.

Flares, the solar phenomena of greatest interest to this study, are sudden brightenings commonly observed best in the Hα or calcium K lines. These brightenings usually occur in the neighborhood of sunspots. Observations of limb flares indicate heights of 7,000 to 16,000 km. Thus flares are an upper chromospheric and lower coronal phenomenon. Rise times of flares are of the order of minutes while decay times are of the order of tens of minutes. The total energy liberated in a typical flare is of the order of 10^{30} erg.

Flare classification is comprised of a dual importance scheme, a numeral followed by a letter, as 1N. The numeral is assigned on the basis of the area of the solar surface encompassed by the flare at its maximum phase. This number ranges from S (subflare, written as -) to 1, 2, 3, and 4. The letter is f (faint), n (normal), or b (brilliant) and is a relative intensity evaluation. The numeral is then an objective parameter while the letter is subjective. Table I lists the five importance classifications and their definitions in terms of both heliographic square degrees and heliographic area in cm^2 to which each importance corresponds.

The outermost layer of the solar atmosphere is the corona. It extends from about 10^4 km above the photosphere to tens of solar radii. The coronal temperature is about 10^6 °K and changes very slowly with increasing radial distance. The density ranges from about 10^9 cm^{-3} at the chromospheric boundary to about 5×10^3 cm^{-3} at 3 solar radii. It was pointed out previously that flares extend into the lower corona.

Another coronal feature of interest is the coronal condensation, a dense region lying over the chromosphere. These have diameters of $1 - 2 \times 10^5$ km, electron density 10 to 20 times the undisturbed coronal electron density, and temperatures of the order of $2 - 4 \times 10^6$ °K.

This discussion of the solar atmosphere is not complete but gives a brief account of the physical region in which solar x-ray bursts are produced. For a more detailed discussion see Zirin [1966] or Kundu [1965].

B. Survey of Previous Solar X-Ray Observations

This survey will concentrate on results obtained in the last several years. Reviews of the subject of solar x-ray emission prior to the last few years and a guide to the earlier literature can be found in Kundu [1965], Mandel'shtam [1965], and Goldberg [1967].

Solar x-ray emission in the 2 - 12 Å range can be divided into three components: the quiet sun component, the slowly varying component, and the burst component [Kundu, 1965; Wende, 1968]. The quiet sun component is the emission radiated by the sun when no solar activity is present. This component varies by an order of magnitude with the 11-year solar cycle period. This emission is thermal in nature with a temperature of $1 - 2 \times 10^6$ °K.

The slowly varying component has a period of 27 days (one solar rotation period) and originates from areas near calcium plage which have a higher density and a higher temperature than the normal corona. Radio emission in the cm-wavelength region

is also produced by these high density, high temperature volumes. Both the radio and x-ray emission for the slowly varying component can be adequately accounted for by thermal emission from localized regions with temperatures 2 - 7 x 10^6 °K [Gibson, 1969].

The third component, the burst component, is the one to be investigated further in this study. X-ray bursts are closely associated with Hα flares. The time scales for x-ray bursts in the 2 - 12 Å (1 - 6 keV) range are rise times of the order of several minutes and decay times of the order of tens of minutes. At higher photon energies the bursts have smaller rise and decay times.

During a burst the intensity increases by factors up to 10^3. The spectrum hardens during a burst [Pounds, 1965; Chubb, Kreplin, and Friedman, 1966]. If the emission is assumed thermal in origin so that a free-free or blackbody spectrum may be used, an effective temperature may be derived from the observed spectrum. A temperature of 10 - 12 x 10^6 °K was obtained in this manner by Bowen et al. [1964] and a temperature of order 10^8 °K by Chubb et al. [1966] for solar x-ray bursts. With the observation of the first hard x-ray burst at photon energies > 20 keV by Peterson and Winckler [1959], non-thermal emission was proposed. Non-thermal emission is thought to be important primarily at higher photon energyes (> 10 keV) and in the rising portion of the more impulsive bursts. However, Acton [1968] claims that

the data of Bowen et al. [1964] can be adequately explained by non-thermal processes.

If an effective temperature can be obtained and if the effective temperature is observed to change faster than the electron-electron energy exchange rate, the electron distribution must be non-Maxwellian. This is found to be the case during the rising portion of a hard x-ray burst by Hudson, Peterson, and Schwartz [1968; 1969a, b].

Kane [1969] has shown that for photon energies > 10 keV there are two components to the burst emission. One component is impulsive and reaches its peak early in the event, nearly coincidental to the peak of the microwave burst. This component of the emission is attributed to bremsstrahlung from a non-thermal electron distribution because the photon spectrum is consistent with a power law in energy and because the duration of this component is of the order of 30 seconds. The other component has a steeper photon spectrum, a duration of the order of 10 minutes, and the exponential rise and decay shape characteristic of soft x-ray bursts. Because of these properties, this component is thought to be of thermal origin.

Hudson, Peterson, and Schwartz [1968; 1969a, b] compared 7.7 - 12.5 keV to 12.5 - 22.0 keV x-ray burst data, assuming an isothermal region producing x radiation by a free-free emission

process. The temperatures they derived were in the range $14 - 50 \times 10^6$ °K. The hardening of the spectrum referred to previously evidences itself as a changing temperature in this analysis. The data within an event fit a curve of constant emission measure of 1.4×10^{47} cm^{-3} with only the temperature changing during the event. The emission measure was found to be constant not only within an event, but from event to event, when the ratios for event peaks were examined. The emission measure was found to be $1 - 2 \times 10^{47}$ cm^{-3} and constant. Their model of a burst is that the time profile of the flux is produced only by a changing temperature in the emission region. This point will be examined further in the present study.

The relationship of Hα flares and x-ray bursts has been examined recently by several investigators [Culhane and Phillips, 1969; Harries, 1968; Hudson, Peterson, and Schwartz, 1968, 1969a, b; Teske and Thomas, 1968; Teske, 1969; Van Allen, Dodson, and Hedeman, 1969]. Teske [1969] finds a loose relationship between flare importance and x-ray burst amplitude. In addition, 8 - 12 Å x-ray bursts were found to start before Hα flares and to reach maximum amplitude about 3 minutes after the Hα maximum time [Teske and Thomas, 1968]. The cm-wavelength radio bursts were found to peak 3 - 5 minutes before the soft x-ray maximum, which puts

their maximum time nearly coincidental with the Hα maximum time. Culhane and Philipps [1969] and Hudson, Peterson, and Schwartz [1968; 1969a, b] find a weak dependence of x-ray burst amplitude on Hα area, which implies a loose relationship between x-ray burst amplitude and Hα flare importance. The nature of this relationship will be examined further in Section VI-B.

It was pointed out by Elwert [1968] that if non-thermal bremsstrahlung produces the rise and maximum of the burst and if the electrons have a preferred direction of motion, then the radiation will be directional and dependent on the particle energy. It is further assumed that the directionality will evidence itself in the probability of occurrence of x-ray bursts as a function of position on the solar disk. By associating an Hα flare with an x-ray burst, the location of the x-ray source on the solar disk is known. The resulting heliographic longitude distribution of x-ray bursts can then be examined to determine if such directionality exists. The flare model of DeJager and Kundu [1963] prescribed that the electrons move radially in the solar atmosphere while the model of Takakura and Kai [1966] required that the electrons move essentially parallel to the solar surface. An examination of the longitude distribution of different energy x-ray bursts might discriminate between these two flare models.

Two workers have completed such studies. Ohki [1969] examined the longitude distributions of 10 - 50 keV and of 1 - 6 keV bursts. He found the occurrence of 10 - 50 keV bursts decreased from center-to-limb while the 1 - 6 keV bursts had a uniform distribution. This is attributed to a directivity effect of non-thermal emission from an anisotropic electron stream. However, the hard x-ray burst statistics were poor (only 46 events) and the center-to-limb variation of Hα flares was not specifically included.

Pinter [1969] used similar x-ray data supplemented by 0.6 - 1.5 keV burst data. The 1 - 6 keV x-ray burst occurrence is not found to be uniform in longitude as Ohki [1969] found. Instead it resembles the distribution of Hα flares with longitude (Section VI-C). He also did not specifically include the Hα heliographic longitude distribution. His conclusion is that a directional effect exists which indicates agreement with the flare model of Takakura and Kai [1966]. This problem is examined in detail in Section VI-C.

The spatial location of x-ray burst sources has only recently been directly observed. Vaiana et al. [1968] photographed in several different soft x-ray wavelength ranges a region flaring in Hα. The burst source was found to coincide with the Hα flare position and to have upper size limits of 1 arc minute by 1 arc minute. During the burst the emission from the flaring region exceeds by a factor of 10 or more the emission from the rest of the solar disk.

C. Free-Free Emission Theory

Several different emission processes could produce x radiation in the 1 - 50 keV range. The more important of these are synchrotron emission, non-thermal bremsstrahlung, and four varieties of thermal emission: free-free, free-bound, bound-bound, and dielectronic recombination emission. Of these possibilites, only free-free thermal emission is considered in detail in this study. The other possibilities are eliminated as follows.

Synchrotron radiation is emitted roughly within a bandwidth of f_c around f_c, where f_c is the critical frequency defined as [Kundu, 1965]

$$f_c(\text{MHz}) = 16.1\ H(\text{gauss})\ E^2\ (\text{MeV})\ . \qquad \text{(I-1)}$$

Above the critical frequency the power decreases as $(f/f_c)^{1/2}$ $\exp(-f/f_c)$. A critical frequency corresponding to a 1 keV photon (2.4×10^{17} Hz) and a field of 10^3 gauss, taken as typical for a solar flare, require an electron energy of 4×10^9 eV. The total power radiated by this electron is given by [Kundu, 1965]

$$P(\text{erg/sec}) = 6 \times 10^{-15} H^2 \text{ (gauss) } E^2 \text{ (MeV)} . \qquad \text{(I-2)}$$

For a 4×10^3 MeV electron and field of 10^3 gauss, the radiated power is 9.6×10^{-2} erg sec^{-1}. The electron energy is 6.4×10^{-3} erg. If the electron energy decreases to 10^{-3} erg, the synchrotron emission at 1 keV will be drastically reduced. The time needed to radiate 5×10^{-3} erg at the rate of $\sim 10^{-1}$ erg sec^{-1} is 5×10^{-2} sec. The short lifetime of such energetic particles, in view of the much longer duration of soft x-ray bursts, requires the production of energetic particles for periods of minutes. This is not thought to occur, nor are such energetic particles thought to exist in any substantial quantity in the solar atmosphere. Synchrotron emission is therefore not a promising possibility.

Non-thermal emission must certainly occur during the rising portions of some impulsive bursts. However, Kane [1969] has observed two components of hard x-ray bursts, one of short time duration consistent with a non-thermal origin and one much slower and apparently thermal in origin. Hudson, Peterson, and Schwartz

[1968; 1969a, b] find agreement with a thermal emission mechanism and disagreement with a non-thermal (power law in energy) mechanism for 7.7 - 22.0 keV bursts. The thermal interpretation holds for burst peaks as well as the decay phase. Wende [1968] finds the decay phase of 1 - 6 keV bursts explainable on the grounds of thermal emission. The results of Section VI-C indicate no substantial non-thermal contribution to the 1 - 6 keV bursts, at least insofar as a directionality effect is concerned. On the basis of the above arguments against non-thermal emission and the lack of argument in favor of it, non-thermal emission is also discarded as a substantial contributor to the 1 - 50 keV burst radiation.

Of the thermal processes, the dominant one for temperatures above 8×10^6 °K is free-free emission. This is shown by calculations by Gibson [1969] and Culhane [1969]. The temperatures obtained when free-free emission is assumed are greater than 10^7 °K. Values in this range have been obtained by a number of different investigators and free-free emission is in agreement with the dominance of the continuum over line emission in the 1 - 50 keV range observed during flares (see Section VII-C). Thus free-free emission emerges as the most probable mechanism for the majority of 1 - 50 keV bursts.

The energy emitted per cm^3 per sec in the source region due to free-free emission from a Maxwellian electron distribution is [Karzas and Latter, 1961; Elwert, 1961]

$$dI(\nu,T) = \frac{2^{11/2}\, e^6}{c^3 k^{1/2}} \left(\frac{\pi}{3M}\right)^{3/2} n_i n_e Z_i^2\, T^{-1/2}\, \bar{g}\, \exp(-h\nu/kT) \qquad (I\text{-}3)$$

where $dI(\nu,T)$ = energy (erg) per cm^3 per sec emitted at frequency ν in the interval $d\nu$ from a Maxwellian electron distribution of electron temperature T

n_i = density of ions of nuclear charge Z_i, cm^{-3}

n_e = density of electrons, cm^{-3}

T = electron temperature, °K

c = speed of light

$\bar{g}$ = temperature averaged free-free Gaunt factor

e = electronic charge

k = Boltzmann's constant

M = mass of electron

ν = photon frequency.

$$\frac{2^{11/2}\, e^6}{c^3\, k^{1/2}} \left(\frac{\pi}{3M}\right)^{3/2} = 6.82 \times 10^{-38} .$$

To obtain the total emission from this region, a sum over the different ion species must be taken. A two-component atmosphere composed of 86% H and 14% He will be assumed [Allen, 1963]. At coronal temperatures these atoms will be completely ionized. The sum then over ion species becomes [Gibson, 1969]

$$\sum_i n_i Z_i^2 = 1.56\, n_H = 1.22\, n_e \,. \qquad \text{(I-4)}$$

The temperature averaged free-free Gaunt factor is taken from Karzas and Latter [1961] as 1.40. This value is good to $\leqslant 5\%$ for the range of energies and temperatures being considered. Then

$$dI(\nu, T) = 1.16 \times 10^{-37}\, n_e^2\, T^{-1/2} \exp(-h\nu/kT) d\nu \,. \qquad \text{(I-5)}$$

Equation (I-5) must be integrated over the source volume and divided by $4\pi R^2$, where R is one astronomical unit, to obtain the flux received at earth at frequency ν in the interval $d\nu$,

$$dF(\nu, T) = 4.12 \times 10^{-65}\, T^{-1/2} \exp(-h\nu/kT)\, d\nu \int n_e^2\, dV. \qquad \text{(I-6)}$$

The emission measure, S, can now be defined as

$$S = \int n_e^2 \, dV. \qquad \text{(I-7)}$$

S has units cm^{-3}. The best form of Equation (I-6) for use in this study is

$$dF(\nu, T) = 4.12 \times 10^{-65} \; S \; T^{-1/2} \; \exp(-h\nu/kT)d\nu \; . \qquad \text{(I-8)}$$

The number of photons per cm^2 per second of energy $h\nu$ is related to the flux by

$$dF(\nu, \; T) = h\nu \; dN_p \; (\nu) \; . \qquad \text{(I-9)}$$

By use of Equations (I-8) and (I-9) and the given detector efficiency function, the detector response can be calculated.

The flux incident at the earth's orbit due to free-free emission in the wavelength range 2 - 12 Å is obtained by integrating Equation (I-8) over the corresponding frequency interval (0.25×10^{18} Hz to 1.5×10^{18} Hz). The resulting expression is

$$F(2 - 12 \text{ Å}) = 8.58 \times 10^{-49} \; S \; T^{1/2} \; \exp(-12/T) \qquad \text{(I-10)}$$

where F is in units of milli-erg $(cm^2 \text{ sec})^{-1}$, T is in units of 10^6 °K, and S is in units of cm^{-3}.

The flux is thus a function of two parameters, S and T, as can be seen from both Equations (I-8) and (I-10). To quantitatively test the emission mechanism two measurements are needed, one to establish the spectral distribution of the flux (T) and one to establish the flux magnitude (S). Such a test requires the assumption that the

temperature and emission measure in different photon energy intervals are identical. Also since the flux depends linearly on the emission measure, and hence the volume, and the Hα importance is based on area, there exist theoretical grounds on which to expect some correspondence between x-ray peak amplitude and flare importance.

D. Flare Models

Two flare models [De Jager and Kundu, 1963, and Takakura and Kai, 1966] which have been used in the literature as a basis for examining data, and a third model [Carlquist, 1968], seldom mentioned in the literature but which seems to possess many features necessary to an adequate model, will be discussed briefly.

The model proposed by De Jager and Kundu [1963] requires that fast electron jets be accelerated in magnetically neutral regions and move in a radial direction. In this situation the same fast electrons which are accelerated radially downward produce both the high-energy (> 10 keV) x rays and the associated cm-wavelength radio burst. The x-ray emission would then be by non-thermal bremsstrahlung and possess directional properties. The electrons accelerated away from the solar surface would produce Type III radio bursts. The electrons in this model are accelerated to energies of at least 10^4 to 10^5 eV.

Takakura and Kai [1966] proposed a model in which the high energy electrons are trapped in the magnetic bottle geometry existing in the region between the two spots of a bipolar spot group. The energetic electrons then have a preferred direction of motion approximately parallel to the solar surface. The cm-wavelength burst is due to synchrotron emission from energetic electrons in stronger field regions. There has been a discrepancy of a factor of 10^3 to 10^4 between the total number of electrons needed to produce the x-ray burst and the number needed to produce the radio burst [Peterson and Winckler, 1959]. This difficulty is overcome in the Takakura and Kai model by requiring that the majority of the energetic electrons be trapped in a region of low field strength and high number density so that the source is invisible at radio frequencies (the frequencies in question lie below the local plasma frequency). A power law electron energy distribution with exponent -3 to -5 is found satisfactory to account for the time profile of the radio burst.

The third flare model [Carlquist, 1968; Jacobsen and Carlquist, 1964; Alfven and Carlquist, 1967] is concerned primarily with the production of the energetic particles needed in the previous models. The proposal is that in low density regions of the solar atmosphere in which the current density is high (along magnetic lines of force) an instability occurs, causing a high impedance region to be formed. The voltage then increases

across the high impedance region until a discharge occurs. Electrons and protons are accelerated to very high energies (10^{10} - 10^{11} eV) during the discharge. This process is shown to have a time scale of 10^2 second and to be energetically feasible. The onset of the instability is related to the radius of the current carrying filament. Typical filament radii sufficient to cause onset of the instability are 200 km, consistent with the fact that source regions for flares have not yet been resolved.

In this model a very small and very hot region would be produced which could then expand and cool, placing the correct temporal order on observed features (see Sections I-B and VII-A). High energy electrons would lose energy much faster than the same energy protons so that soon after the discharge, protons would be the dominant higher energy particles. Boldt and Serlemitsos [1969] demonstrate that for the 28 September 1961 solar flare, the observed hard x-ray emission is consistent with a suprathermal proton source emitting bremsstrahlung. In addition to these features, a number of other observational features are consistent with this theory [Carlquist, 1968].

E. Objectives

Solar x rays in the wavelength range 2 - 12 Å (1 - 6 keV) have been monitored by University of Iowa detectors on the satellites Explorer 33 (since July 1966) and Explorer 35 (since

July 1967). From July 1966 to July 1967 Explorer 33 obtained x-ray data 55% of the time. From July 1967 to September 1968 Explorer 35 obtained x-ray data 75% of the time. These x-ray data have been converted into absolute flux values by computer for the above data [Drake, Gibson and Van Allen, 1969].

In this large quantity of data, thousands of x-ray bursts are observed. A means was devised to examine the burst component of the flux by computer. A total of 4028 bursts have been indentified in this manner for the period July 1966 to September 1968. This burst sample was examined for possible parameters by which to classify bursts. Previously the largest number of solar x-ray bursts included in a study was 472 [Harries, 1968]. The present study then provides results derived from the largest data base obtained to date on the subject of soft (1 - 6 keV) solar x-ray bursts.

In a comparison with other flare data, the relationship between Hα flare occurrence and x-ray burst occurrence was examined. The distribution of soft x-ray bursts with heliographic longitude was determined in order to test the non-thermal, directional emission proposal discussed in Section I-B.

A comparison was made with harder (photon energy greater than 6 keV) solar x-ray bursts to study the temporal and amplitude relationship of the two phenomena. In particular the suggestion of Hudson, Peterson, and Schwartz [1968; 1969a, b], based on

7.7 - 22.0 keV burst data, that x-ray bursts are adequately explained as free-free emission from a region with constant emission measure and with temperature only changing was examined over the extended range of 1 - 50 keV with data obtained from three different experiments [Arnoldy, Kane, and Winckler, 1968; Kane and Winckler, 1969; Hudson, Peterson, and Schwartz, 1969].

II. OBSERVATIONAL TECHNIQUES

A. Satellites

The absolute x-ray flux from the whole disc of the sun has been measured over a prolonged period of time (see Section II-C) by a 1 kg University of Iowa equipment on the earth-orbiting satellite Explorer 33 and the moon-orbiting satellite Explorer 35, both of the Goddard Space Flight Center/National Aeronautics and Space Administration. Explorer 33 was launched at 1602 UT on 1 July 1966. It has a far ranging earth-orbit which is strongly perturbed from time to time by passage by the moon. Over a three-year period the perigean radial distance has been between 32,000 and 274,000 km, the apogean radial distance between 436,000 and 859,000 km, and the orbital inclination to the earth's equator between 7° and 60°. Thus Explorer 33 is exposed almost continuously to the sun and makes occasional brief passes through the earth's magnetosphere. Explorer 35 was launched at 1419 UT on 19 July 1967 and injected into lunar orbit at 0919 UT on 22 July 1967. The subsequent orbit has been a stable one with periselene at a mean radial distance of 2576 km, aposelene at 9386 km, a mean orbital period of 11.53 hr, and an orbital inclination of 168° to the ecliptic (retrograde). One to two hours of x-ray data from

Explorer 35 are lost during each orbit because of passage through the optical shadow of the moon and of lunar occulation of the spacecraft as viewed from the earth (loss of telemetry signal). Data from both satellites are transmitted in an essentially real-time mode only. GSFC/NASA has maintained exceptionally continuous telemetry coverage.

Both satellites are "spin-stabilized" (i.e., set spinning about the axis of maximum moment of inertia during the launching operation). The rotational period of Explorer 33 has varied cyclically with a one-year period within the range 2.2 to 3.6 seconds; that of Explorer 35 has been within the range 2.3 to 2.4 seconds. The celestial coordinates of the spin-axis of each satellite are approximately constant, though there are weak torques due to solar radiation pressure which cause gradual changes. The spin-axis of Explorer 33 has been within 6° of the ecliptic plane throughout its flight. That of Explorer 35 can be reoriented by means of gas jets upon ground command; it has been maintained in the direction of the south ecliptic pole to within 7°.

B. Detectors

The pertinent portions of the detector complements on both satellites are nominally identical, consisting of three mica-window Geiger-Mueller tubes (EON type 6213) arranged as shown in Figure 1.

Detector GM1 has a fan-shaped collimator whose central axis is perpendicular to the satellite spin-axis. The opening angles of the collimator were measured experimentally with the collimated beam

from a small laboratory x-ray machine (electron energy 2.0 keV) in vacuo. The same experimental method was used to determine the opening angles of GM2 and GM3. The window thickness of detector GM1 on Explorer 33 [$(GM1)_{33}$] is 1.7 mg cm^{-2} and of detector GM1 on Explorer 35 [$(GM1)_{35}$] is 1.3 mg cm^{-2}.

By virtue of the orientation of the respective spin-axes of the two satellites, detectors GM2 and GM3 on Explorer 35 never view the sun, whereas these detectors on Explorer 33 do so periodically. $(GM2)_{33}$ has a conical aperture with axis parallel to the satellite spin-axis; the window thickness is 1.3 mg cm^{-2}. $(GM3)_{33}$ is identical in construction and arrangement to $(GM2)_{33}$, except that the axis of $(GM3)_{33}$ is anti-parallel to the satellite spin-axis; the window thickness is 1.3 mg cm^{-2}.

The GM tubes are self-quenching ones filled to a total nominal pressure of 429 mm Hg (at 0° C) with a mixture of neon (410 mm), argon (7 mm), and chlorine (12 mm). The effective volume of the tubes for soft x rays is a cylinder approximately 0.7 cm in length and 0.24 cm in diameter. The spectral efficiency of the tubes for soft x rays has been determined by two methods: by calculation and by experimental comparison with a tube whose efficiency can be calculated with better accuracy [Van Allen, 1967a; Wende, 1969]. Both methods agree to within 15% for $\lambda > 2.6$ Å, yielding the spectral efficiency curve shown in Figure 2. Pulses from $(GM2)_{33}$ and $(GM3)_{33}$ are accumulated continuously in separate storage

registers during a 25.57-second interval every 163.62 seconds and are read out in every other telemetry sequence. The center of the 25.57 second sampling period is 33.2 seconds after the beginning of the sequence.

The pulses from GM1 are gated into four separate storage registers, one register for each quadrant of rotation, by an electronic sector generator triggered by a "see-sun" pulse from a narrow-angle photo-electric sensor. The sectoring scheme is shown in Figure 3. The total accumulation time for the four sectors is 25.57 seconds, or 6.39 seconds per sector. The accumulation and read-out cycle is repeated every 81.81 seconds (every telemetry sequence). The center of the sampling period of GM1 is also 33.2 seconds after the beginning of the sequence. Sector III records solar x rays as well as galactic and solar energetic particles, whereas Sectors I, II, and IV record only galatic and solar energetic particles. Each telemetered sample of accumulated counts in Sector III comprises n subsamples, one per rotation of the spacecraft. Since the telemetry cycle is not synchronous with the rotational period, n varies as the rotational period varies and lies in the range 7 to 12. This fact in itself has no effect on the number of counts observed since the fraction of each rotation that the detector views the sun is independent of spin period. There is, however, a fluctuation in the fraction of the sampling interval that is devoted

to Sector III. For example, if n = 7.5, the data from Sector III may be obtained from as few as 7 rotations or as many as 8. The maximum fluctuation from the mean counting rate is $\pm$ 7%. This effect appears as a quasi-periodic "beat note" in the counting rate of Sector III (as well as in the counting rates of the other sectors). The GSFC telemetry system reports the position in each telemetry cycle at which the first "see-sun" pulse occurs. It is therefore possible to correct for this effect but has not been thought worthwhile to do so.

The in-flight accuracy of the sector generator on Explorer 35 is checked automatically on every 16th sequence by counting pulses from an auxiliary 10 kHz oscillator. The accuracy of the sector generator on Explorer 33 is checked occasionally at the data reduction level using the galactic cosmic ray counting rate of $(GM1)_{33}$.

C. Data Coverage

As Explorer 33 moves with the earth around the sun, the angle α between its spin-axis (approximately fixed in celestial coordinates) and the spacecraft-to-sun vector changes by about 1° per day, going from nearly zero through 90° to nearly zero again in a year. Hence the three detectors view the sun successively in the cyclic order GM1, GM2, GM1, GM3, GM1, GM2, GM1, etc., as the sun moves across the celestial sphere. There are gaps in the data when the sun is viewed by none of the three detectors; these

gaps average 23 days in length. The time interval between 2 July 1966 and 27 July 1967 during which solar x-ray observations with Explorer 33 were possible on geometrical grounds alone are:

2 July - 21 September 1966	GM1
9 October - 1 December 1966	GM2
29 December 1966 - 27 March 1967	GM1
20 April - 14 June 1967	GM3
4 July - 27 July 1967	GM1

For the entire period 2 July 1967 to 27 July 1967 the Explorer 33 coverage is 55% complete, if every break in the data of ≥ 5 minutes duration is counted as a data gap. During the five sub-intervals listed above, useable data are available for 78% of the time, on the same criterion. A sample coverage plot is given in Figure 4.

Detector GM1 on Explorer 35 observes the sun throughout the year, since the spin-axis of this spacecraft is approximately normal to the ecliptic. There are, however, several hours per day of lost data because of eclipse and occultation of the spacecraft by the moon and loss of signal during range-and-range rate interrogations through the spacecraft telemetry system. Certain data gaps are attributable to high particle intensities (Section III-A). For the entire period 26 July 1967 to 18 September 1968, useable x-ray data are available for 75% of the time, again using the

$\geq$ 5 minute criterion for summarizing the total of data gaps. A sample coverage plot is shown in Figure 5.

It is often possible by means of careful hand reduction to retrieve useable data during periods of time that have been discarded in the computer-reduced data analysis because of the stringent validity criteria which have been applied in the preparation of the basic catalog.

D. In-Flight Operation of Detectors

All six of the selected EON Geiger-Mueller tubes on Explorers 33 and 35 have operated properly and without apparent degradation since launch until the present date of writing (October 1969), despite the accumulation of over 10^{10} counts by each of those that has viewed the sun--$(GM1)_{33}$, $(GM2)_{33}$, $(GM3)_{33}$, and $(GM1)_{35}$. There have been occasional incidents (about 10) of high, spurious counting rates by a detector that has been exposed simultaneously to high x-ray intensity and high particle intensity. These incidents, which have never occurred under any other circumstances, have a duration of some hours. Even during such periods the detector continues to respond to x-ray bursts. In the scanning detectors $(GM1)_{33}$ and $(GM1)_{35}$, the spurious effect is pronounced in Sector III, much less in IV, still less in I, and absent in II during each rotation. Hence, the effect is characterized by a short-term recovery time of about one

second. The onset of the effect is abrupt (between data samples); and in every case the effect has disappeared after a period of less than 12 hours and the solar x ray and other rates have returned accurately to their pre-incident values. This observation has been established with special clarity in several cases of simultaneous Explorers 33 and 35 coverage. It is thought, tentatively, that the problem may arise from electrostatic charging of the poorly-conducting mica window under high intensity conditions.

Overall, there is a good level of confidence in the long-term validity of the Explorer 33 and Explorer 35 data. The impressive quality of the agreement between simultaneous observations with different detectors is particularly reassuring.

Only one spacecraft fault has been of importance: On 22 July 1967 the 10th flip-flop in the storage register that records counts from $(GM3)_{33}$ stuck in a monostable state. Since that date $(GM3)_{33}$ rates greater than 511/25.57 = 20 count sec^{-1} have not been transmitted unambiguously.

The temperature of the University of Iowa equipment on Explorer 33 and Explorer 35 has been within the respective ranges +5° to +42° C and -3° to +25° C, with brief exceptions (lower temperature) during several terrestrial eclipse periods, and the regulated power supply voltage has been accurately constant at its nominal value.

III. REDUCTION OF DATA

A. Conversion of Counting Rates to Absolute Fluxes

It has been shown previously [Van Allen, 1967a] that the type 6213 Geiger-Mueller tube (Figure 2) can be considered accurately equivalent to an x-ray detector whose absolute photon efficiency $\epsilon(\lambda)$ = const. for the wavelength range $\lambda_1 \leq \lambda \leq \lambda_2$ with λ_1 and λ_2 having the same values for a wide variety of spectra. The numerically determined values of λ_1 and λ_2 [Van Allen, 1967a; Wende, 1969] are 2 and 12 Å, respectively. The author has additionally verified numerically the constancy of $\epsilon(\lambda)$ with the given λ_1 and λ_2 for a blackbody spectrum corresponding to temperatures of up to 10^8 °K.

Thus the absolute solar x-ray flux F(2 - 12 Å) in milli-erg $(cm^2\ sec)^{-1}$ at the point of observation is given by

$$F(2 - 12\ \text{Å}) = (1.8 \times 10^{-3}) \cdot R \qquad \text{(III-1)}$$

where R is the true counting rate of the detector in count sec^{-1}. Equation (III-1) is applicable to a tube whose mica-window is 1.3 mg cm^{-2} in thickness and whose axis is fixed through the center of the sun.

For the actual conditions of observation of the rotating satellites Explorer 33 and 35

$$F(2 - 12\ \text{Å}) = (1.8 \times 10^{-3}) \cdot R \cdot f(\alpha) \qquad \text{(III-2)}$$

where $F(2 - 12\ \text{Å})$ is the absolute flux of solar x rays in the wavelength range 2 - 12 Å in milli-erg $(\text{cm}^2\ \text{sec})^{-1}$, R is the true counting rate in count sec^{-1} caused by the x rays from the whole disk of the sun, and $f(\alpha)$ is a "geometric obliquity factor" which, for a given detector, is a function only of the angle α between the spin-axis of the spacecraft and the spacecraft-to-sun vector.

The counting rate R in equation (III-2) is the true rate caused solely by solar x rays. For the sectored detectors $(GM1)_{33}$ and $(GM1)_{35}$ the quantity R is calculated from the formula

$$R = R_{III} - (R_I + R_{II} + R_{IV})/3 \qquad \text{(III-3)}$$

where R_i is the counting rate of the i^{th} sector.

For detectors $(GM2)_{33}$ and $(GM3)_{33}$, R is calculated from the formulae

$$R = R(GM2) - R(GM3) \qquad \text{(III-4a)}$$

or

$$R = R(GM3) - R(GM2) \qquad \text{(III-4b)}$$

as appropriate.

Formulae (III-3) and (III-4) are ordinarily adequate for the subtraction of counting rate contributions from galactic cosmic rays, solar electrons, protons, and alpha particles, and magnetospheric electrons and protons. Certain periods of high particle intensity and/or substantial but strongly anisotropic particle intensity have been omitted from the basic catalog.

B. Dead Time Corrections

The detector system has an especially wide dynamic range for the measurement of solar x-ray flux. In favorable cases it extends from 0.01 to over 1000 milli-erg $(cm^2\ sec)^{-1}$ in the 2 to 12 Å range.

The relationship between the true counting rate R (the rate that would be observed if the detector had zero dead time) and the apparent rate r (the rate that is actually observed) was determined by a careful series of pre-flight calibrations in the laboratory using a small dc x-ray machine and running a family of overlapping inverse square law curves. The r-R relationship at high counting rates is, in general, different for each detector and is also sensitive to temperature and to the precise choice and physical arrangement of associated electronic components. It was found possible to make the r-R relationship almost completely independent of temperature over

the range -25° to +50° C (a range considerably greater than observed in flight). The final r-R curves were run for each individual detector on the completed flight packages.

The final r-R curves for $(GM2)_{33}$ and $(GM3)_{33}$ are shown in Figures 6 and 7, respectively. These are directly applicable to flight data since these detectors view the sun continuously (on a short term basis).

Similarly determined r-R curves for $(GM1)_{33}$ and $(GM1)_{35}$ are shown as the solid curves in Figures 8 and 9, respectively. These detectors, however, spin past the sun once per spacecraft rotation. The instantaneous counting rate is not transmitted. The quantity which is transmitted is the accumulated number of counts within Sector III for 7 to 12 rotations during each of which there is a brief burst of counts. A further correction to the pre-flight r-R curves (as determined with a dc x-ray source) is therefore necessary. This correction was computed point-by-point during a rotation by use of the solid curves in Figures 8 and 9 and the curve of counting rate versus rotational angle (Figure 10) as also determined (at low counting rates) in pre-flight laboratory tests. The normalized form of this latter curve was found to be substantially independent of α. The dashed curves in Figures 8 and 9 are the finally adopted ones for $(GM1)_{33}$ and $(GM1)_{35}$. They are valid for any α and for any rotational rate.

All Explorer 35 data as well as Explorer 33 data after 27 July 1967 have been properly corrected for dead time using the appropriate dashed r-R curve.

The cataloged data from $(GM1)_{33}$ of Explorer 33 during the period 2 July 1966 to 27 July 1967 were reduced using the solid r-R curve in Figure 8. Upon re-examination of the data it was found that the peak fluxes of only ten bursts were significantly in error (10% to 25% too low). These bursts are listed in Table II with their apparent peak counting rates and the properly corrected true counting rates.

C. Geometric Obliquity Factor $f(\alpha)$

The geometric obliquity factor $f(\alpha)$ (cf. Equation (III-2)) is a function of α only and is that factor by which the true counting rate R of a given detector must be multiplied to yield the counting rate that would have existed if the standard detector had been viewing the sun fixedly with its axis through the center of the sun. Provisional values of $f(\alpha)$ for each detector were calculated from pre-flight experimental determinations of the angular response functions for its collimator using heterochromatic x-ray beams from a 2 kV and a 5 kV x-ray machine in vacuo.

The finally adopted values of $f(\alpha)$ were determined in the ideal manner, using simultaneous flight observations on the sun by successive pairs of detectors on the two spacecraft.

The GM tube for which the absolute $\epsilon(\lambda)$ versus λ curve (Figure 2) was determined was flown on Mariner V. Of the four detectors used on Explorers 33 and 35, $(GM2)_{33}$, $(GM3)_{33}$, and $(GM1)_{35}$ have essentially the same window thicknesses as the Mariner V detector (measured with an α-particle source). $(GM2)_{33}$ was adopted as the absolute standard, $f(0°) = 1.00$ in Equation (III-2).

Since $(GM1)_{35}$ observes solar x rays throughout the year with α approximately constant ($\approx 90°$), its rate was adopted as the reference standard for the rates of the three different detectors on Explorer 33. The values of α for each spacecraft at any one moment are provided directly to a nominal accuracy of $\pm 0.5°$ by the GSFC aspect sensors.

The comparison of rates of $(GM1)_{33}$, $(GM2)_{33}$, and $(GM3)_{33}$ with simultaneous rates of $(GM1)_{35}$ was done by overlaying translucent graphs on a light table, taking the data in one-day blocks for the period 27 July 1967 to 31 March 1968. Observed values of the ratio $(GM1)_{35}/(GM2 - GM3)_{33}$ as a function of α are plotted in Figure 11. The accuracy of the adopted curve is judged to be $\pm$ 10% for $\alpha < 15°$ and $\pm$ 50% for $\alpha > 22°$. To obtain $f(\alpha)$ versus α for (GM2 - GM3) the factor is found that brings the ratio $(GM1)_{35}/(GM2 - GM3)_{33}$ to unity at $\alpha = 0°$. The curve of Figure 11 is multiplied by this factor (5.9) to give the adopted curve of $f(\alpha)$ versus α for $(GM2 - GM3)_{33}$ (Figure 12).

This process also determines the absolute geometric obliquity factor $f(\alpha)$ for $(GM1)_{35}$ at $\alpha \approx 90°$. Since α_{35} is always $\approx 90°$, the value $f(90°) = 5.9$ ($\pm$ 10%) was adopted as the appropriate constant factor for this detector for use in Equation (III-2).

It is assumed that $f(180° - \alpha)$ for $(GM3 - GM2)_{33}$ is equal to $f(\alpha)$ for $(GM2 - GM3)_{33}$ since the respective tubes and their collimators are essentially identical. A partial set of overlapping flight data for $(GM3 - GM2)_{33}$ and $(GM1)_{35}$ agrees well with the curve of Figure 11 and supports this assumption.

In determining $f(\alpha)$ for $(GM1)_{33}$, a discrepancy was found when plotting the ratio $D = (GM1)_{35}/(GM1)_{33}$ as a function of α. The data points corresponding to α increasing did not lie along the same smooth curve as those corresponding to α decreasing. In addition the curves did not coincide for α and $(180° - \alpha)$ as they should for a GM tube with a symmetrical collimator. Also the minima in the curve of D versus α indicated a value of $\alpha_{min} = 90.5°$ for α decreasing with time and $\alpha_{min} = 92.0°$ for α increasing with time, the angle α being that read from the GSFC optical aspect sensor.

This discrepancy may be attributable to either an up-down asymmetry of $(GM1)_{33}$ or to a systematic error in the GSFC optical aspect sensor. Two different optical aspect sensors are used to measure α, one for $0° \leq \alpha \leq 90°$ and a second one for $90° \leq \alpha \leq 180°$. The transition from one sensor to the other is made at $\alpha \approx 90°$. When α versus time was plotted, there was discontinuity in the curve

when this switch should have occurred. The curves of D versus time for the two periods (days 207 to 268, 1967, α decreasing, and days 357, 1967 to 90, 1968, α increasing) were symmetrical. In the first period, D was a minimum at day 227.7 and $D(227.7 + \Delta t) = D(227.7 - \Delta t)$ for $\Delta t \leq 22$ days (Δt taken to be a positive quantity). In the second period D was a minimum at day 48.0 and $D(48.0 - \Delta t)$ for $\Delta t \leq 27$ days. Even more significant was the fact that $D(227.7 + \Delta t)$ from the first period was accurately equal to $D(48.0 - \Delta t)$ from the second period, as was $D(227.7 - \Delta t)$ equal to $D(48.0 + \Delta t)$. This confirms the belief in the up-down symmetry of $(GM1)_{33}$ and suggests that a better parameter than α for this detector is $t_{min} \pm \Delta t$.

The ratio $(GM1)_{35}/(GM1)_{33}$ as a function of Δt is shown on Figure 13. The solid circles denote ratios taken while the sun was quiet; the X's are ratios obtained during bursts. The fact that the counting rate of $(GM1)_{35}$ is 1.84 times the counting rate of $(GM1)_{33}$ when both $\alpha_{33} = 90°$ and $\alpha_{35} = 90°$ is consistent with the greater window thickness of $(GM1)_{33}$ (1.7 mg cm^{-2} compared to 1.3 mg cm^{-2} for $(GM1)_{35}$). From Figure 13 it is seen that a smooth curve, which when multiplied by 5.9 becomes $f(\Delta t)$ for $(GM1)_{33}$ (Figure 14), can be defined to an uncertainty $\leq 10\%$ for $\Delta t \leq 20$ days, $\leq 30\%$ for $20 \leq \Delta t \leq 30$ days, and $\leq 50\%$ for $30 \leq \Delta t \leq 55$ days.

The principal value of the work described in this section is in bringing the data from three different detectors on Explorer 33 for the period of over one year before the launch of Explorer 35 to

a common absolute basis and in obtaining the absolute value of $f(90°)$ for $(GM1)_{35}$.

To determine the geometric obliquity factor for $(GM1)_{33}$ for the time before the launch of Explorer 35, t_{min} was assigned to the time when $\alpha = 90.5°$ for α decreasing with time and to the time when $\alpha = 92.0°$ for α increasing with time. The t_{min} values so determined were day 220.7, 1966 and day 41.0, 1967, respectively.

The finally adopted geometric obliquity factors f(t) determined as described above for 2 July 1966 to 27 July 1967 are summarized in Figure 15. The result of using the values of f(t) so obtained is to yield a flux which would have been recorded by $(GM2)_{33}$ if it had been pointed continuously at the sun with $\alpha = 0°$. The factor $f(90°) = 5.9$ in Equation (III-2) for $(GM1)_{35}$ further brings all Explorer 35 fluxes to the same basis.

It is evident that the adopted values of $f(\alpha)$ and f(t) for the several detectors are such as to lump together in a single factor both purely geometric factors and all other factors that differ from detector to detector (window thicknesses, gas pressures, etc.).

D. Reduced Data Forms

As described in the previous sections, University of Iowa equipments on Explorers 33 and 35 have provided a homogeneous body of basic data on the x-ray flux F(2 - 12 Å) from the whole disc of

the sun beginning on 2 July 1966 and continuing at the present date of writing (October 1969).

A comprehensive catalog of absolute values of F(2 - 12 Å) as a function of time has been completed as follows:

From Explorer 33: 2 July 1966 to 30 March 1969
From Explorer 35: 26 July 1967 to 7 May 1969
The data are presented in two forms, tabular and graphical.

Two specimen pages of tabular data are given in Figures 16 and 17. The first column is the decimal day of the year to five decimal places at the beginning of the telemetry sequence in the second column. Note that 0000 UT of 1 January of each year = decimal day 0.00000. The geometric obliquity factor is given in the third column. In following columns are the last two digits of the year, the month of the year, the day of the month, and the hour, minute, and second of the center time of the x-ray sampling interval associated with the specified telemetry sequence. The absolute value of F(2 - 12 Å) is given in the last column in milli-erg $(cm^2\ sec)^{-1}$. Three digit accuracy has been maintained in the computer program although it is clear that the right-hand digit is insignificant.

The graphical form of the data is illustrated in Figures 18 to 27, inclusive. The flux in milli-erg $(cm^2\ sec)^{-1}$ is plotted against time, universal time being given along the bottom scale

and decimal days along the upper scale. These graphs were computer drawn on a microfilm plotter. A wide variety of solar activity is illustrated.

Corrections for the varying distance from the sun to the earth ($< 3\%$) and for the varying electromagnetic propagation time over the different path lengths involved in the observational system ($\lesssim 5$ sec) and in the location of the source on the spherical sun (≤ 2 sec) have been considered trivial and have not been made. The times given are the times of arrival of solar photons at the earth, not their times of emission at the sun.

The relative uncertainty of the Explorer 35 data and of normalized Explorer 33 data during periods of overlapping observation is thought to be less than $\pm$ 15% throughout. The relative uncertainty of the prior Explorer 33 data (2 July 1966 - 27 July 1967) is greater--being $\pm$ 20% for $f(t) \leq 30$, $\pm$ 50% for $50 \leq f(t) \leq 200$, and greater for $f(t) > 500$. The absolute uncertainty in the factor 1.8×10^{-3} in Equation (III-2) is $< \pm$ 50% for a wide variety of spectra.

IV. BURST IDENTIFICATION PROCEDURE

A method was developed to both identify the occurrence of an x-ray burst and to determine several parameters of the burst by computer using as input the magnetic tape of reduced solar x-ray flux. A computer approach was used because of the extent of the data to be analyzed and to reduce the subjectivity of the process to a minimum.

A. Method of Identification

The program used compares, at each data point, the flux value to a background flux value which has been determined manually and fed into the program. When the ratio of the observed flux to the background flux exceeds a certain arbitrary value, a burst has been found, its parameters are subsequently determined, and output occurs. The arbitrary value for the ratio was adopted as 1.5 after trying several values from 1.25 to 4.0; a value less than 1.5 produces an excessive number of spurious burst outputs.

The burst parameters obtained and their method of determination can best be discussed by examining a sample page of the burst output listing, as shown on Figure 28. The beginning time of the burst is the interpolated time when the rising flux curve equals the

local background flux plus 20% of the peak flux increase above background. The year, month, and day of month of the beginning time are recorded in the first three columns. The next three columns are the beginning time in hours, minutes, and seconds.

The time, in units of hours, minutes, and seconds, under "PEAK" corresponds to the time of the maximum flux of the burst. The ending time is the interpolated time when the falling flux curve equals the local background flux plus 20% of the peak flux increase above background and appears under "END" in units of hours, minutes, and seconds. All times used have been corrected to correspond to the central time of the flux sampling period. A "U" on a beginning, peak, or ending time indicates that the time is uncertain because the corresponding data point was in or on the edge of a data gap. A record mark on a beginning (ending) time indicates that the time value was not determined by the previously discussed interpolation scheme because another burst occurred before (after) the flagged time such that the flux was never small enough in value to meet the interpolation requirement. In this case the flagged time corresponds to the time of the minimum flux value attained.

A burst is listed as one burst with two peaks if after the first peak the flux decreased to a value less than 80% of the total flux value at the time of the first peak and then rises again to a value equal to, or exceeding, the total flux value at the time

of the first peak. This procedure can be repeated to produce bursts with several peaks, always using the immediately preceding peak to compare against. In cases of multiply peaked bursts, the beginning time is determined from the first peak and the ending time from the last peak in the interpolation previously described.

The column "PEAK VALUE" lists, in units of milli-erg $(cm^2\ sec)^{-1}$, the flux increase above the background level for the maximum flux in the burst. The ratio of the maximum total flux to the background flux appears in the column "RATIO". The number of data losses of five consecutive minutes or more which occurred during the burst are recorded under the heading "GAPS".

The rise time, decay time, and total duration of the burst appear under the broad heading of "TIME" under the appropriate sub-headings. These values are determined directly from the beginning, peak, and ending times. For single bursts the rise time plus decay time equals the total burst duration. For multiply peaked bursts this will not be true due to the manner of determination of the beginning and ending times for these bursts.

The time integral of the flux increase above the background level for each burst is listed in the column "SUMF" in units of erg cm^{-2}. The flux is summed from the beginning time to the ending time of the burst. The contribution to the integral occurring before the beginning time and after the ending time were obtained, to a

first approximation, by a triangular extrapolation formula based on the two data points nearest to each end. The value appearing then is once corrected to obtain more accurately the total time integral of the flux for each burst.

The columns headed by "R/D", "R/T", and "D/T", list the ratios of rise time to decay time, rise time to total burst duration, and decay time to total burst duration, respectively. These quantities are calculated directly from parameters obtained previously.

The final column, "TLOS", contains the ratio of the time lost in gaps to the total time of the burst. This value can range from 0.000 for complete coverage to 1.000 if each point in the burst is on the edge of a gap. The non-zero values given in this column can provide an approximate correction to the flux time integral values to partially compensate for the contribution to the integral lost during a gap.

The results of the computer analysis were examined together with the graphical form of the data for each listed burst to eliminate, or identify, listings which disagreed strongly with a subjective, visual impression of the event. Less than 10% of the bursts were in disagreement by this test. Bursts in question were done by hand and substituted for the erroneously listed bursts. After examination and correction, the burst list was transferred to magnetic tape.

A total of 3515 bursts and 513 secondary burst peaks were listed in this manner for the time interval 2 July 1966 to 18 September 1968 for a total of 4028 burst peaks. Based on the data from August 1967 through August 1968 there were an average of 8 bursts per day. The burst occurrence per month for the total time period of this study is given in Table III.

B. Error Discussion

The uncertainty associated with the time of peak flux occurrence is of the order of one-half the time between detector sampling intervals, or 41 seconds, except for the periods 9 October to 1 December 1966 and 2 April to 14 June 1967 when this uncertainty is 82 seconds. The background flux value was defined to ± 20% during the majority of the data. During multiply peaked bursts the background value for the secondary peaks is difficult to determine, even when all work is done by hand, and may have a greater uncertainty than for the majority of the events. Secondary peaks accounted for 15% of the total number of peaks found so that at least 85% of the events have a background flux good to ± 20%.

The uncertainty in the beginning time due to the ± 20% possible uncertainty in the background flux value is ± 4% for the most common rise time (4 minutes). The uncertainty in the ending time due to this effect is less than ± 1% for the most common decay time (12 minutes). The rise and decay times have in addition to

the above possible uncertainty in beginning and ending times the possible uncertainty in the peak time. For a rise time of 4 minutes this uncertainty is ± 17% (± 34%). The value in parentheses refers to the two intervals cited in which the delay between flux samplings was longer; this notation will retain its significance for the duration of this section. For a decay time of 12 minutes the uncertainty is ± 6% (± 12%). The rise time uncertainty is then ± 21% (± 38%) and for the decay time is ± 7% (± 13%). The uncertainty values given here are representative and correspond to the most common rise and decay times.

The total flare time has a possible uncertainty of ± 5%. The ratio of rise to decay time has a ± 28% (± 51%) uncertainty, the ratio of rise to total time ± 26% (± 33%) uncertainty, and the ratio of decay to total time ± 12% (± 18%) uncertainty.

The uncertainty in both the absolute value of the flux and in the relative flux values has been discussed previously (Section III-D). Since the relative uncertainty of flux values is at most ± 7% and the background flux values were determined to at least ± 20%, there is at most a possible ± 27% possible uncertainty in the ratio of peak flux to background flux. The flux time integral has a ± 20% uncertainty due to the background flux uncertainty. In addition, there may be up to a 20% underestimation of the flux time integral due to not completely including the contributions to the integral occurring before the beginning time and after the ending

time even though a first attempt at correction by an extrapolation formula, mentioned previously, has been included. There is thus a 0% to -40% possible uncertainty in the flux time integral value.

In the studies made using these parameters, a large number of events were used. A wide range of values for each parameter was obtained. The uncertainties should occur at random and tend to cancel in the use of a large sample so that the errors expected in the distributions should be much less than those given above. Only in consideration of an individual event could the uncertainty be as great as that given previously.

V. BURST PARAMETER DISTRIBUTIONS

A study of the burst parameters was completed to determine if there were parameters which would allow classification of bursts, which classification might provide insight into the production mechanism.

As a listing on magnetic tape has been produced containing both the parameters for each burst and information detailing the quality of the burst (if and where in the burst a data gap had occurred), the distribution of parameters was also obtained by computer. Only events of best quality in each parameter were used; the exclusion of events in each category will be discussed in the various parameter distribution sections.

A. Rise Time

No rise times were included which were based on a flagged beginning or peak time or for which there was a data gap between the beginning and peak times. The number of events passing these criteria was 2206. Figure 29 shows the distribution of 94% of the events with good quality rise times. The number of events in each class, the number of those events shown on the corresponding plot, and the percentage of the total number of events in each class

appearing on the plots is given in Table IV and will not be specifically stated in the text for the remaining distributions.

The most common rise time was 4 minutes; no events were observed having a rise time of less than one minute, the limiting time resolution of the system. A linear least-squares fitting program with weighting equal to the square root of the number of events in each interval was used to fit the data. The data from 4 minutes to 38 minutes, comprising 75% of the events in this distribution, is represented by the equation

$$N = 11.9 \exp[(-0.1004 \pm 0.0009)\ T_R] \qquad (V\text{-}1)$$
$$T_R \geq 4 \text{ minutes} \ .$$

T_R is the rise time in minutes and N is the percentage of the total number of events in this class which have rise times in the interval $T_R \pm 0.5$ minutes. Thus N is the percentage probability for the occurrence of a burst in the differential interval $T_R \pm 0.5$ minutes.

The uncertainty expressed in the exponent is the standard deviation of the exponent as determined in the fitting program. The uncertainties expressed for all following exponents determined for parameter distributions were determined in this same manner unless specifically stated otherwise. In addition, the parameters used correspond to those actually observed; there has been no correction

or elimination of events which may be the superposition of two or more different solar events. This will not affect significantly the most prominent features of the distribution as solar events, evidenced by Hα flare reports, overlap in time rarely. The effect may be more significant for the finer details in the distributions.

B. Decay Time

No decay times were included which were determined from flagged peak or ending times or for which there was a data gap between the peak and ending times. The distribution of decay times so obtained is shown on Figure 30. The most common decay time is 10 - 13 minutes; a nominal value of 12 minutes will be used henceforth to denote this time.

There are two peaks, one at 18 minutes and one at 29 minutes, which are not quite within the limits of statistical uncertainty of the adjoining values. However, the widths of these apparent peaks are the minimum width possible (one interval only) and are only slightly outside the statistical uncertainty limit. On this basis, it is thought that these peaks do not represent significant decay time peaks but owe their existence to the sample size used and to statistical fluctuations. There is then only one significant peak in this distribution at a nominal value of 12 minutes.

C. Total Duration

Only single bursts continuous at the 5-minute interval level and without flagged beginning or ending times were included in this distribution. The total burst duration distribution is shown on Figure 31. No bursts were observed with a duration of less than 2 minutes. A nominal value for the most common burst duration is 16 minutes, although the peak is rather broad (8 - 24 minutes). There is no evidence of more than one peak in the total burst duration distribution.

D. Ratio of Rise (Decay) Time to Total Duration

Using the same criteria as were used before in the rise time, decay time, and total duration distributions, the distribution of bursts with respect to the ratio of the rise (decay) time to total duration was examined. The distributions so obtained are shown in Figures 32 and 33, respectively. The solitary peak in the distribution of the rise (decay) time divided by the total duration is at 0.25 (0.75).

E. Ratio of Rise to Decay Time

The same criteria as before were again used to define good quality rise and decay times. The distribution of events with respect to the ratio of rise to decay time is shown on Figure 34. From a ratio of 0.3 to a ratio of 2.7, comprising 69% of the events in this category, the distribution can be represented by

$$N = 32.5 \exp[(-2.309 \pm 0.018)\ T_R/T_D] \qquad (V\text{-}2)$$

where N is the percentage of events, relative to the total number of events in the distribution, per 0.1 interval centered on the ratio of rise to decay time, T_R/T_D. The significant peak in this distribution occurs at a ratio of rise to decay time of 0.3.

F. Discussion of Temporal Parameters

There is no evidence in the temporal parameter distributions for the existence of more than one class of x-ray burst in the 2 - 12 Å (1 - 6 keV) range. More classes may exist but they can not occur for a substantial number of bursts. It appears adequate to consider bursts as being of one standard form with wide latitude in all parameters. The temporal description of this standard (most common) 2 - 12 Å burst is a rise time of 4 minutes, ratio of rise (decay) time to total time of 0.25 (0.75), and ratio of rise to decay time of 0.3.

These typical values for 1 - 6 keV bursts may be compared with the values reported for 3.0 - 4.5 keV bursts and 7.7 - 12.5 keV bursts. A 10% to 90% rise time and 90% to 10% fall time were given for the typical 3.0 - 4.5 keV bursts by Culhane and Phillips [1969]. An e-folding rise and fall time for a typical 7.7 - 12.5 keV burst was given by Hudson, Peterson, and Schwartz [1969b]. The given rise and decay times were then used to compute temporal parameters

comparable to those obtained in this study. The comparison of typical parameters is presented in Table V. There is a progressive increase in energy of the bursts being sampled by the three groups, so the change of the parameters with increasing x-ray hardness will be seen. This is immediately evident in the rise time comparison. A decreasing rise time with increasing burst hardness is clearly seen. The trend of the decay time to decrease is clearly seen from the 1 - 6 keV bursts to harder bursts, although between the two harder bursts the decay time actually increases with increasing hardness. The total duration of the softer bursts is clearly seen, although the two harder bursts have the same duration. For the remaining ratio parameters the 1 - 6 keV values in all three cases lie nearly midway between the other two values. If the average were taken, the 1 - 6 keV values would be very nearly attained. The ratio values are strongly affected by any uncertainty in the rise or decay times so that less agreement would be expected among them.

G. Flux to Background Ratio at Burst Peak

Three parameters related to the intensity of the burst were examined: the ratio of the total flux to the background flux evaluated at the burst peak; the flux increase from background evaluated at the burst peak, called the "peak flux"; and the time integral of the flux increase from background during the event.

The distribution for ratio of total flux to background flux evaluated at burst maximum utilized no events for which the peak intensity occurred on the edge of a data gap (the maximum intensity was not definitely observed). Since the burst identification criterion was set for a ratio of at least 1.5, the observed number of events in the ratio interval 1.5 to 2.0 was doubled to yield the number in the ratio interval of 1.0 to 2.0. The resulting distribution is shown in Figure 35. The data can be well represented for four decades by the equation

$$N = 190 \left(\frac{F}{B}\right)_P^{-2.62 \pm 0.01} \qquad \text{(V-3)}$$

where

$$\left(\frac{F}{B}\right)_P = \left(\frac{\text{total observed flux}}{\text{background flux}}\right)_{\text{maximum burst intensity}}$$

and N is the percentage of events occurring in the interval $(F/B)_p \pm 0.5$. This distribution could be fit by an empirical relation better than any other studied.

It is interesting to note that only 16% of the events have a ratio, $(F/B)_p$, of 4.0 or more. Such a ratio value is adopted for the burst to be included in the solar x-ray flare listing published in the ESSA bulletin Solar-Geophysical Data [Van Allen,

1967b]. Thus, 84% of the events represented on Figure 35 were not included in the published flare listings.

H. Peak Flux

The peak flux, F_p, is defined as the flux increase above the background level, evaluated at the peak or maximum intensity of the burst or,

$$F_p = (F - B)_p \quad . \tag{V-4}$$

There is the additional constraint that

$$\left(\frac{F}{B}\right)_p \geq 1.5 \quad . \tag{V-5}$$

These two conditions combined restrict the peak flux values to

$$F_p \geq \left(\frac{B}{2}\right)_p \quad . \tag{V-6}$$

For example, a peak flux value less than 1.0 milli-erg $(cm^2\ sec)^{-1}$ can not be recorded if the background flux exceeds 2.0 milli-erg $(cm^2\ sec)^{-1}$. The data analysis method used thus discriminates against low intensity bursts on the basis of the background flux value.

An attempt was made to correct for this effect by preparing a frequency of occurrence histogram for the background flux. The factor was then determined by which to multiply the number of events in each flux interval to normalize this number to a 100% frequency of background flux occurrence. The greatest correction factor used was 1.7 for the 0.0 - 1.0 milli-erg $(cm^2\ sec)^{-1}$.

There is a tendency for the degree of solar burst activity and the background flux level to track one another. A greater percentage of the bursts tend to occur when the background flux level is higher. Since the number of events in the lower peak flux intervals were necessarily obtained during relatively quiet periods, it is probable that the correction applied does not provide enough of an increase for these events. It is believed that the correction applied does bring the data closer to the natural distribution, but that the number of events in the lower peak flux intervals may yet be too low.

The distribution obtained after correcting the data as described, again excluding any peak flux values observed on the edge of a data gap, is shown on Figure 36. There is an apparent peak in the distribution seen at a peak flux value of 1.0 - 2.0 milli-erg $(cm^2\ sec)^{-1}$. The reality of this peak is not claimed; it is most likely due to the background flux and the selection problem discussed previously.

The peak flux distribution can be approximated by a power law relation. Excluding the lowest peak flux interval, the most questionable one, the equation for $1.0 \leq F_p \leq 100.0$ milli-erg $(cm^2\ sec)^{-1}$ is

$$N = 59.9\ F_p^{-1.66} \pm 0.02 \qquad (V\text{-}7)$$

where N is the percentage of bursts with peak flux F_p in the interval $F_p \pm 0.5$. The distribution falls below this curve at the higher peak flux values. If the second most questionable interval is excluded, so that the peak flux range used is $2.0 \leq F_p \leq 100.0$ milli-erg $(cm^2\ sec)^{-1}$, the equation is

$$N = 82.5\ F_p^{-1.84} \pm 0.02 \qquad (V\text{-}8)$$

with the symbols retaining their previous definitions. These two equations represent 85% and 56% of the total number of events in Figure 36.

It is concluded that the distribution of bursts by peak flux can be represented by a power law relation with exponent -1.75 ± 0.1 over a range of two orders of magnitude in peak flux value. At higher flux values the distribution falls off more rapidly than the given power law relation. There were only 14 bursts with peak flux

greater than 100.0 milli-erg $(cm^2\ sec)^{-1}$ in the time interval under consideration.

I. Flux Time Integral

The flux time integral distribution was constructed using only events which had no data gaps during the event and for which the beginning and ending points were definitely known (these points were unflagged). The flux time integral was corrected for end contributions by the extrapolation method discussed in Section IV-A. In addition, the uncertainty discussed in the previous section concerning the number of events for the smaller peak flux values must also affect the number of events for the smaller flux time integral values. No simple correction can be attempted for the smaller flux time integral values as it was for the smaller peak flux values. No correction was applied to the data, except that the lowest interval, 0.0 - 1.0 erg cm^{-2} which should be most affected, was excluded from the distribution.

The distribution of flux time integral values is presented in Figure 37. The distribution can be represented by

$$N = 43.1 \left(\int F\ dt\right)^{-1.44 \pm 0.01} \qquad (V\text{-}9)$$

where N is the percentage of events occurring with a flux time integral value, $\int F\ dt$ in erg cm^{-2}, in the interval $\int F\ dt \pm 0.5$. The flux time integral values are in the range 1 - 100 erg cm^{-2}.

J. Discussion of Intensity Parameters

The examination of burst intensity parameters again indicates no need to consider more than one class of burst. There is a smooth variation seen in all three distributions such that a power law relation can represent the data.

The concept of a solar x-ray burst arising from this study is of one standard form of event with the individuality of events owing to the departure of one or more parameters from their typical or most common values. Nine parameters were examined in this study. A burst may appear to depart substantially from the standard if, for example, two parameters depart from their most common values. The most common values might be the result of approximately the same physical conditions existing for the production of the majority of burst x-rays while their departure from typical values might indicate the departure of one or more of the pertinent physical parameters in the emission region from its usual state. The true complexity of the flaring process is then manifested in the observed x-ray bursts.

VI. COMPARISON WITH Hα FLARES

The soft x-ray bursts were compared with Hα flares listed in Solar-Geophysical Data (1966-1969). An Hα flare and an x-ray burst were considered associated if either the start time of the two phenomena coincided within 5 minutes or if the peak flare and peak burst times coincided within 10 minutes. Both confirmed and small or unconfirmed Hα flares were included in the study, the confirmed data being examined first. The relative occurrence statistics were determined, the dependence of peak x-ray flux upon flare importance was examined, and the heliographic longitude distributions of both Hα flares and soft x-ray bursts were studied.

A. Relative Occurrence Statistics

Of the 4028 x-ray bursts listed, 176 had uncertain peak times or occurred during periods of no Hα flare patrol. Of the remaining 3852 events, 70% could be associated with Hα flares in the manner described. This agrees closely with the correlation of 69% between 7.7 - 12.5 keV bursts and Hα flares [Hudson, Peterson, and Schwartz, 1968; 1969a, b] but differs considerably from the correlation of 46% between 3.0 - 4.5 keV bursts with Hα

flares [Culhane and Phillips, 1969]. A correlation of 71 - 82% was found between 3 keV bursts and Hα flares by Harries [1968].

During the time period under consideration in this study, 16,468 Hα flares occurred. Hα flares occurring during periods of no x-ray data for several hours or more were excluded. Periods of no x-ray data of less than several hours occur more frequently and have no relationship to Hα flare occurrence. This will, however, affect the percentage of Hα flares associated with x-ray bursts. For instance, the correlation of Hα flares (16,468) with soft x-ray bursts (2698) is only 16%. This is very low compared to the values of 65% for Hα flares and 3.0 - 4.5 keV bursts [Culhane and Phillips, 1969] and 88% for Hα flares and 7.7 - 12.5 keV bursts [Hudson, Peterson, and Schwartz, 1968; 1969a, b].

However, the number of Hα flares accompanied by x-ray bursts depends strongly on the sensitivity of the x-ray detection method. The number of x-ray bursts increases strongly with decreasing peak x-ray flux. A factor of 3 or 4 increase in the number of x-ray bursts listed might be realized by decreasing the arbitrary burst identification criterion from 1.5 to 1.2 for the flux ratio to background at burst peak. Also small bursts occurring during the rise or decay of a larger burst may be obscured and not listed. To illustrate these points, the data for the month of March 1968 was examined in detail.

The results of this comparison are presented in Table VI. The comparison was broken down by flare importance. The four categories into which Hα flares were sorted are: an Hα flare accompanied by a listed x-ray burst; an Hα flare accompanied by an x-ray increase too small to be listed as a burst but still noticeable in visual examination of the data; an Hα flare during periods of no x-ray data coverage; and an Hα flare with no detectable x-ray burst. The dependence within each category on flare importance and the contrast between the total number of Hα flares accompanied by listed x-ray bursts and those accompanied by unlisted but noticeable x-ray bursts exemplify the strong dependence of the number of Hα flares accompanied by x-ray bursts on the x-ray burst sensitivity. Furthermore, of 98 Hα flares with no detectable x-ray bursts, only 3 flares are of importance greater than a subflare. Figure 27 is the x-ray data for the time during which one of the 1N Hα flares with no detectable x-ray bursts occurred. This confirmed flare started on 28 March 1968 at 0745, was at maximum phase as determined from area measurements at 0801, and ended at 0836. The heliographic coordinates were S23, W78 in McMath plage region 9282. No x-ray enhancement greater than the statistical fluctuations in the data is seen during the entire time of the Hα flare.

The total number of Hα flares given for the month of March 1968 is 528. The number which occurred during periods of x-ray

data coverage is 405. The percentage association of Hα flares and listed x-ray bursts is then 17% or 22%, depending on whether the total number of flares for the month or the number of flares during periods of x-ray coverage only are used. If the number of Hα flares accompanied by unlisted but noticeable x-ray bursts is included, the percentage association becomes 76%, using flare data only during periods of x-ray observations. The range of the percentage association is seen to be large and strongly dependent on the criteria used. This detailed comparison for March 1968 is thought to give typical, representative results. The mean value of the relative occurrence probability, shown on Figure 43, for the entire period July 1966 to September 1968 is 17%, the same as that for March 1968 when all Hα bursts were included.

The total number of x-ray bursts associated with each Hα importance classification as a function of the classification is shown on Figure 38. It is clear from this plot that the number of associated bursts increases strongly with decreasing flare importance, as Table VI also shows.

It has been asserted previously that all Hα flares produce x-ray bursts [Teske, 1969; Hudson, Peterson, and Schwartz, 1968; 1969a, b]. With the demonstrated dependence on sensitivity of the percentage association between Hα flares and x-ray bursts shown in this study, the assertion that all Hα events produce x-ray bursts is strongly supported.

B. Amplitude Relationship

Several additional studies were developed after associating the 2698 x-ray bursts with Hα flares. The dependence of the x-ray burst peak flux on Hα importance was examined. The x-ray data were broken into two groups for scaling purposes in plotting. Those having a peak burst flux less than 10.0 milli-erg $(cm^2\ sec)^{-1}$ comprised one group, while those with peak flux greater than 10.0 milli-erg $(cm^2\ sec)^{-1}$ comprised the second. The data for the first group is shown in Figure 39. The most significant features of this plot are the rapid increase in the number of x-ray bursts at smaller flare importances and that the number of x-ray bursts increases with decreasing peak flux value.

The plot of events with peak flux greater than 10.0 milli-erg $(cm^2\ sec)^{-1}$ is shown in Figure 40. In this plot, a loose dependence of peak flux on flare importance can be seen. The largest peak flux value within an importance classification increases from F to N to B in each case except for importance 3, in which the statistics are not significant. Also the largest peak flux in each classification increases in going from class to class at the same brightness level. The one exception to this trend is the high, circled point of 1N importance. This confirmed flare occurred on 6 July 1968 with maximum phase at 0956. This event was reported by ten stations. It was reported as -N by 3 stations, as 1N by 3, as 1B and 2F by one each, and as 2B by 2 stations. The maximum flare times reported

ranged from 0944 to 0957. On the basis of the wide variability in the optical reports of this flare, it is argued that the labeling of this flare as 1N is questionable and that this one flare which does not agree with the general trend of the data is of little significance. There does appear a general increase in a gross sense, then, of the x-ray flux both with increasing flare area and with increasing relative intensity evaluation of the brightness. However, on an individual basis, it is seen that at smaller flux values an x-ray burst could be produced by an Hα flare of any importance.

It was pointed out in the introduction that the x-ray flux is dependent on the volume of the activated region. The Hα flare importance is based on the area of the Hα flare region. Since the two phenomena are related temporally and since they do occur in the same general area on the sun [Vaiana et al., 1968], this provides some basis for expecting a dependence of x-ray flux on flare importance. A plot of the median x-ray burst flux against flare importance is shown in Figure 41. This plot again shows a dependence of x-ray flux both on flare area and brilliance. The median burst flux increases both within a classification but with increasing brightness and from class to class at the same brightness. Statistics were insufficient to include the importance 3 data.

The general trend of increasing x-ray flux both with flare area and with flare brightness are shown by the data presented

in this section. The increase in the number of x-ray bursts with decreasing flare importance, similar to the trend in Hα flare occurrences, is also evidenced by this data.

C. Heliographic Longitude Dependences

The position on the solar disk of the source of an x-ray burst is assumed to be the same as that of the associated Hα flare. The 2698 x-ray bursts which were associated with Hα flares were examined to determine if any directionality exists in the x radiation.

The east-west symmetry of the x-ray sources was examined first. It was found that 1366 bursts occurred at east longitudes and 1332 occurred at west longitudes. These numbers do not differ by a statistically significant factor. No east-west asymmetry is observed.

The heliographic longitude distribution of x-ray bursts was next examined. The longitude distribution of University of Iowa observed 1 - 6 keV bursts has been studied by Ohki [1969] and Pinter [1969]. On the basis of this and other x-ray data, they both conclude directivity of the emission is present and both attribute the directivity to non-thermal bremsstrahlung produced by anisotropic, energetic electron streams.

The conclusion reached by Ohki [1969] is based upon the nonuniform longitude distribution of 46 hard (> 10 keV) x-ray

bursts. The conclusion of Pinter [1969] is based on the apparent peak in the longitude distribution of three different energy range x-ray bursts (0.6 - 1.6 keV, 1 - 6 keV, 10 - 50 keV) moving from 0° to ~ 50° with increasing photon energy. Again the number of events used for the hard x-ray bursts was small (46). Considering statistical fluctuations, the trend in neither author's distributions seems significant. Also, Ohki [1969] finds the 1 - 6 keV burst occurrence uniform in longitude while Pinter [1969] claims a peak in their distribution at 30° - 40° heliographic longitude. The 1 - 6 keV longitude distribution is the statistically most significant distribution either author uses, but they disagree on its form.

In addition, neither author takes into account explicitly the longitude distribution of the Hα flares against which the x-ray bursts were compared. Ohki [1969] mentions that there is a 29% decrease in the number of Hα flares observed at 60° - 90° compared to those observed at 0° - 30° but assumes this effect small enough to be negligible.

The number of Hα flares per 10° of heliographic longitude for the period July 1966 to September 1968 is shown on Figure 42. The error bars are $\pm\sqrt{N}$ where N is the number of Hα flares in each 10° longitude interval. It is seen that there is a significant decrease in the number of events at higher longitude values. There is also a weak peak in the distribution at 30° - 40° longitude,

just as Pinter [1969] found for the 1 - 6 keV burst longitude distribution. These two distributions are very similar. It is clear that care must be taken to properly take into account the Hα flare longitude distribution.

This was done by using the relative occurrence probability of x-ray bursts compared to Hα flares per 10° longitude. That is, the number of x-ray bursts per 10° of longitude was divided by the number of Hα flares which occurred in that same 10° interval. This should remove any Hα longitude dependence irregularities and leave only the x-ray burst longitude dependence in evidence. The results so obtained are shown on Figure 43. The mean value of the relative occurrence probability, 0.17, indicates that about 6 times as many Hα flares occur as do x-ray bursts. This point was discussed in Section VI-A where it was shown that this ratio is a strong function of the criteria of the x-ray burst identification process. The error bars on Figure 43 were determined by the largest change possible in the ratio due to counting statistics. On this basis, some real variations do appear to occur at longitudes 70° - 90°. However, the variation in these two intervals is thought to be a result of the variation in the number of Hα flares observed at 70° - 90°, as seen on Figure 42. Too few Hα flares are seen from 70° - 80° and too many, relatively, from 80° - 90°. This may be the result of the difficulty of assigning a longitude value to a

flare at longitudes of 70° - 90°. Also, bursts occurring up to 10° beyond the limb may be visible, increasing the number observed from 80° - 90°, as seen on Figure 42. If in Figure 43 the 70° - 80° relative occurrence probability and the 80° - 90° value are averaged, the average of the other 7 intervals is closely approached. For these reasons the variation in the x-ray burst relative occurrence probability longitude distribution at 70° - 90° is thought not to reflect the x-ray longitude dependence and is therefore drawn as a heavy dashed line.

The central light dashed line is the mean value of the relative occurrence probability for the 9 intervals. The upper and lower dashed lines are one standard deviation from the mean value as determined from the interval values. All the relative occurrence probability values, except the 70° - 90° values, lie within one standard deviation of the mean. It has been pointed out that the average of the 70° - 90° values is very close to the mean value. There is a gradual rise to, and fall from, an apparent peak at 40° - 50° in the distribution. However, in view of the error bars shown and that all points, except 70° - 90°, lie within one standard deviation of the mean, this peak is not thought to be statistically significant. This figure is taken to show that there is no significant directivity to the 1 - 6 keV x radiation.

It would seem quite fortuitous, in view of the simplicity of the two models assumed and of the complexity of different individual

events, and their corresponding geometries, if directivity were actually discerned in a longitudinal burst occurrence distribution.

A lack of directivity in 3.0 - 4.5 keV bursts is also found by Culhane and Phillips [1969], supporting the results of the present study and additionally contradicting the results of Ohki [1969] and Pinter [1969].

VII. COMPARISON WITH HARD (> 6 keV) X-RAY BURSTS

The 1 - 6 keV burst x-ray flux recorded by Explorer 33 and Explorer 35 is insensitive to the spectral distribution of the x radiation and provides only the magnitude of the flux in this energy range. Both the magnitude and the spectral distribution must necessarily be known to examine quantitatively the observational data in terms of possible emission mechanisms. To this end a comparison of the 1 - 6 keV bursts was made with two different experimental observations of hard (photon energy > 6 keV) x-ray bursts.

A. Comparison with 10 - 50 keV Bursts

X-ray bursts in the energy range 10 - 50 keV were observed by the University of Minnesota Cosmic Ray Group with ionization chambers on the satellites OGO I and OGO III for the time interval 5 September 1964 to 31 December 1967. The cataloged form of these observations [Arnoldy, Kane, and Winckler, 1968; Kane and Winckler, 1969] was used in a comparison study with the 1 - 6 keV bursts. The increase in the ionization chamber rate and the time of the peak of the hard x-ray burst were taken from the plots given in

the hard x-ray atlas. The ionization chamber rate increases could be read with at most a ± 10 % possible uncertainty and the peak time could be read to ± 1 minute accuracy.

There were 134 hard x-ray bursts listed during times when University of Iowa equipment provided soft x-ray data. Of these 134 hard x-ray bursts, accompanying soft x-ray bursts as listed by the burst program could be found for 100 bursts. The criterion for association was that the peaks coincide within ± 10 minutes. The degree of association by this criterion is then 75%. Of the 34 hard x-ray bursts for which no associated soft x-ray bursts were found, 17 occurred with a time difference of ± 12 to ± 35 minutes between peaks and 7 occurred on 3 May 1967 when the soft x-ray flux was high.

Both the hard x-ray burst counting rate and the corresponding soft x-ray flux for two typical events are shown in Figures 44 and 45. The symbols shown correspond to the actual data points through which the smoothed curves were drawn to present a continuous impression of the event. The peak hard x-ray flux is seen to precede the peak soft x-ray flux, the soft x-ray event has a greater total duration than the hard x-ray event, and the soft x-ray flux appears to initially begin to increase before the hard x-ray rate increases.

The time difference between the peaks of the associated hard and soft x-ray bursts was examined. Soft x-ray bursts with an

uncertain peak time were excluded from this study, leaving 86 good quality associated events. The number of events as a function of Δt, the time of the soft x-ray burst peak minus the time of the hard x-ray burst peak, is shown on Figure 46. It is seen that in nearly all events the hard x-ray peak occurs before the soft x-ray peak ($\Delta t > 0$). On the average the hard x-ray peaks occurred 3 minutes before the soft x-ray peaks.

A delay in the time of maximum flux occurrence such that the peaks occur first with higher energy photons and then progressively for less energetic photons is in agreement with other observations. Culhane and Phillips [1969] find time differences of several minutes between 1 - 3 Å and 6 - 18 Å peaks. A delay of the order of 1 minute between 0 - 3 Å and 0 - 8 Å peaks can be seen in the data presented by Kreplin, Moser, and Castelli [1969]. In each case the hardest peak occurs first.

If the radiation were due to free-free emission from a region with a constant emission measure, the peak should occur simultaneously at all energies. Since this is not what is observed, by at least three independent observers free-free emission with a constant emission measure must not be the case. Either free-free emission is not the dominant emission mechanism or one or more of the assumptions of free-free emission from a region with constant emission measure must be incorrect.

Another test of the free-free emission with a constant emission measure proposal is to examine the relationship of the hard and soft x-ray peak fluxes. According to theory, there should be a unique correspondence between the two peak fluxes. The 1 - 6 keV peak flux was plotted against the 10 - 50 keV peak counting rate, as shown on Figure 47, to test this prediction. Again, only soft x-ray bursts with well-defined peak times were used. The straight line in Figure 47 was arbitrarily drawn to demonstrate that a power law relation could approximately fit the data. It is worth noting the wide range of values found in this data sample, nearly 3 orders of magnitude in the soft x-ray flux and nearly 5 orders of magnitude in the hard x-ray counting rate. Also, to be noted is that the departure of the individual data points from a straight line fit is independent of the size of the soft x-ray flux or of the hard x-ray counting rate; no systematic departures are seen.

To examine this peak flux relationship quantitatively, the free-free emission formula must be integrated with the appropriate detector response functions. To obtain the ionization chamber counting rate due to free-free emission, the response curve given by Kane [1967] was integrated together with Equations (I-8) and (I-9). The ratio of the ionization chamber counting rate to the emission measure (I/S) as a function of temperature is shown on Figure 48.

For the Explorer detector the response is effectively constant throughout the bandwidth, as pointed out previously. Since the observed quantity as used in this study is the flux in the 2 - 12 Å range, this quantity must be theoretically calculated; this is given by Equation (I-10). A plot of the ratio of the flux to the emission measure (F/S) as a function of temperature is shown on Figure 49.

The ratio of the hard x-ray counting rate to the soft x-ray flux is a function of the temperature only, assuming free-free emission from an isothermal volume, so that the temperature and emission measure in the two ranges are identical. The theoretically calculated ratio as a function of temperature can be obtained from Figures 48 and 49. The observed ratios can then be interpreted in terms of temperatures. Once the temperature is determined in this manner, the emission measure can be calculated from the observed flux or counting rate, or curves of given constant emission measure can be superimposed on the data plot.

The experimentally determined ratio of 10 - 50 keV peak x-ray counting rate to 1 - 6 keV peak x-ray flux plotted against the 1 - 6 keV peak flux is shown on Figure 50. The data points represented by triangles had a peak separation of ± 2 minutes or less; the points had a difference of more than ± 2 minutes. There is no separation of the data on this parameter.

The temperatures obtained by this procedure vary from $14 - 39 \times 10^6$ °K. To account for all the data, the emission measure must vary from 3.6×10^{47} cm^{-3} - 2.1×10^{50} cm^{-3}. It is seen on Figure 50 that at a constant temperature the emission measure has a range of 10 - 100 and so is not constant from event to event in this data. The data is not ordered on this type figure, indicating agreement with no simple emission mechanism, particularly free-free emission from a constant emission measure region. Since the variability from event to event is so large, it is clear that ascribing the emission to a different mechanism will not improve the situation as the basic experimental ratios remain the same.

If the ratio is plotted against the 10 - 50 keV counting rate, the agreement with a constant emission measure free-free emission process appears to be better (Figure 51). However, the apparent better agreement is thought due to the greater range of the 10 - 50 keV counting rate compared to the range of the 1 - 6 keV flux.

The results of this study are that the emission measure is not constant within an event (temporal study) or from event to event (amplitude study) and that the temperature is in the range $14 - 39 \times 10^6$ °K if the theory of free-free emission from a constant emission measure region is assumed.

B. Comparison with 7.7 - 12.5 keV Bursts

X-ray bursts in the energy ranges 7.7 - 12.5 keV and 12.5 - 22.0 keV were observed by use of a collimated scintillation counter

with spectrum analysis on the OSO-III satellite by the University of California, San Diego [Hudson, Peterson, and Schwartz, 1968; 1969a, b]. These data were used to show that x-ray bursts in this energy range could be explained as due to free-free emission from a constant emission measure region. The soft (1 - 6 keV) x-ray bursts were also compared to the 7.7 - 12.5 keV bursts (courtesy of Hudson, Peterson, and Schwartz [1969]) to determine the form of the relationship in these energy ranges.

From a list of 37 events in the 7.7 - 12.5 keV range during periods when soft x-ray data coverage existed, 18 corresponding soft x-ray bursts were found in the computer listing of soft x-ray bursts. The largest soft x-ray peak flux was ~ 6 milli-erg $(cm^2\ sec)^{-1}$, quite small compared to the fluxes used in the previous study. The 19 unassociated hard x-ray bursts were for the most part accompanied by soft x-ray events too small to classify as a burst by the criterion used. Thus, this sample is composed entirely of small events.

The ratio of the peak 7.7 - 12.5 keV flux to the peak 1 - 6 keV flux as a function of the 1 - 6 keV flux for each of the 18 events is shown on Figure 52. The ratio of these fluxes has been calculated assuming free-free emission from an isothermal volume so that each ratio corresponds to a temperature. The range of temperatures indicated by this data are 12 - 18 x 10^6 °K. The range of soft x-ray fluxes is so small that a constant emission measure might be said to fit the data to within a factor of 3. However, the fit is not

good to a factor of 2 and the possibly constant (within a factor of 3) emission measure might be the result of using too limited a range of flux values. The conclusion which will be drawn from Figure 52 is that the emission measure is not constant to within a factor of 2 from event to event.

It is encouraging to note that the temperatures and corresponding soft x-ray fluxes given in Figure 52 and derived from 7.7 - 12.5 keV/1 - 6 keV burst fluxes are consistent with those given in Figure 50 and derived from the 10 - 50 keV counting rate/1 - 6 keV flux. The data obtained by three different observational techniques and groups yield consistent results when analyzed by similar methods.

The ratio of 7.7 - 12.5 keV flux to 1 - 6 keV flux plotted against the 1 - 6 keV flux during three arbitrarily chosen events is shown on Figure 53. The three different events are denoted by different symbols. The circles around particular symbols indicate points occurring before the peak of the soft x-ray event. In general, points move toward higher temperatures during the rise of the event and toward smaller temperatures during the decay phase. Two curves corresponding to given constant emission measures and the indicated temperatures have been drawn through the data to facilitate comparison of the experimental data with theory. It is seen that the emission measure describing the two bursts is less than one-half the emission measure describing the third burst. Again, the emission measure is seen to be not constant to within a factor of 2.

Within the event individual data points depart from the theoretical curve by more than the experimental uncertainty in the data. The data point departing furthest from the experimental curve is different by 60%. The experimental uncertainty associated with this point is 7%, leaving at least 53% variation between theory and experiment. Within an event then the emission measure varies by at least 50%. The variation of the emission measure within the event is also supported by the fact that for the 18 events shown on Figure 52, the 7.7 - 12.5 keV peak flux occurred an average of 3 minutes before the 1 - 6 keV peak flux.

The comparison with 7.7 - 12.5 keV bursts reveals that the emission measure is not constant (within a factor of 2) within an event or from event to event and that temperatures of 12 - 18 x 10^6 °K for free-free emission account for the data.

C. Discussion of Comparison Results

The results of the comparison of the soft x-ray bursts with both the 10 - 50 keV bursts and the 7.7 - 12.5 keV bursts consistently indicate that the emission measure in a free-free emission mechanism explanation of the radiation is constant neither within an event nor from event to event. This disagrees with the results of Hudson, Peterson, and Schwartz [1968, 1969a, b] who claim that the emission measure is constant both within an event and from event to event.

Possible arguments both for and against the results obtained in this study will be considered. These results would be invalidated

if the emission mechanism for x-ray bursts in one of the energy ranges used were not free-free emission. Either the hard x-ray bursts might be attributed to non-thermal bremsstrahlung or the soft x-ray bursts to predominantly a line emission process. Kane [1969] has shown that hard x-ray bursts are composed of 2 components. One component is impulsive in nature, has a very short total duration (~ 30 seconds), and is attributed to non-thermal bremsstrahlung. The other component reaches maximum later in the event, has a greater duration (5 - 10 minutes), and has a steeper photon energy spectrum. This component has many properties marking it as thermal in origin, which it is assumed to be. The hard x-ray bursts used in this study were then most likely composed of this thermal component as the predominant component due to the short duration of the non-thermal component and to the longer duration (~ 5 - 10 minutes) of the 10 - 50 keV bursts. On this experimental basis, the hard x-ray bursts used in this study are thought to be of thermal origin.

Line emission is not thought to contribute substantially to the 1 - 6 keV burst flux for the following reasons. Meekins, Kreplin, Chubb, and Friedman [1968] from crystal spectrometer data found that the continuum from 1 - 10 Å during solar flares always dominated the line emission by more than an order of magnitude. Data presented by Rugge and Walker [1968] show that shortly after two class 1 flares

the continuum dominated the lines in the wavelength range 7 - 12 Å. Spectra presented by Neupert, Gates, Swartz, and Young [1967] also show that in the wavelength range 2 - 12 Å during flares the continuum emission dominated the line emission.

On theoretical grounds, calculations performed by Gibson [1969] show that for temperatures greater than ~ 6×10^6 °K free-free emission exceeds both free-bound and bound-bound emission, including the effects of dielectronic recombination. In addition, the free-bound emission is always greater than the bound-bound contribution. The calculations of Culhane [1969] for free-free and free-bound thermal continuum radiation show that in the wavelength interval 2 - 12 Å free-free dominates free-bound emission for temperatures greater than ~ 8×10^6 °K. Since the free-bound exceeds the bound-bound emission, the free-free emission then dominates at temperatures greater than ~ 8×10^6 °K. Thus, both on experimental and theoretical grounds, line emission is not thought to contribute significantly to the 1 - 6 keV burst flux and free-free emission appears to be the correct mechanism.

The temperatures and emission measures obtained by attributing x-ray bursts in the 1 - 50 keV range to free-free emission are in the range of values for these parameters being obtained by a number of workers. Chubb, Friedman, and Kreplin [1964] found a temperature of about 10^7 °K from the slope of the photon spectrum for energies from 2 - 4 keV during times of subflare activity

Meekins, Kreplin, Chubb, and Friedman [1968] derived temperatures of 15 - 20 x 10^6 °K from the slope of the photon spectrum from 3.3 - 8.5 Å during solar flares ranging from class 1 to class 3. Hudson, Peterson, and Schwartz [1968, 1969a, b], as mentioned previously, found temperatures in the range 10 - 50 x 10^6 °K for solar x-ray bursts in the energy range 7.7 - 22.0 keV. Neupert [1968] finds consistency between the 1.87 Å line emission and a model in which the temperature is in the range 20 - 40 x 10^6 °K. Culhane and Phillips [1969] determined temperatures of 10 - 30 x 10^6 °K for impulsive x-ray bursts at energies less than 10 keV observed with instruments on OSO-4.

Thus, agreement is emerging on temperatures of 10 - 40 x 10^6 °K as the range during solar flares, in agreement with the present work, with free-free emission being the dominant process. The non-constancy of the emission measure during an event is necessary to account for the more energetic photon peak fluxes occurring before the less energetic photon peak fluxes. From event to event, the emission measure also changes as evidenced by the analysis presented here.

The flare concept emerging from this study is that a small region is first quickly heated and then loses energy to surrounding regions such that the temperature attained in the larger region is 10 - 40 x 10^6 °K . The same process occurs for all flares but the exact conditions differ from event to event to cause the apparent

individuality of bursts. As energy is lost from the hot core, the effective emission measure changes. The flare model of Carlquist [1968] does provide a sufficiently rapid acceleration in a sufficiently small volume and with a large enough energy release to account for the production of the hot core. This hot core would be the source of non-thermal electrons needed to cause rapid excitation of energetic iron lines observed to occur first in an event and to then be followed by the occurrence of less energetic lines. Some of the non-thermal electrons would emit the microwave impulsive burst, depending on their position in the magnetic field, etc. Others would thermalize, producing the heating needed to create the observed x-ray emission. Such a flare model is consistent with the observational facts and is in agreement with the models suggested by Meekins, Kreplin, Chubb, and Friedman [1968] and by Neupert (1968].

VIII. CONCLUSIONS

The conclusions of this thesis are:

1. The most frequently occurring rise time (20% to peak burst intensity) for 2 - 12 Å solar x-ray bursts is 4 minutes. The most common decay time is 12 minutes and the most common total duration is 16 minutes. The differential rise time distribution can be represented by an exponential with exponent -0.1004 for rise times greater than 4 minutes.

2. The differential distribution of the ratio of rise time to decay time has a maximum at 0.3. From a ratio of 0.3 to 2.7 the distribution can be represented by an exponential with exponent -2.31 ± 0.02.

3. The differential distribution of the ratio of rise time to total burst duration has a maximum at 0.25.

4. The differential distribution of the ratio of the total observed flux to the background flux at the burst peak can be represented by a power law with exponent -2.62 ± 0.01 for $1.5 < (F/B)_p < 32$.

5. The differential distribution of the peak burst fluxes can be represented by a power law with exponent -1.75 ± 0.01 over the range 1 - 100 milli-erg $(cm^2\ sec)^{-1}$.

6. The differential distribution of the flux time integral values can be represented by a power law with exponent -1.44 ± 0.01 over the range 1 - 50 erg cm^{-2} .

7. The number of Hα flares which can be correlated with x-ray bursts is demonstrated to be strongly dependent on the criteria of the x-ray identification scheme. This strongly supports the assertion that all Hα events produce x-ray bursts. The correlation of x-ray bursts with Hα flares is ~ 70%.

8. A general trend for larger peak x-ray fluxes to occur with both larger flare areas and with brighter events is definitely seen.

9. The heliographic longitude dependence of Hα flares from July 1966 to September 1968 is found to be non-uniform. The relative occurrence probability of 2 - 12 Å x-ray bursts (properly taking into account the non-uniformity of the Hα flare distribution) as a function of heliographic longitude is found to be uniform. This result detracts from the proposal that a significant portion of the x radiation is due to non-thermal bremsstrahlung from energetic electrons moving in preferred geometries.

10. The relationship of 1 - 6 keV bursts to 10 - 50 keV bursts, assuming free-free emission for the x-ray burst production, was examined. Temperatures of $14 - 39 \times 10^6$ °K and emission measures of 3.6×10^{47} cm^{-3} - 2.1×10^{50} cm^{-3} were obtained. The

emission measure was found to vary both within the individual event and from event to event.

11. In a similar manner, 7.7 - 12.5 keV bursts were compared with 1 - 6 keV bursts. Temperatures obtained were 12 - 18 x 10^6 °K and emission measures varied from 5.1 x 10^{47} - 3.8 x 10^{48} cm^{-3}. The emission measure was again found to vary, both from event to event and within the event, by more than a factor of 2.

12. The burst data studied in the range 1 - 50 keV are consistent with a free-free emission mechanism with temperatures of 12 - 39 x 10^6 °K and an emission measure which varies both within the event and from event to event from 3.6 x 10^{47} cm^{-3} - 2.1 x 10^{50} cm^{-3}.

TABLE I

Hα FLARE IMPORTANCE DEFINITIONS

Importance	Heliographic square degrees	Area (cm^2) x 10^{-18}
S(-)	≤ 2.0	≤ 2.96
1	2.1 - 5.1	3.11 - 7.55
2	5.2 - 12.4	7.70 - 18.4
3	12.5 - 24.7	18.5 - 36.6
4	> 24.7	> 36.6

TABLE II

EXPLORER 33 BURST CORRECTIONS
(2 JULY 1966 TO 26 JULY 1967)

Year	Decimal Day	Month	Day	Peak Time (UT)	r_{III}(c/sec)	R_{III}(c/sec)	Bk.(c/sec)
1967	31	February	1	1252	1755	1920	39
1967	33	February	3	0317	1244	1350	94
1967	34	February	4	1701	1441	1640	62
1967	37	February	7	0137	1374	1540	39
				1038	2255	2810	47
1967	43	February	13	1825	1351	1505	125
1967	48	February	18	1043	1290	1410	2
1967	52	February	22	0513	1246	1368	1
				1850	2082	2530	1
1967	57	February	27	1700	1410	1595	1

TABLE III

MONTHLY TOTAL OF X-RAY BURSTS OBSERVED FROM JULY 1966 TO SEPTEMBER 1968

Year	Month	Total number of peaks	Number of Individual Bursts
1966	July (beginning on the 3rd)	102	93
1966	August	123	109
1966	September (ending on the 21st)	33	26
1966	October (beginning on the 9th)	137	106
1966	November	122	105
1966	December (beginning on the 29th)	9	8
1967	January	166	146
1967	February	199	171
1967	March (ending on the 27th)	120	100
1967	April (beginning on the 20th)	52	46
1967	May	175	153

TABLE III (CONT.)

Year	Month	Total number of peaks	Number of Individual Bursts
1967	June (ending on the 14th)	55	44
1967	July (beginning on the 4th)	178	145
1967	August	180	166
1967	September	142	132
1967	October	212	184
1967	November	190	165
1967	December	247	212
1968	January	235	208
1968	February	180	159
1968	March	135	121
1968	April	162	143
1968	May	187	167
1968	June	179	158
1968	July	198	171
1968	August	215	189
1968	September (ending on the 18th)	95	88
TOTAL		4028	3515

TABLE IV

PARAMETER DISTRIBUTION STATISTICS

Parameter	Total number of events in distribution	Number of events in plot	Percentage of events in plot
Rise time	2206	2070	94
Decay time	2227	2059	93
Total time	1586	1426	90
Rise time/Total time	1586	1586	100
Decay time/Total time	1586	1586	100
Rise time/Total time	1626	1598	98
Peak flux/Background	3154	3139	99
Peak flux	3154	3140	99
Flux time integral	1586	1185	75

TABLE V

COMPARISON OF DERIVED BURST TEMPORAL PARAMETERS
WITH PREVIOUSLY REPORTED VALUES

	Rise Time (min)	Decay Time (min)	Total Duration (min)	Rise Time / Decay Time	Rise Time / Total Time	Decay Time / Total Time
This Study (1-6 keV)	4.0	12.0	16.0	0.30	0.25	0.75
Culhane and Phillips (1969) (3.0 - 4.5 keV)	2.8	6.3	9.1	0.44	0.31	0.69
Hudson, Peterson, and Schwartz (1969b) (7.7 - 12.5 keV)	1.4	7.6	9.1	0.19	0.16	0.84

TABLE VI

RESULTS OF DETAILED STUDY OF Hα FLARE AND X-RAY BURST OCCURRENCES FOR MARCH 1968

Hα importance	-F	-N	-B	1F	1N	1B	2F	2N	2B	Total
Hα flare with x-ray burst	16	45	10	4	8	6			1	90
Hα flare with unlisted but noticeable x-ray burst	103	93	14	2	1	3		1		217
Hα flare but no x-ray data	58	50	5	3	2	1				119
Hα flare with no detectable x-ray burst	55	38	2	1	2					98

REFERENCES

Acton, L. W., X-Radiation of the Sun, Ph. D. Thesis, University of Colorado, Boulder, 1964.

Acton, L. W., X-Ray and Microwave Emission of the Sun with Special Reference to the Events of July, 1961, Ap. J., 152, 305, 1968.

Alfven, H. and P. Carlquist, Currents in the Solar Atmosphere and a Theory of Solar Flares, Solar Physics, 1, 220, 1967.

Allen, C. W., Astrophysical Quantities, 291 ff., 2nd edition, The Athlone Press, London, 1963.

Arnoldy, R. L., S. R. Kane, and J. R Winckler, An Atlas of 10 - 50 keV Solar Flare X-Rays Observed by the OGO Satellites 5 September 1964 to 31 December 1966, University of Minnesota Cosmic Ray Technical Report CN-108, January, 1968.

Boldt, E. and P. Serlemitsos, Cosmic X-Ray Bremsstrahlung Associated with Suprathermal Protons, Ap. J., 157, 557, 1969.

Bowen, P. J., K. Norman, K. A. Pounds, P. W. Sanford and A. P. Willmore, Measurements of the Solar Spectrum in the Wavelength Band 4 to 14 Å, Proc. Roy. Soc. London, A, 281, 538, 1964.

Carlquist, P., Solar Flares Caused by High Impedance Regions in Current Filaments, Division of Plasma Physics, Royal Institute of Technology, Research Report No. 68-11, Stockholm, May, 1968.

Chubb, T. A., H. Friedman, and R. W. Kreplin, Spectrum of Solar X-Ray Emission from 2 - 20 keV During Subflare Activity, Space Research IV, Edited by P. Muller, 759, John Wiley and Sons, Inc., New York, 1964.

Chubb, T. A., R. W. Kreplin, and H. Friedman, Observations of Hard X-Ray Emission from Solar Flares, J. Geophys. Res., 71, 3611, 1966.

Culhane, J. L., Thermal Continuum Radiation from Coronal Plasmas at Soft X-Ray Wavelengths, Mon. Not. Roy. Astron. Soc., 144, 375, 1969.

Culhane, J. L. and K. J. H. Phillips, Solar X-Ray Bursts at Energies Less Than 10 keV Observed with OSO 4, Mullard Space Science Laboratory Research Report, University College London, 1969.

De Jager, C. and M. R. Kundu, A Note on Bursts of Radio Emission and High Energy (> 20 keV) X-Rays from Solar Flares, Space Research III, 836, 1963.

Drake, J. F., Sr. J. Gibson, O. S. B., and J. A. Van Allen, Iowa Catalog of Solar X-Ray Flux (2 - 12 Å), Solar Physics, 11, 1969.

Elwert, G., Theory of X-Ray Emission of the Sun, J. Geophys. Res., 66, 391, 1961.

Elwert, G., The Significance of the Polarization of Solar Short-Wavenlength X-Rays, Structure and Development of Solar Active Regions, edited by K. O. Kiepenheuer, D. Reidel Publishing Company, Dordrecht, Holland, 444, 1968.

Gibson, Sr. J., O. S. B., The Correlation of X-Ray Radiation (2 - 12 Å) with Microwave Radiation (10.7 cm) from the Non-Flaring Sun, Ph. D. Thesis, University of Iowa, Iowa City, 1969.

Goldberg, L., Ultraviolet and X-Rays from the Sun, Ann. Rev. Astronomy and Astrophysics, 5, 279, 1967.

Harries, J. R., Variable X-Ray Fluxes from Celestial Objects, Ph. D. Thesis, The University of Adelaide, South Australia, 1968.

Hudson, H. S., L. E. Peterson, and D. A. Schwartz, The Hard Solar X-Ray Spectrum Observed from the Third Orbiting Solar Observatory, University of California Report (UCSD-SP-68-6), December 1968 (submitted to Ap. J.).

Hudson, H. S., L. E. Peterson, and D. A. Schwartz, Solar and Cosmic X-Rays above 7.7 keV, Solar Physics, 6, 205, 1969a.

Hudson, H. S., L. E. Peterson, and D. A. Schwartz, The Hard Solar X-Ray Spectrum Observed from the Third Orbiting Solar Observatory, Ap. J., 157, 389, 1969b.

Jacobsen, C. and P. Carlquist, Solar Flares Caused by Circuit Interruptions, Icarus, 3, 270, 1964.

Kane, S. R., Observations of Two Components in Energetic Solar X-Ray Bursts, Ap. J., 157, L139, 1969.

Kane, S. R. and J. R. Winckler, An Atlas of 10 - 50 keV Solar Flare X-Rays Observed by the OGO Satellites 1 January to 31 December 1967, University of Minnesota Cosmic Ray Technical Report CR-134, April, 1969.

Karzas, W. J. and R. Latter, Electron Radiative Transitions in a Coulomb Field, Ap. J. Suppl., 6, No. 55, 1961.

Kreplin, R. W., P. J. Moser, and J. P. Castelli, Flare X-Ray and Radio Wave Emission, Paper presented at the XII Plenary Meeting of COSPAR May 21, 1969, Prague, Czechoslovakia, June, 1969.

Kundu, M. R., Solar Radio Astronomy, 10 ff., John Wiley and Sons, Inc., New York, 1965.

Mandel'shtam, S. L., X-Ray Emission of the Sun, Space Science Reviews, 4, 587, 1965.

Meekins, J. F., R. W. Kreplin, T. A. Chubb, and H. Friedman, X-Ray Line and Continuum Spectra of Solar Flares from 0.5 to 8.5 Angstroms, Science, 162, 891, 1968.

Neupert, W. M., Comparison of Solar X-Ray Line Emission with Microwave Emission During Flares, Ap. J., 153, L59, 1968.

Neupert, W. M., W. Gates, M. Swartz, and R. Young, Observation of the Solar Flare X-Ray Emission Line Spectrum of Iron from 1.3 to 20 Å, Ap. J., 149, L79, 1967.

Ohki, K.-I., Directivity of Solar Hard X-Ray Bursts, Solar Physics, 7, 260, 1969.

Peterson, L. E. and J. R. Winckler, Gamma-Ray Burst from a Solar Flare, J. Geophys. Res., 64, 697, 1959.

Pinter, S., Longitudinal Distribution of X-Bremsstrahlung on the Solar Disk, Solar Physics, 8, 142, 1969.

Pounds, K. A., Recent Solar X-Ray Studies in the United Kingdom, Annales D'Astrophysique, 28, 132, 1965.

Rugge, H. R. and A. B. C. Walker, Jr., Solar X-Ray Spectrum Below 25 Å, Space Research VIII, edited by A. P. Mitra, L. G. Jacchia, and W. S. Newman, 439, North-Holland Publishing Co., Amsterdam, 1968.

Solar-Geophysical Data, issued by the Institutes for Environmental Research, U. S. Department of Commerce, Nos. 264-295, August 1966-March 1969.

Takakura, T. and K. Kai, Energy Distribution of Electrons Producing Microwave Impulsive Bursts and X-Ray Bursts from the Sun, Publications of the Astronomical Society of Japan, 18, 57, 1966.

Teske, R. G., Observation of the Solar Soft X-Ray Component; Study of its Relation to Transient and Slowly-Varying Phenomena Observed at Other Wavelengths, Solar Physics, 6, 193, 1969.

Teske, R. G. and R. J. Thomas, Solar Soft X-Rays and Solar Activity I. Relationships Between Reported Flares and Radio Bursts, and X-Ray Bursts, University of Michigan Report, 1968.

Vaiana, G. S., W. P. Reidy, T. Zehnpfennig, L. Van Speybroeck, and R. Giacconi, X-Ray Structure of the Sun During the Importance 1N Flare of 8 June 1968, Science, 161, 564, 1968.

Van Allen, J. A., The Solar X-Ray Flare of July 7, 1966, J. Geophys. Res., 72, 5903, 1967a.

Van Allen, J. A., Catalog of Solar X-Rays, Solar-Geophysical Data, issued by the Institutes for Environmental Research, U. S. Department of Commerce, July 1967-August 1969, 1967b.

Van Allen, J. A., H. W. Dodson, and E. R. Hedeman, Comparison of Hα and Solar X-Ray Emission ($2 < \lambda < 12$ Å) for the Major Flare on 1966 August 28, (to be submitted to Ap. J.), 1969.

Wende, C. D., The Correlation of Solar Microwave and Soft X-Ray Radiation, Ph.D. Thesis, University of Iowa, Iowa City, 1968.

Wende, C. D., Correlation of Solar Microwave and Soft X-Ray Radiation 1. The Solar Cycle and Slowly Varying Components, J. Geophys. Res., 74, 4649, 1969.

Zirin, H., The Solar Atmosphere, 1 ff., Ginn and Company, Waltham, Mass., 1966.

FIGURE CAPTIONS

Figure 1. Physical arrangement of the three thin-windowed GM tubes on Explorer 33 and Explorer 35.

Figure 2. Absolute photon efficiency of "standard" EON type 6213 GM tube, $(GM2)_{33}$, for a soft x-ray beam parallel to the axis of the end-window tube. $\epsilon(\lambda)$ is the number of counts per photon of wavelength λ incident within the effective diameter of the tube (0.24 cm). The labeled absorption edges are ones for components of the mica window and the fill gas [Van Allen, 1967a].

Figure 3. Sectoring scheme for assigning output pulses from the GM1 detector to four successive quadrants. β is the angle of rotation of the spacecraft, referenced to the meridian plane of the spacecraft through the see-sun sensor located at $\beta = 230°$. Pulses are assigned to Sector I from the moment at which the axis of the detector passes $\beta = 0°$ to the moment at which it passes $\beta = 90°$.

Figure 4. Sample diagram of observational coverage of solar x rays during October 1966 by Explorer 33. The darkened areas represent data gaps. During the early part of the month no detectors were viewing the sun. During the remainder of the month $(GM2)_{33}$ viewed the sun continuously.

Figure 5. Sample diagram of observational coverage of solar x rays during June 1968 by Explorer 35. The darkened areas represent data gaps. Note the systematic diagonal movement of lunar eclipse and occultation periods across the diagram.

Figure 6. Experimental relationship of apparent counting rate r to true counting rate R for $(GM2)_{33}$.

Figure 7. Experimental relationship of apparent counting rate r to true counting rate R for $(GM3)_{33}$.

Figure 8. Solid curve is experimental relationship of apparent counting rate r to true counting rate R for $(GM1)_{33}$ if detector is not rotating with respect to the beam. Dashed curve is calculated r-R relationship for rotating case. The effective dead time is larger in the second case (cf. Figure 10).

Figure 9. Solid curve is experimental relationship of apparent counting rate r to true counting rate R for $(GM1)_{35}$ if detector is not rotating with respect to the beam. Dashed curve is calculated r-R relationship for rotating case. The effective dead time is larger in the second case (cf. Figure 10).

Figure 10. Explanatory diagram to show the manner in which spacecraft rotation causes the difference between the solid and dashed r-R curves in Figures 8 and 9. The curve labeled R shows the true counting rate as a function of the rotation angle β, with a maximum of 10,000 count sec^{-1} at $\beta = 230°$. The curve labeled r is derived from it by using the solid curve in Figure 9. Neither of

these curves is observable in flight. The observed quantity is the Sector III averaged, apparent rate $\langle r \rangle$ (= 1656 count sec^{-1} in this example). The rate that would be observed by a zero deadtime detector is $\langle R \rangle$ (= 2107 count sec^{-1}). If the solid curve of Figure 9 had been used a true rate $\langle R \rangle$ = 1670 count sec^{-1} would have been inferred. The effect is greater at greater values of R.

Figure 11. Daily averages of observed values of the ratio $(GM1)_{35}/(GM2 - GM3)_{33}$ for simultaneous flight data 16 October to 9 December 1967.

Figure 12. Adopted geometric obliquity factor $f(\alpha)$ for $(GM2 - GM3)_{33}$.

Figure 13. Daily averages of observed values of the ratio $(GM1)_{35}/(GM1)_{33}$ for simultaneous flight data 27 July to 26 September 1967 (α decreasing) and 24 December 1967 to 31 March 1968 (α increasing). Solid circles are from quiet sun background, the X's from bursts.

Figure 14. Adopted geometric obliquity factor $f(\Delta t)$ for $(GM1)_{33}$ [= $(G1X)_{33}$] as a function of the time Δt in days from the moment at which the observed ratio $(GM1)_{35}/(GM1)_{33}$ has a minimum value (derived from Figure 13 as described in text).

Figure 15. Adopted geometric obliquity factor f(t) for the three Explorer 33 detectors as a function of time for 1 July 1966 to 27 July 1967.

Figure 31. Differential distribution of 2 - 12 Å x-ray bursts with respect to the total burst duration; the number of events per 2-minute interval is shown.

Figure 32. Differential distribution of 2 - 12 Å x-ray bursts with respect to the ratio of the rise time to the total burst duration.

Figure 33. Differential distribution of 2 - 12 Å x-ray bursts with respect to the ratio of the decay time to the total burst duration.

Figure 34. Differential distribution of 2 - 12 Å x-ray bursts with respect to the ratio of the rise time to the decay time. The straight line is least-squares fit over the region indicated.

Figure 35. Differential distribution of 2 - 12 Å x-ray bursts with respect to the ratio of the total observed flux to the background flux, evaluated at the time of peak burst intensity. The straight line is least-squares fit over the region indicated.

Figure 36. Differential distribution of 2 - 12 Å x-ray bursts with respect to the peak burst flux. The straight lines are least-squares fit over the regions indicated.

Figure 37. Differential distribution of 2 - 12 Å x-ray bursts with respect to the value of the integral of the burst flux with respect to time for the duration of the burst and with end corrections added as described in the text (Section IV-A). The straight line was least-squares fit over the region indicated.

Figure 38. Distribution of x-ray bursts which could be associated with Hα flares as a function of Hα flare importance.

Figure 39. Distribution of x-ray bursts which could be associated with Hα flares as functions of both the Hα flare importance and the peak burst flux, for peak burst fluxes less than 10.0 milli-erg $(cm^2\ sec)^{-1}$. The Hα flare importance by area is given at the top of each of the four plots while the relative intensity evaluations are indicated by different symbols and lines, as given on the fourth plot.

Figure 40. Distribution of x-ray bursts which could be associated with Hα flares as functions of both the Hα flare importance and the peak burst flux, for peak burst fluxes greater than 10.0 milli-erg $(cm^2\ sec)^{-1}$.

Figure 41. Median burst flux 2 - 12 Å as a function of Hα flare importance.

Figure 42. Heliographic longitude distribution of Hα flares during the period July 1966 to September 1968 when x-ray data coverage was possible.

Figure 43. Relative occurrence probability of 2 - 12 Å solar x-ray bursts with respect to Hα flares as a function of heliographic longitude for x-ray bursts observed from July 1966 to September 1968.

Figure 44. Comparison plot between the soft (1 - 6 keV) x-ray flux (F) and the hard (10 - 50 keV) x-ray counting rate (I) as functions of time. Hard x-ray rate from Arnoldy, Kane, and Winckler [1968].

Figure 45. Comparison plot between the soft (1 - 6 keV) x-ray flux (F) and the hard (10 - 50 keV) x-ray counting rate (I) as functions of time. Hard x-ray rate from Kane and Winckler [1969].

Figure 46. Distribution of the associated 1 - 6 keV and 10 - 50 keV x-ray bursts according to the time difference, Δt, between the burst peaks. Δt is the time of the 1 - 6 keV peak minus the time of the 10 - 50 keV peak. Positive Δt results from the 10 - 50 keV peak occurring earlier than the 1 - 6 keV peak.

Figure 47. Peak flux of the 2 - 12 Å bursts as a function of the peak excess ion chamber rate due to corresponding 10 - 50 keV x-ray bursts. The latter rates were taken from Arnoldy, Kane, and Winckler [1968] and Kane and Winckler [1969].

Figure 48. The ratio of the ion chamber rate observed at the orbit of the earth due to a free-free emission mechanism in the 10 - 50 keV range and ion chamber characteristics as given by Kane [1967] to the emission measure as a function of temperature.

Figure 49. The ratio of 2 - 12 Å flux observed at the orbit of the earth to the emission measure as a function of temperature, calculated assuming free-free emission.

Figure 50. Ratio of the 10 - 50 keV peak counting rate to the 1 - 6 keV peak flux as a function of the 1 - 6 keV peak flux. The temperatures to which these ratios correspond, assuming free-free emission, are given on the right axis. The horizontal lines in the plot

correspond to the behavior expected due to a constant temperature decay with only the emission measure changing; various emission measures are ticked in. The near vertical lines correspond to a decay with constant emission measure and changing temperature only. Data points represented by triangles had a peak separation of $\pm$ 2 minutes. Hard x-ray rates from Arnoldy, Kane, and Winckler [1968] and Kane and Winckler [1969].

Figure 51. Ratio of the 10 - 50 keV peak counting rate to the 1 - 6 keV peak flux as a function of 10 - 50 keV rate. The temperatures to which these ratios correspond, assuming free-free emission, are given on the right axis. The lines drawn through the data correspond to decay curves of constant (given) emission measure and changing temperature only. Data points represented by triangles had a peak separation of $\pm$ 2 minutes or less; filled circles had a difference of more than $\pm$ 2 minutes. Hard x-ray rates from Arnoldy, Kane, and Winckler [1968] and Kane and Winckler [1969].

Figure 52. Ratio of 7.7 - 12.5 keV burst flux to 1 - 6 keV peak flux as a function of 1 - 6 keV peak flux. The temperatures corresponding to these ratios, assuming free-free emission, are given on the right axis. Lines corresponding to given constant emission measures and changing temperature only are drawn through the data. The hard (7.7 - 12.5 keV) x-ray fluxes are courtesy of Hudson, Peterson, and Schwartz [1969].

Figure 53. Soft (1 - 6 keV) flux versus the ratio of 7.7 - 12.5 keV flux to 1 - 6 keV flux during three individual events. The three events are distinguished by the three different symbols. Circled points occurred before the peak in the 1 - 6 keV flux. Temperatures to which these ratios correspond, assuming free-free emission, are given along the top axis. Two curves of given constant emission measure and changing temperature only are drawn through the data. Hard (7.7 - 12.5 keV) x-ray fluxes courtesy of Hudson, Peterson, and Schwartz [1969].

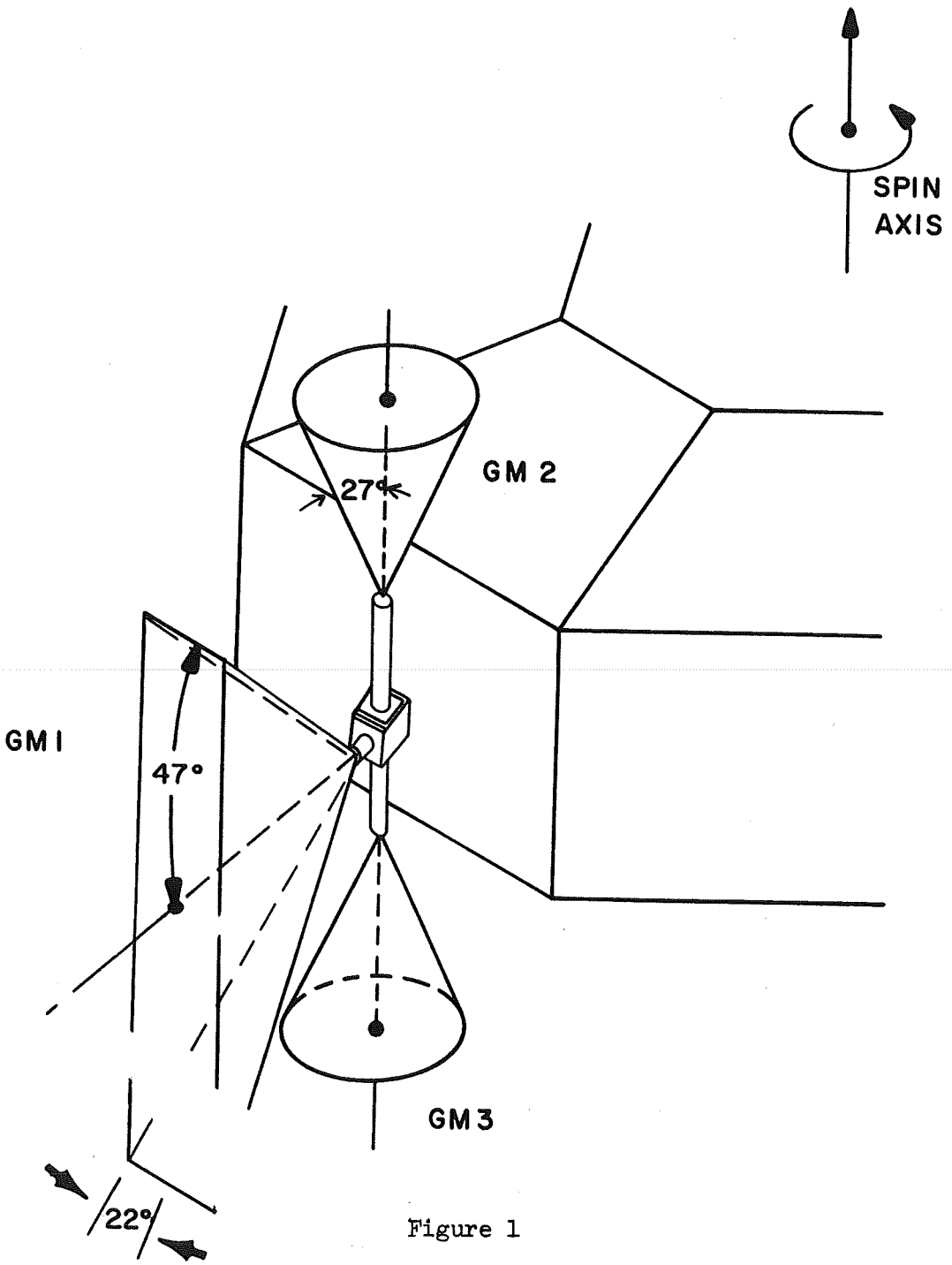

Figure 1

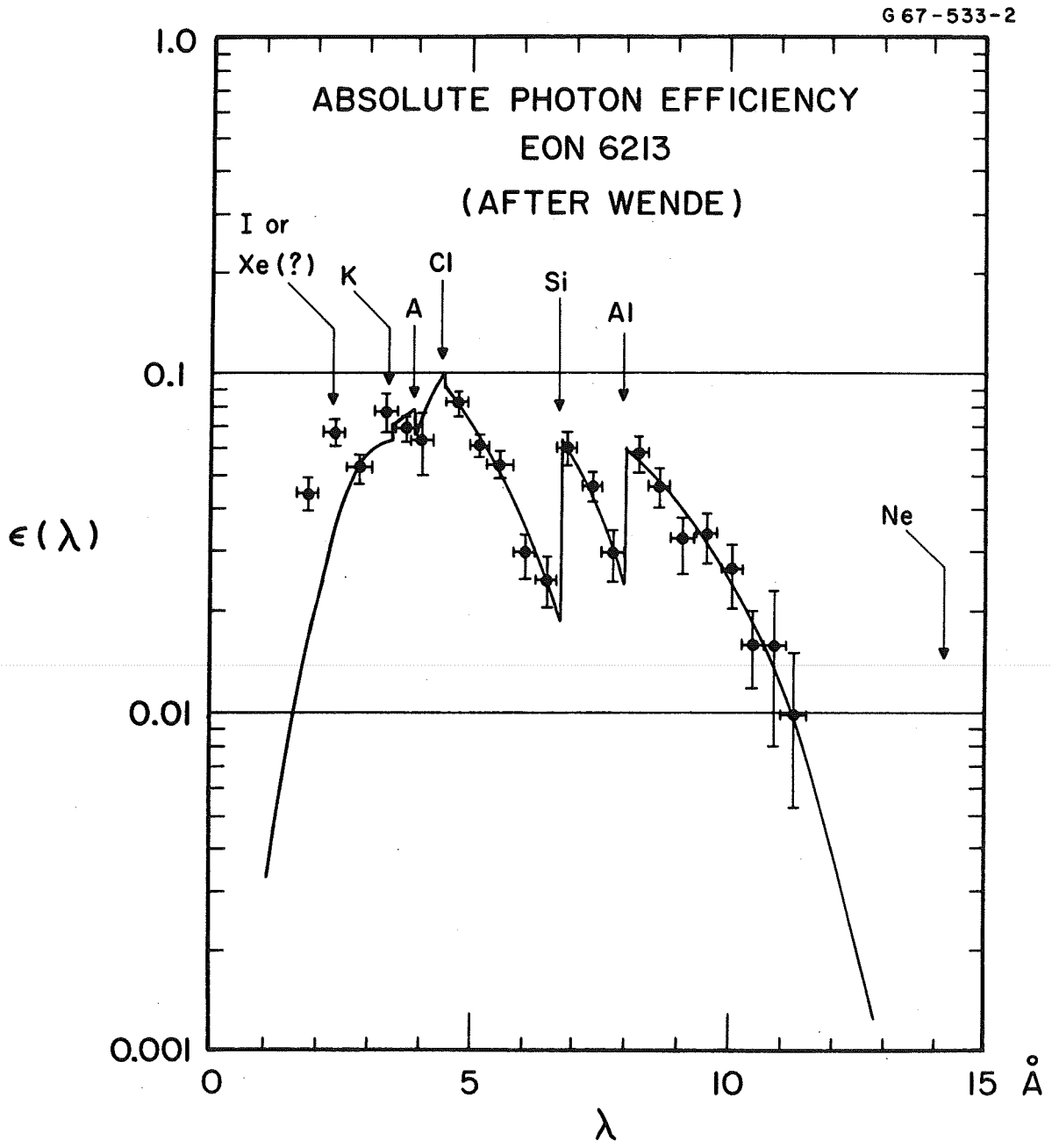
G 67-533-2
ABSOLUTE PHOTON EFFICIENCY
EON 6213
(AFTER WENDE)
I or
Xe (?)
K
A
Cl
Si
Al
Ne
1.0
0.1
0.01
0.001
ε(λ)
0
5
10
15 Å
λ

Figure 2

G 67-738-3

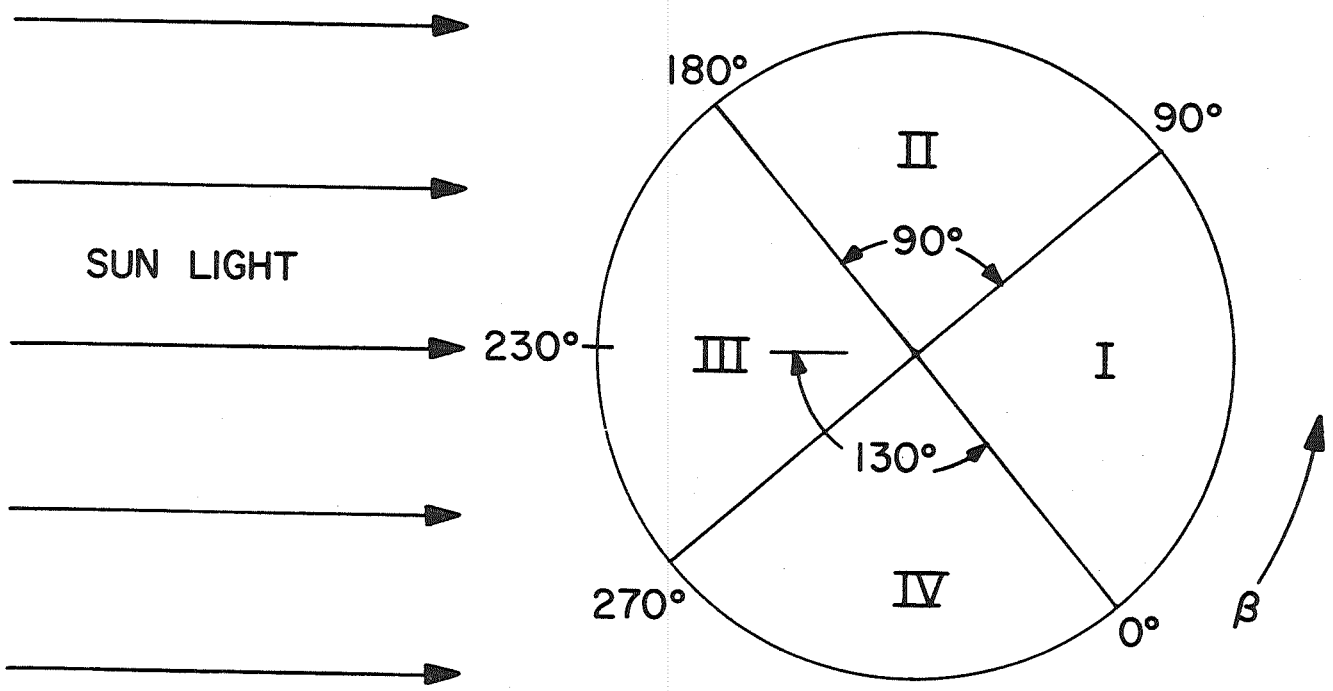

SECTORING SCHEME – EXPLORER 33 AND EXPLORER 35

Figure 3

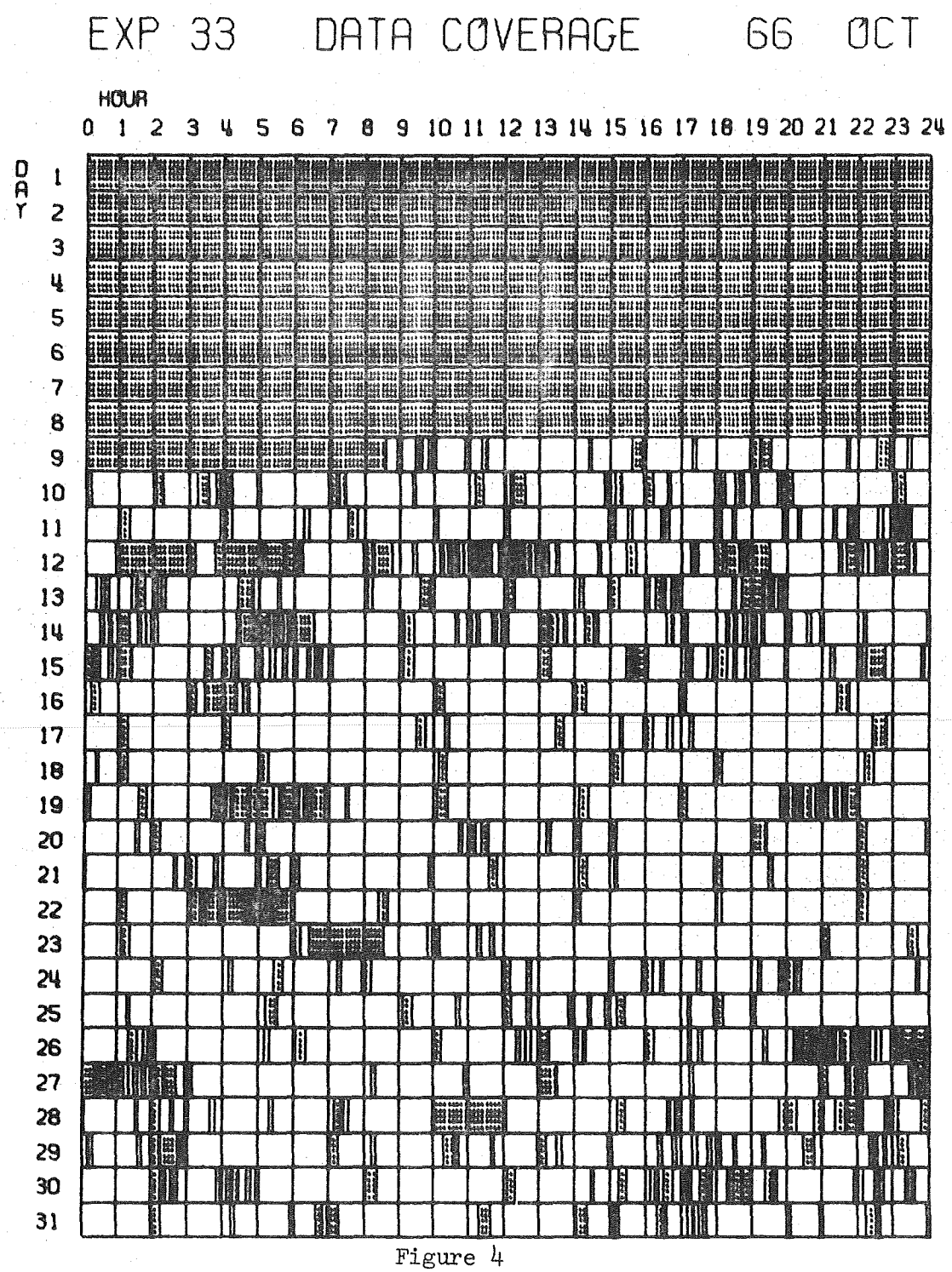
EXP 33 DATA COVERAGE 66 OCT
HOUR
0 1 2 3 4 5 6 7 8 9 10 11 12 13 14 15 16 17 18 19 20 21 22 23 24
DAY
1
2
3
4
5
6
7
8
9
10
11
12
13
14
15
16
17
18
19
20
21
22
23
24
25
26
27
28
29
30
31

Figure 4

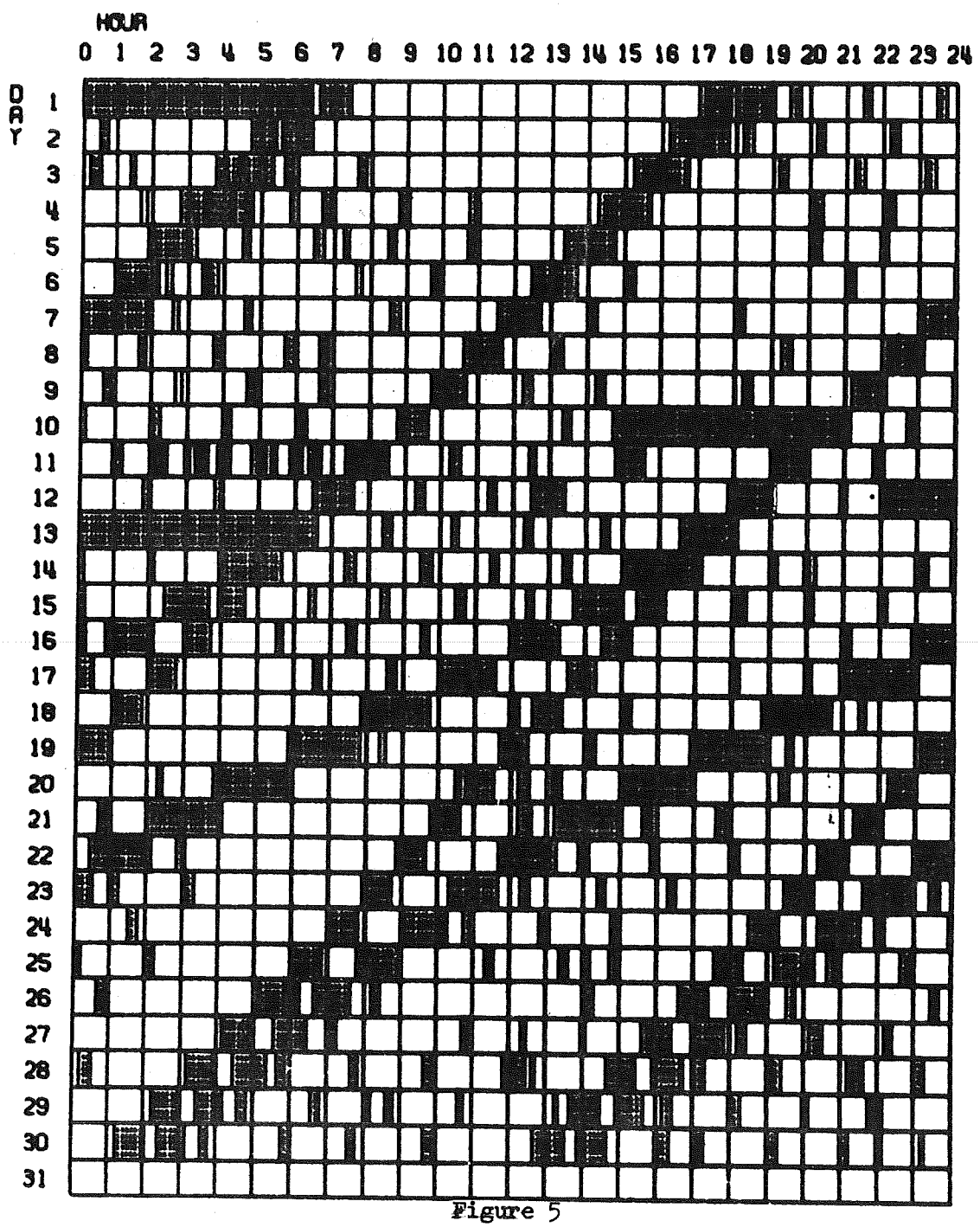
EXP 35 DATA COVERAGE 68 JUN
HOUR
0 1 2 3 4 5 6 7 8 9 10 11 12 13 14 15 16 17 18 19 20 21 22 23 24
DAY
1
2
3
4
5
6
7
8
9
10
11
12
13
14
15
16
17
18
19
20
21
22
23
24
25
26
27
28
29
30
31

Figure 5

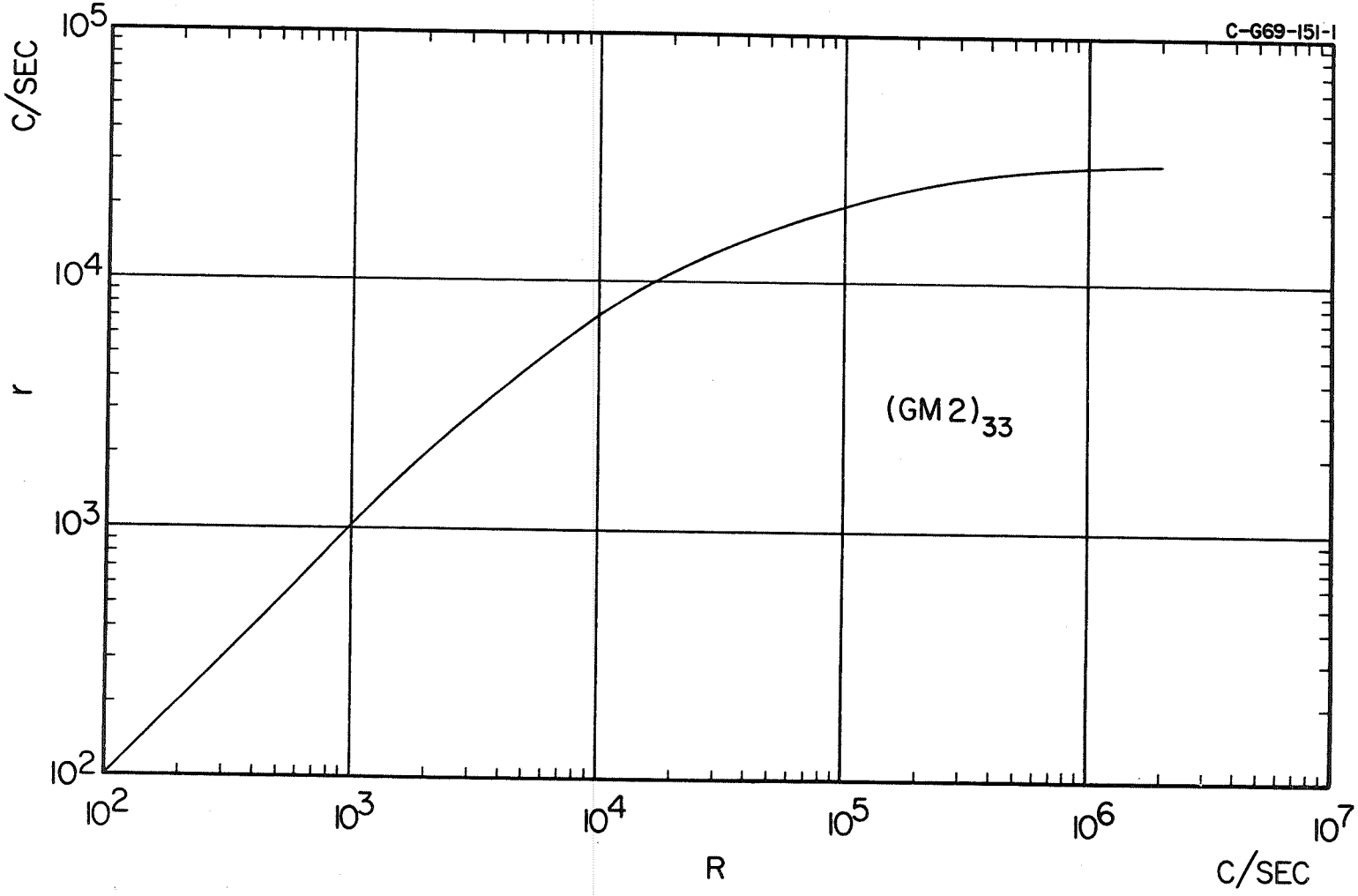
C-G69-151-1
10^5
C/SEC
r
10^4
10^3
10^2
$(GM2)_{33}$
10^2
10^3
10^4
10^5
10^6
10^7
R
C/SEC

Figure 6

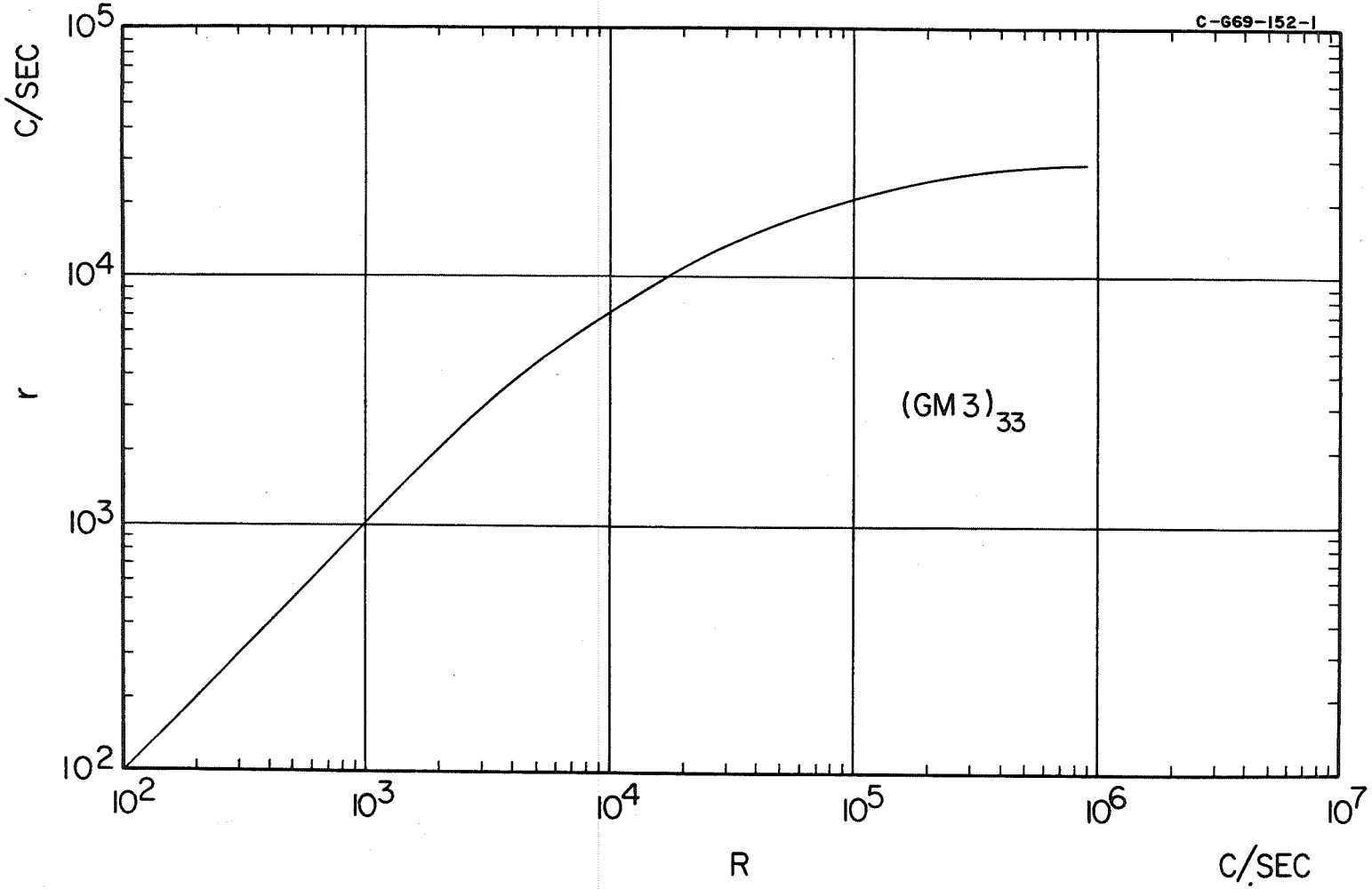
C-G69-152-1
r
C/SEC
10^5
10^4
10^3
10^2
$(GM3)_{33}$
10^2
10^3
10^4
10^5
10^6
10^7
R
C/SEC

Figure 7

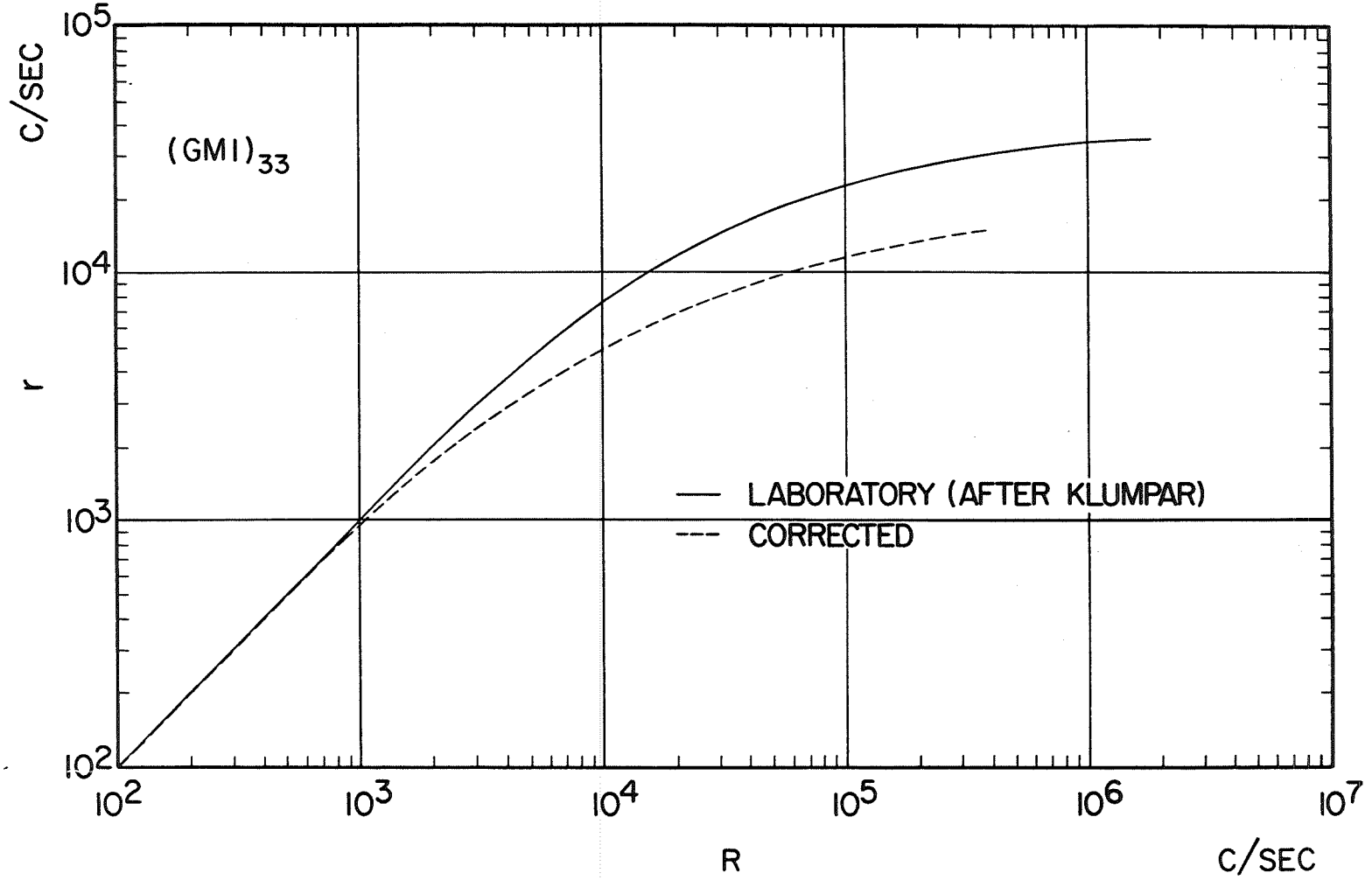
10^5
C/SEC
$(GM1)_{33}$
10^4
r
10^3
LABORATORY (AFTER KLUMPAR)
CORRECTED
10^2
10^2
10^3
10^4
10^5
10^6
10^7
R
C/SEC

Figure 8

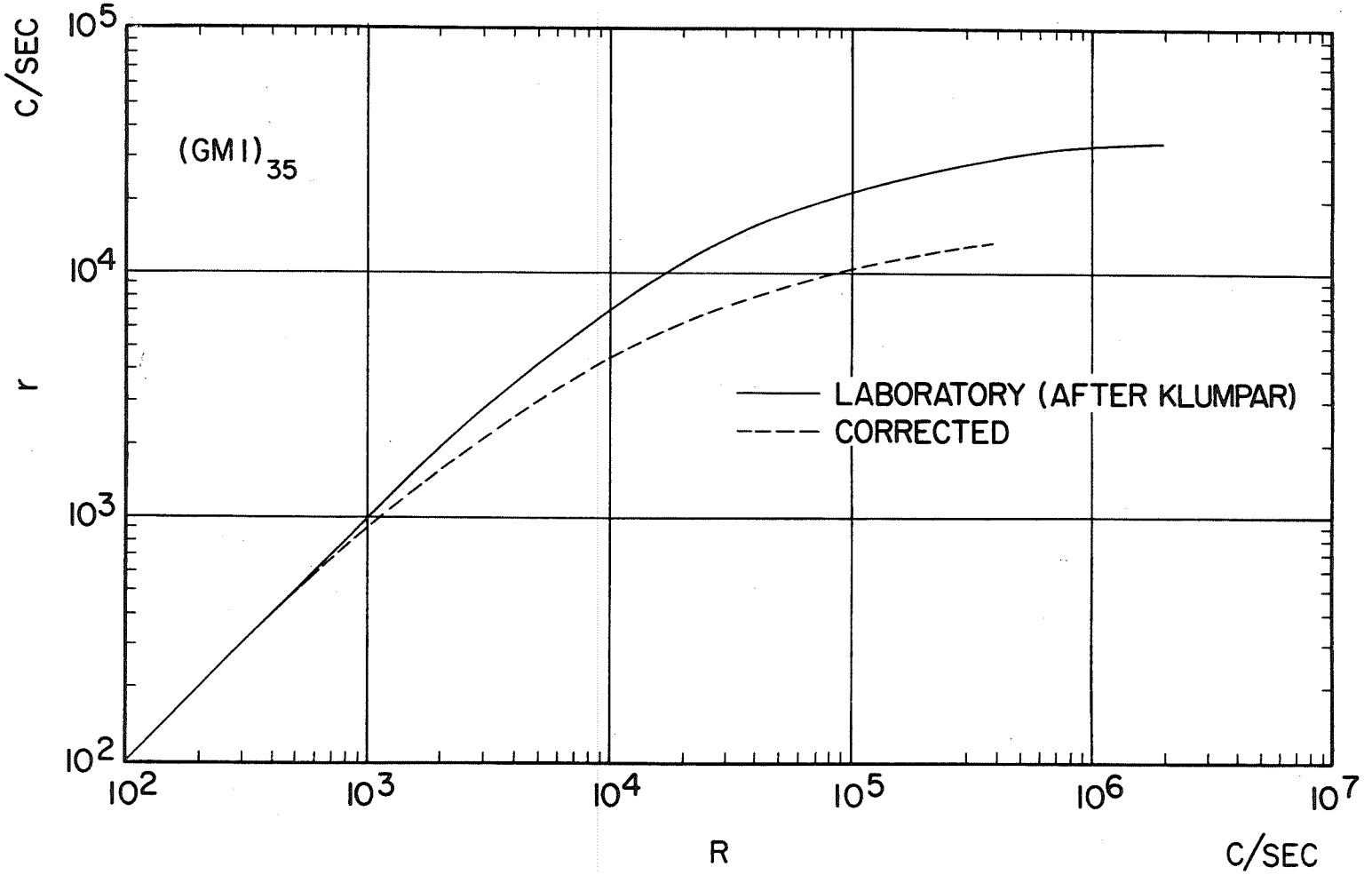
C/SEC
r
10^5
10^4
10^3
10^2
$(GM1)_{35}$
LABORATORY (AFTER KLUMPAR)
CORRECTED
10^2
10^3
10^4
10^5
10^6
10^7
R
C/SEC

Figure 9

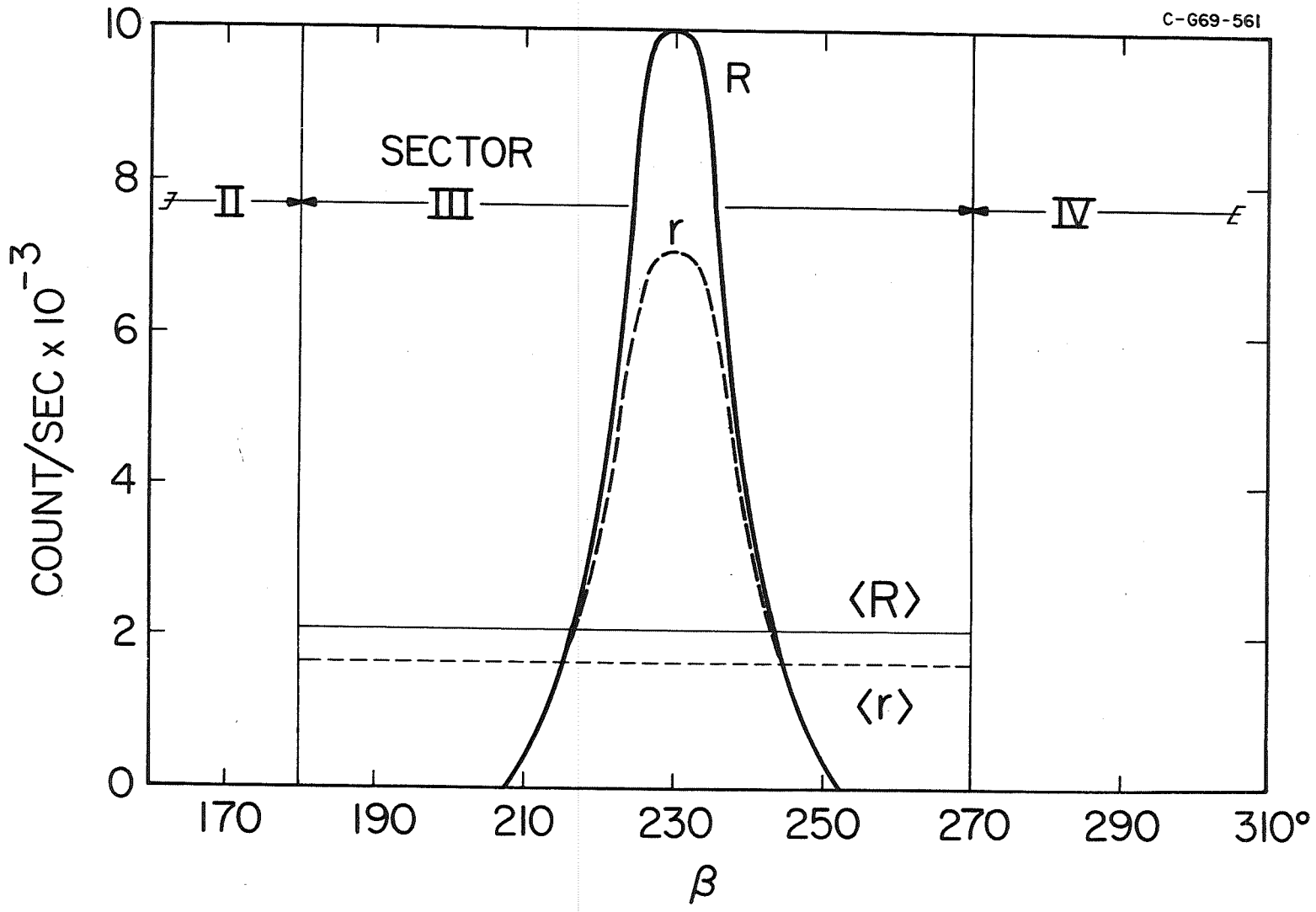
C-G69-561
10
8
6
4
2
0
COUNT/SEC x 10⁻³
SECTOR
II
III
IV
R
r
⟨R⟩
⟨r⟩
170
190
210
230
250
270
290
310°
β

Figure 10

G68-907-1

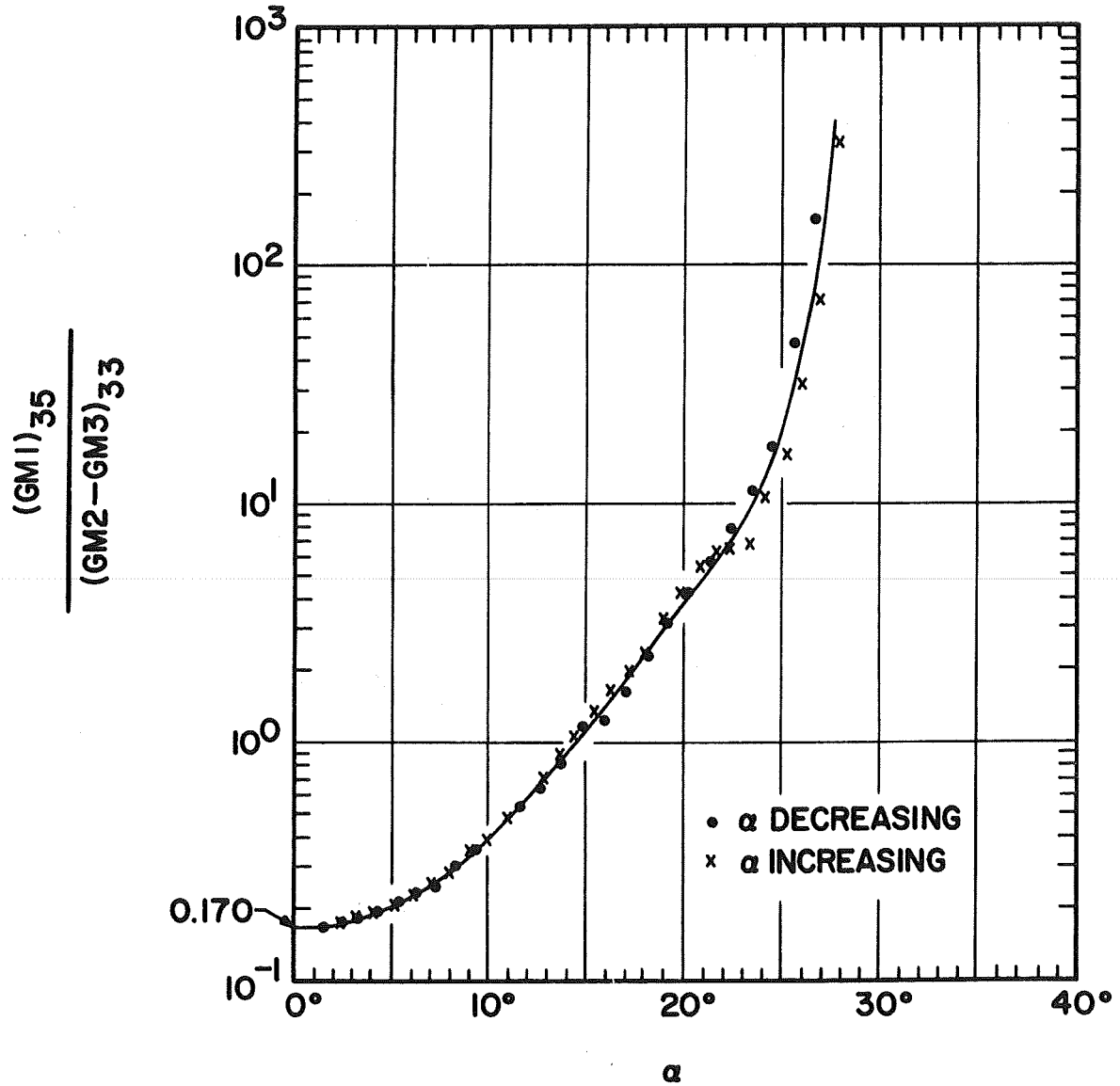

Figure 11

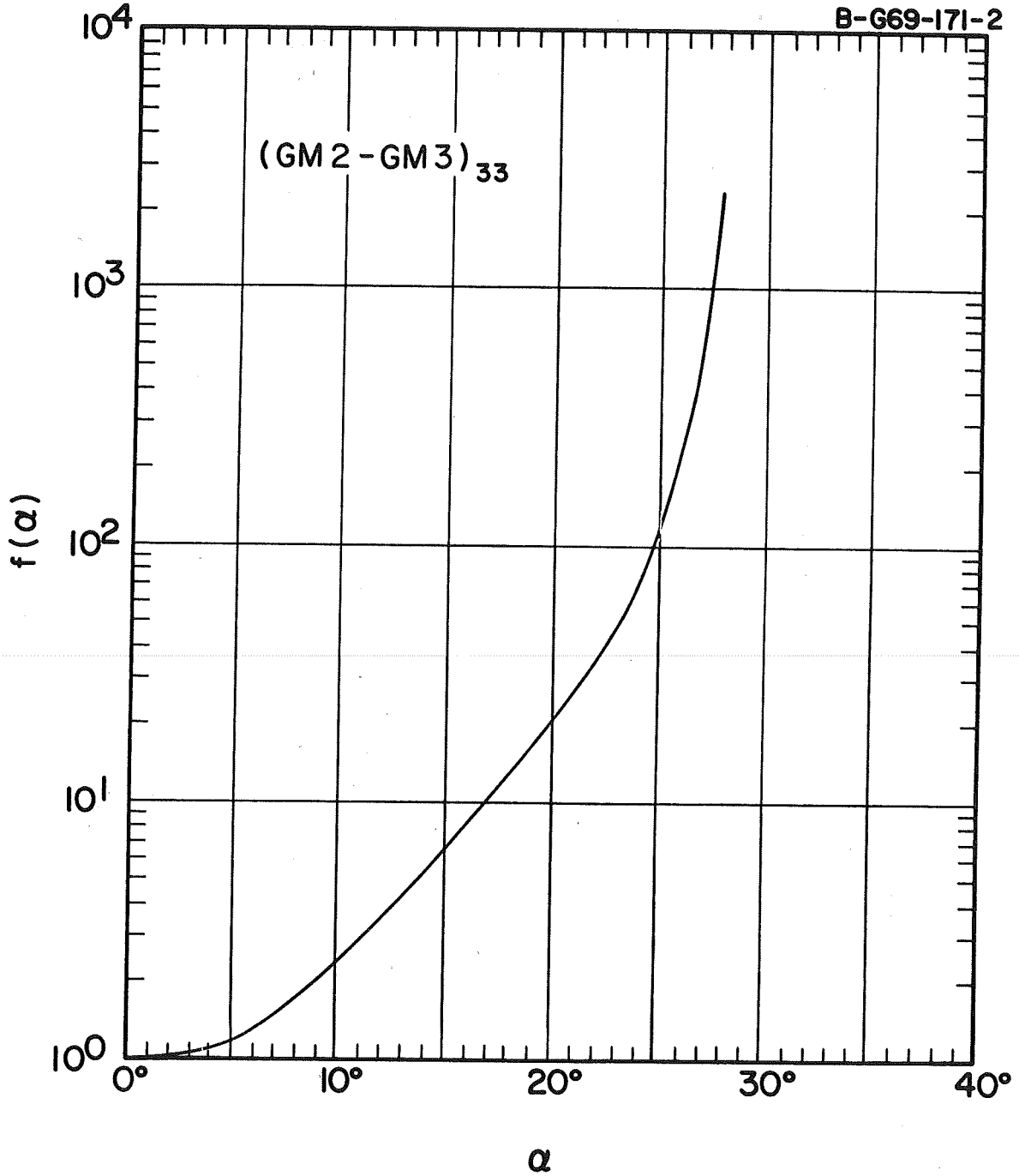

Figure 12

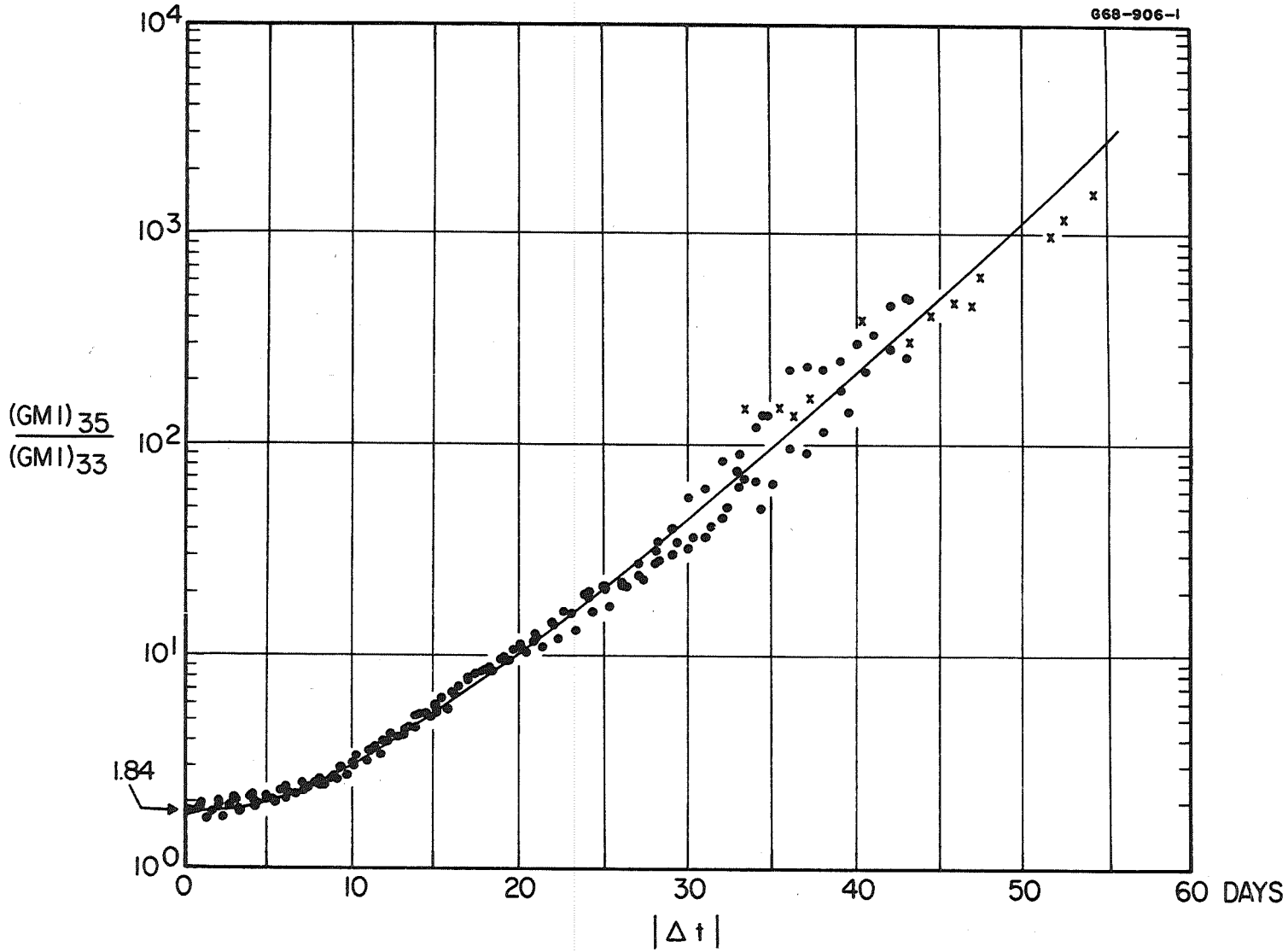
668-906-1
10^4
10^3
10^2
10^1
10^0
1.84
$\frac{(GM1)_{35}}{(GM1)_{33}}$
0
10
20
30
40
50
60 DAYS
$|\Delta t|$

Figure 13

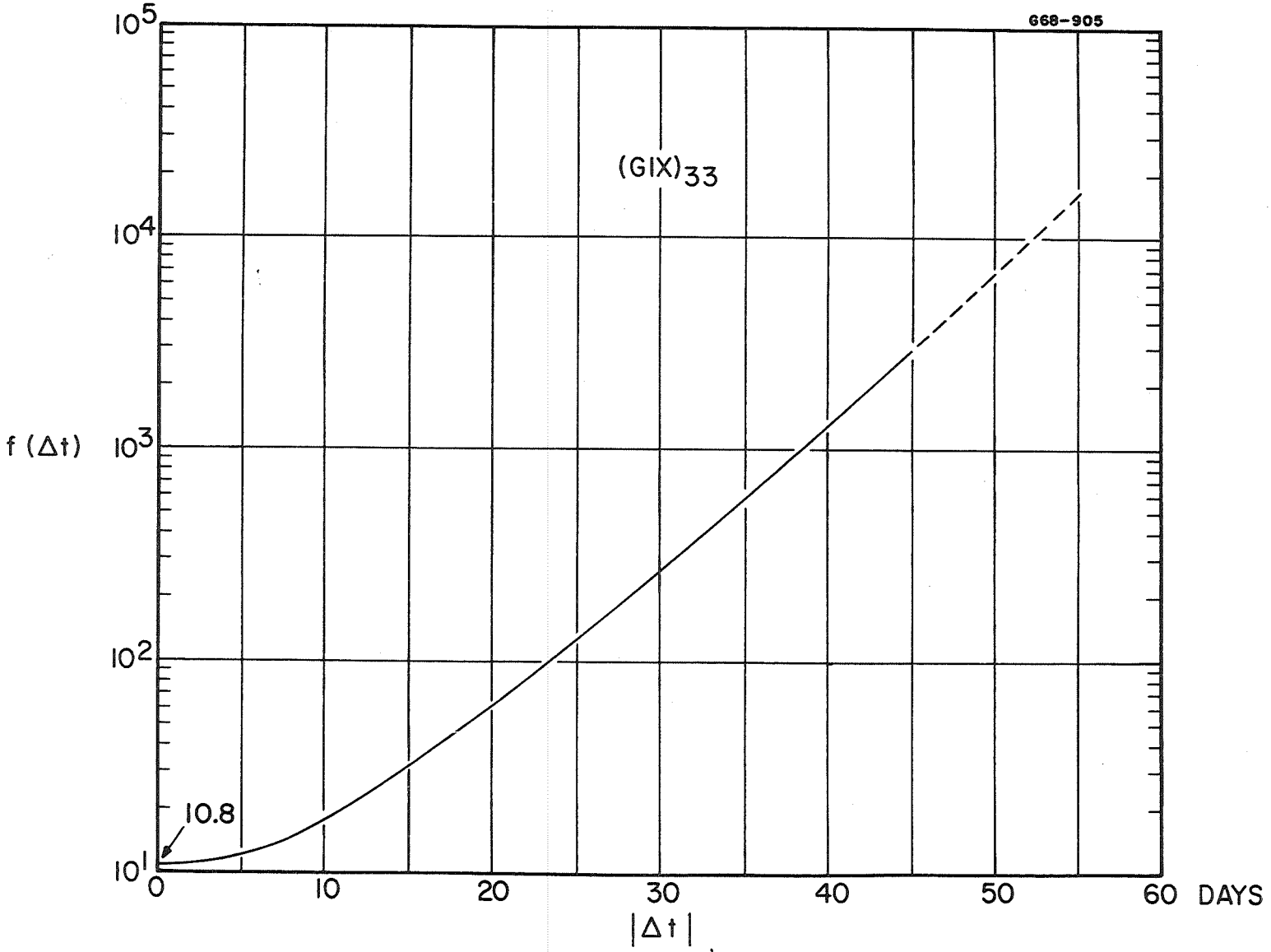
G68-905
10^5
10^4
10^3
10^2
10^1
$(GIX)_{33}$
f (Δt)
10.8
0
10
20
30
40
50
60 DAYS
|Δt|

Figure 14

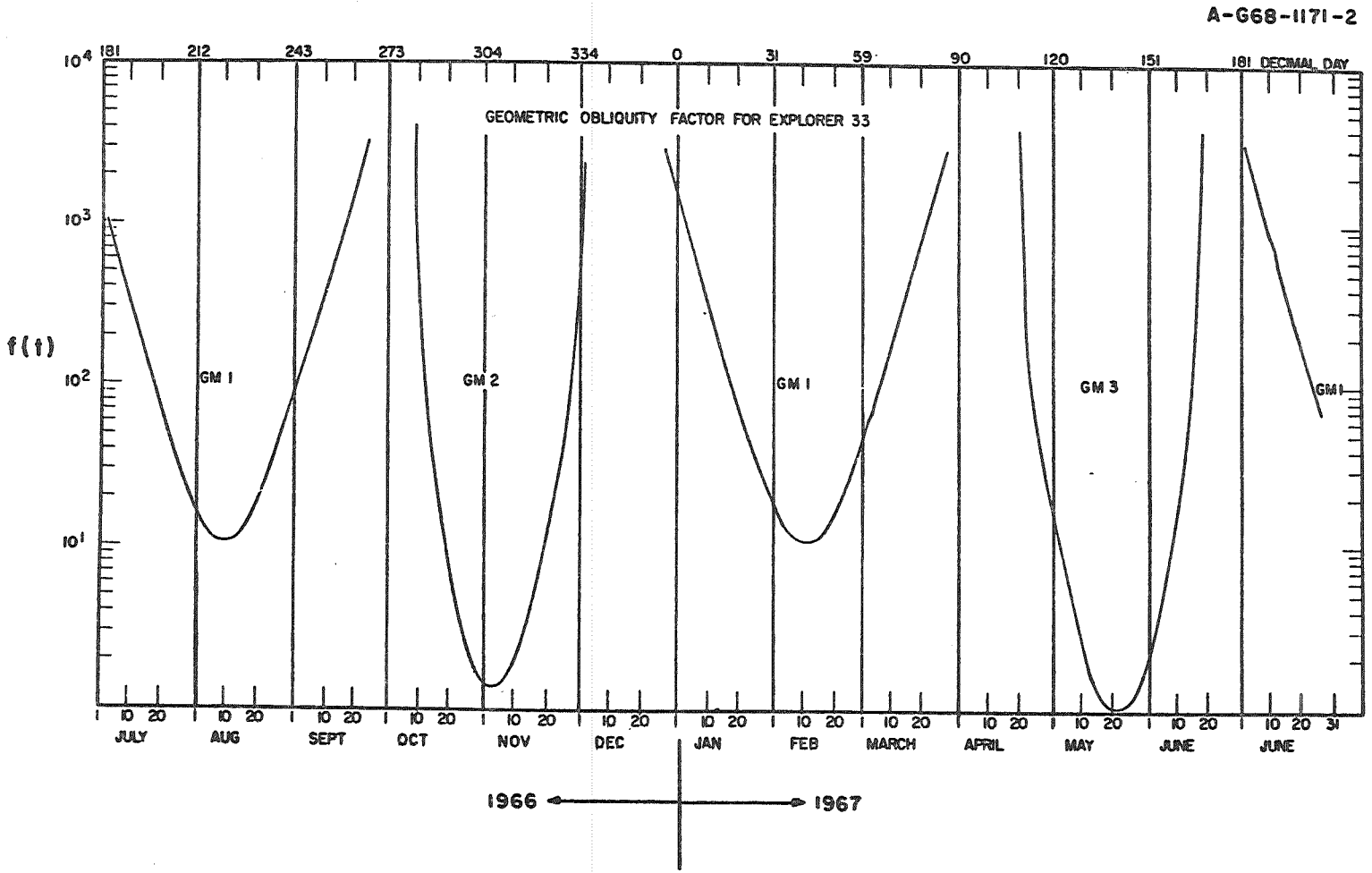
A-G68-1171-2
GEOMETRIC OBLIQUITY FACTOR FOR EXPLORER 33
f(t)
10^4
10^3
10^2
10^1
181 212 243 273 304 334 0 31 59 90 120 151 181 DECIMAL DAY
GM 1
GM 2
GM 1
GM 3
GM 1
10 20 JULY
10 20 AUG
10 20 SEPT
10 20 OCT
10 20 NOV
10 20 DEC
10 20 JAN
10 20 FEB
10 20 MARCH
10 20 APRIL
10 20 MAY
10 20 JUNE
10 20 31 JUNE
1966
1967

Figure 15

DEC. DAY	SEQUENCE	FALPHA	YEAR	MONTH	DAY	HR	MIN	SEC	FLUX
140.70657	385938.	1.03	67	MAY	21	16	58	1	2.73
140.70846	385940.	1.03	67	MAY	21	17	0	44	2.78
140.71036	385942.	1.03	67	MAY	21	17	3	28	2.79
140.71225	385944.	1.03	67	MAY	21	17	6	12	2.86
140.71414	385946.	1.03	67	MAY	21	17	8	55	2.83
140.71604	385948.	1.03	67	MAY	21	17	11	39	3.24
140.71982	385952.	1.03	67	MAY	21	17	17	5	3.25
140.72172	385954.	1.03	67	MAY	21	17	19	50	3.18
140.72361	385956.	1.03	67	MAY	21	17	22	33	3.11
140.72551	385958.	1.03	67	MAY	21	17	25	17	3.13
140.72740	385960.	1.03	67	MAY	21	17	28	1	3.09
140.72929	385962.	1.03	67	MAY	21	17	30	44	3.49
140.73119	385964.	1.03	67	MAY	21	17	33	28	3.41
140.73308	385966.	1.03	67	MAY	21	17	36	11	3.81
140.73497	385968.	1.03	67	MAY	21	17	38	54	5.85
140.73687	385970.	1.03	67	MAY	21	17	41	39	5.54
140.73876	385972.	1.03	67	MAY	21	17	44	22	5.27
140.74066	385974.	1.03	67	MAY	21	17	47	6	5.22
140.74255	385976.	1.03	67	MAY	21	17	49	50	4.78
140.74444	385978.	1.03	67	MAY	21	17	52	33	4.48
140.74634	385980.	1.03	67	MAY	21	17	55	17	4.35
140.74823	385982.	1.03	67	MAY	21	17	58	0	4.13
140.75012	385984.	1.03	67	MAY	21	18	0	43	4.01
140.75202	385986.	1.03	67	MAY	21	18	3	28	3.87
140.75391	385988.	1.03	67	MAY	21	18	6	11	3.70
140.75581	385990.	1.03	67	MAY	21	18	8	55	3.49
140.75770	385992.	1.03	67	MAY	21	18	11	38	3.42
140.75959	385994.	1.03	67	MAY	21	18	14	22	3.31
140.76149	385996.	1.03	67	MAY	21	18	17	6	3.26
140.76338	385998.	1.03	67	MAY	21	18	19	49	3.34
140.76527	386000.	1.03	67	MAY	21	18	22	32	3.30
140.76717	386002.	1.03	67	MAY	21	18	25	17	3.28
140.76906	386004.	1.03	67	MAY	21	18	28	0	3.05
140.77096	386006.	1.03	67	MAY	21	18	30	44	2.98
140.77285	386008.	1.03	67	MAY	21	18	33	27	3.07
140.77474	386010.	1.03	67	MAY	21	18	36	11	3.23
140.77664	386012.	1.03	67	MAY	21	18	38	55	3.36
140.77853	386014.	1.03	67	MAY	21	18	41	38	3.48
140.78042	386016.	1.03	67	MAY	21	18	44	21	3.64
140.78232	386018.	1.03	67	MAY	21	18	47	5	3.82
140.78421	386020.	1.03	67	MAY	21	18	49	49	4.11
140.78611	386022.	1.03	67	MAY	21	18	52	33	3.96
140.78800	386024.	1.03	67	MAY	21	18	55	16	3.95
140.78989	386026.	1.03	67	MAY	21	18	58	0	4.21
140.79179	386028.	1.03	67	MAY	21	19	0	44	4.89
140.79557	386032.	1.03	67	MAY	21	19	6	10	4.64
140.79747	386034.	1.03	67	MAY	21	19	8	54	4.15
140.79936	386036.	1.03	67	MAY	21	19	11	38	3.97
140.80126	386038.	1.03	67	MAY	21	19	14	22	4.04
140.80315	386040.	1.03	67	MAY	21	19	17	5	4.11
140.80504	386042.	1.03	67	MAY	21	19	19	49	4.32
140.80694	386044.	1.03	67	MAY	21	19	22	33	5.64
140.80883	386046.	1.03	67	MAY	21	19	25	16	102.
140.81072	386048.	1.03	67	MAY	21	19	27	59	223.
140.81262	386050.	1.03	67	MAY	21	19	30	43	154.
140.81451	386052.	1.03	67	MAY	21	19	33	27	115.
140.81641	386054.	1.03	67	MAY	21	19	36	11	91.2
140.81830	386056.	1.03	67	MAY	21	19	38	54	81.5
140.82019	386058.	1.03	67	MAY	21	19	41	37	71.6
140.82209	386060.	1.03	67	MAY	21	19	44	22	62.5
140.82398	386062.	1.03	67	MAY	21	19	47	5	54.8
140.82587	386064.	1.03	67	MAY	21	19	49	48	48.3
140.82777	386066.	1.03	67	MAY	21	19	52	32	40.7
140.82966	386068.	1.03	67	MAY	21	19	55	16	33.0
140.83156	386070.	1.03	67	MAY	21	19	58	0	25.8
140.83345	386072.	1.03	67	MAY	21	20	0	43	21.2
140.83534	386074.	1.03	67	MAY	21	20	3	26	17.8
140.83724	386076.	1.03	67	MAY	21	20	6	11	15.4
140.83913	386078.	1.03	67	MAY	21	20	8	54	13.5
140.84102	386080.	1.03	67	MAY	21	20	11	37	11.9

Figure 16

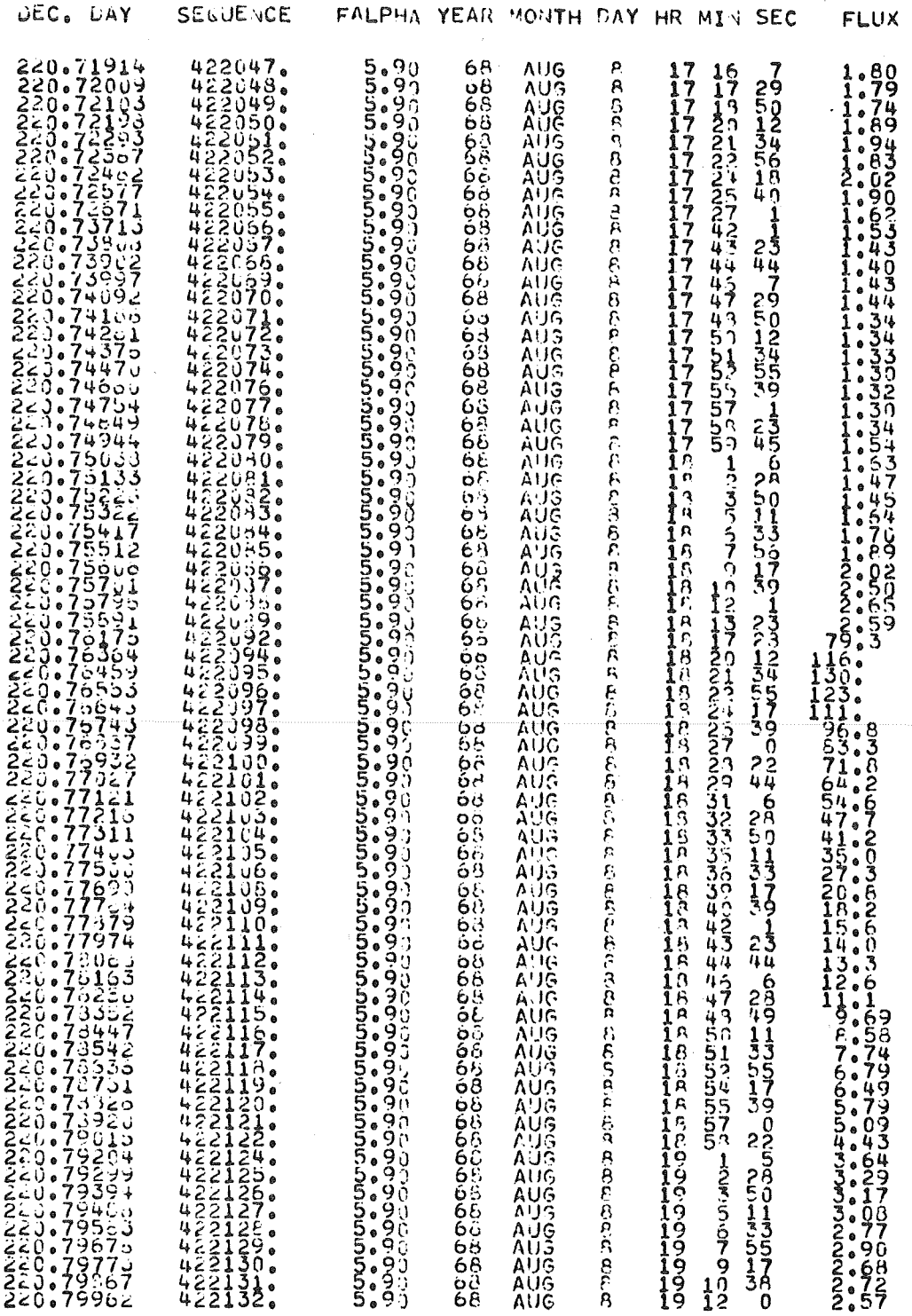

DEC. DAY	SEQUENCE	FALPHA	YEAR	MONTH	DAY	HR	MIN	SEC	FLUX
220.71914	422047.	5.90	68	AUG	8	17	16	7	1.80
220.72009	422048.	5.90	68	AUG	8	17	17	29	1.79
220.72103	422049.	5.90	68	AUG	8	17	18	50	1.74
220.72198	422050.	5.90	68	AUG	8	17	20	12	1.89
220.72293	422051.	5.90	68	AUG	8	17	21	34	1.94
220.72387	422052.	5.90	68	AUG	8	17	22	56	1.83
220.72482	422053.	5.90	68	AUG	8	17	24	18	2.02
220.72577	422054.	5.90	68	AUG	8	17	25	40	1.90
220.72671	422055.	5.90	68	AUG	8	17	27	1	1.62
220.73713	422066.	5.90	68	AUG	8	17	42	1	1.53
220.73908	422067.	5.90	68	AUG	8	17	44	23	1.43
220.73902	422068.	5.90	68	AUG	8	17	44	44	1.40
220.73997	422069.	5.90	68	AUG	8	17	45	7	1.44
220.74092	422070.	5.90	68	AUG	8	17	47	29	1.44
220.74186	422071.	5.90	68	AUG	8	17	48	50	1.34
220.74281	422072.	5.90	68	AUG	8	17	50	12	1.34
220.74375	422073.	5.90	68	AUG	8	17	51	34	1.33
220.74470	422074.	5.90	68	AUG	8	17	52	55	1.30
220.74660	422076.	5.90	68	AUG	8	17	55	39	1.32
220.74754	422077.	5.90	68	AUG	8	17	57	1	1.30
220.74849	422078.	5.90	68	AUG	8	17	58	23	1.34
220.74944	422079.	5.90	68	AUG	8	17	59	45	1.54
220.75038	422080.	5.90	68	AUG	8	18	1	6	1.63
220.75133	422081.	5.90	68	AUG	8	18	2	28	1.47
220.75227	422082.	5.90	68	AUG	8	18	3	50	1.45
220.75322	422083.	5.90	68	AUG	8	18	5	11	1.54
220.75417	422084.	5.90	68	AUG	8	18	6	33	1.70
220.75512	422085.	5.90	68	AUG	8	18	7	56	1.89
220.75606	422086.	5.90	68	AUG	8	18	9	17	2.02
220.75701	422087.	5.90	68	AUG	8	18	10	39	2.55
220.75795	422088.	5.90	68	AUG	8	18	12	1	2.65
220.75891	422089.	5.90	68	AUG	8	18	13	23	2.59
220.76175	422092.	5.90	68	AUG	8	18	17	33	79.3
220.76364	422094.	5.90	68	AUG	8	18	20	12	116.
220.76459	422095.	5.90	68	AUG	8	18	21	34	130.
220.76553	422096.	5.90	68	AUG	8	18	22	55	123.
220.76648	422097.	5.90	68	AUG	8	18	24	17	111.
220.76743	422098.	5.90	68	AUG	8	18	25	39	96.8
220.76837	422099.	5.90	68	AUG	8	18	27	0	83.3
220.76932	422100.	5.90	68	AUG	8	18	28	22	71.8
220.77027	422101.	5.90	68	AUG	8	18	29	44	64.2
220.77121	422102.	5.90	68	AUG	8	18	31	6	54.6
220.77216	422103.	5.90	68	AUG	8	18	32	28	47.7
220.77311	422104.	5.90	68	AUG	8	18	33	50	41.2
220.77405	422105.	5.90	68	AUG	8	18	35	11	35.0
220.77500	422106.	5.90	68	AUG	8	18	36	33	27.3
220.77690	422108.	5.90	68	AUG	8	18	39	17	20.6
220.77784	422109.	5.90	68	AUG	8	18	40	39	18.2
220.77879	422110.	5.90	68	AUG	8	18	42	1	15.6
220.77974	422111.	5.90	68	AUG	8	18	43	23	14.0
220.78068	422112.	5.90	68	AUG	8	18	44	44	13.3
220.78163	422113.	5.90	68	AUG	8	18	46	6	12.6
220.78258	422114.	5.90	68	AUG	8	18	47	28	11.1
220.78352	422115.	5.90	68	AUG	8	18	48	49	9.69
220.78447	422116.	5.90	68	AUG	8	18	50	11	8.58
220.78542	422117.	5.90	68	AUG	8	18	51	33	7.74
220.78636	422118.	5.90	68	AUG	8	18	52	55	6.79
220.78731	422119.	5.90	68	AUG	8	18	54	17	6.49
220.78826	422120.	5.90	68	AUG	8	18	55	39	5.79
220.78920	422121.	5.90	68	AUG	8	18	57	0	5.09
220.79015	422122.	5.90	68	AUG	8	18	58	22	4.43
220.79204	422124.	5.90	68	AUG	8	19	1	5	3.64
220.79299	422125.	5.90	68	AUG	8	19	2	28	3.29
220.79394	422126.	5.90	68	AUG	8	19	3	50	3.17
220.79488	422127.	5.90	68	AUG	8	19	5	11	3.08
220.79583	422128.	5.90	68	AUG	8	19	6	33	2.77
220.79678	422129.	5.90	68	AUG	8	19	7	55	2.90
220.79772	422130.	5.90	68	AUG	8	19	9	17	2.68
220.79867	422131.	5.90	68	AUG	8	19	10	38	2.72
220.79962	422132.	5.90	68	AUG	8	19	12	0	2.57

Figure 17

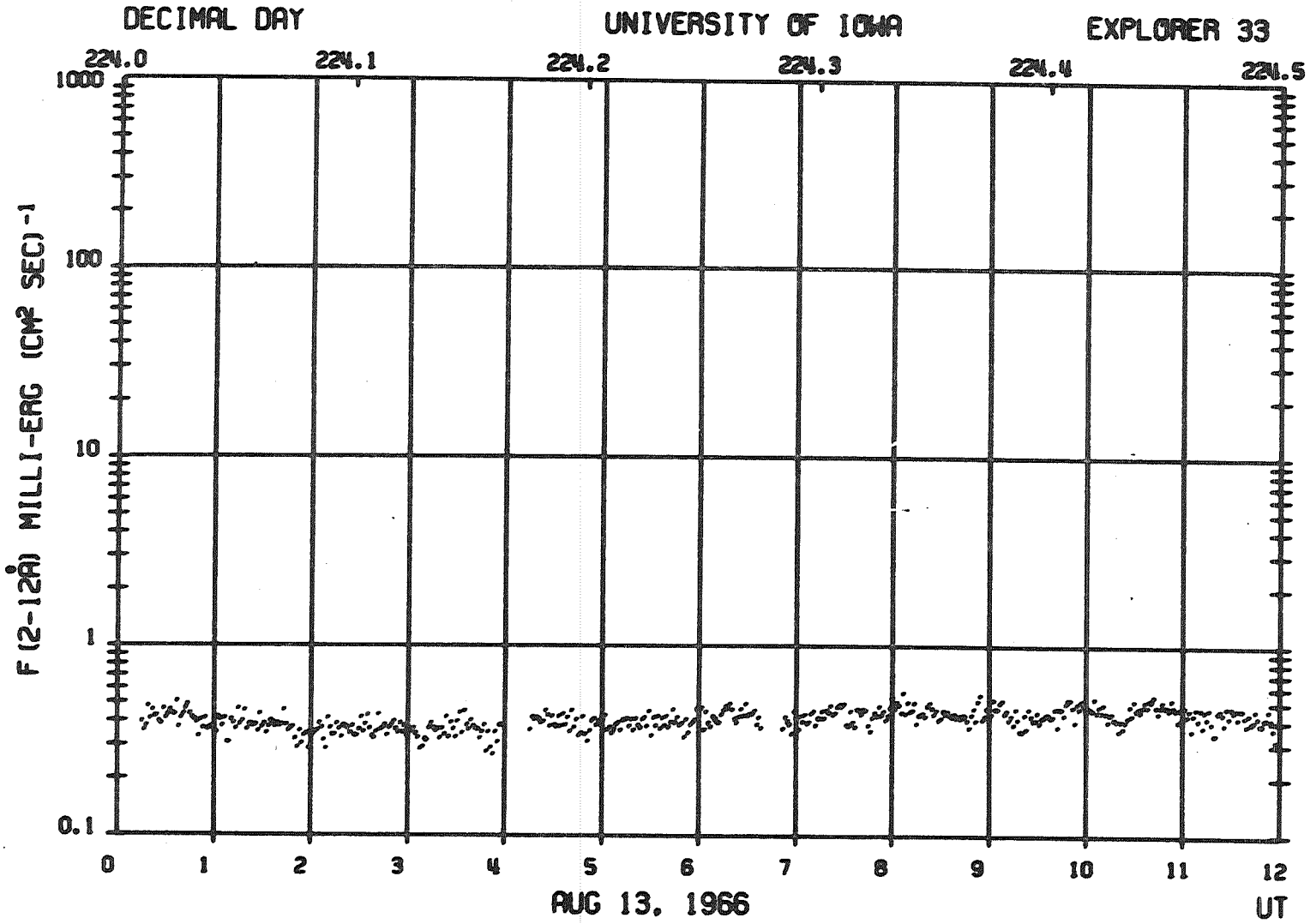
DECIMAL DAY
UNIVERSITY OF IOWA
EXPLORER 33
224.0
224.1
224.2
224.3
224.4
224.5
1000
100
10
1
0.1
F (2-12Å) MILLI-ERG (CM² SEC)⁻¹
0
1
2
3
4
5
6
7
8
9
10
11
12
AUG 13, 1966
UT

Figure 18

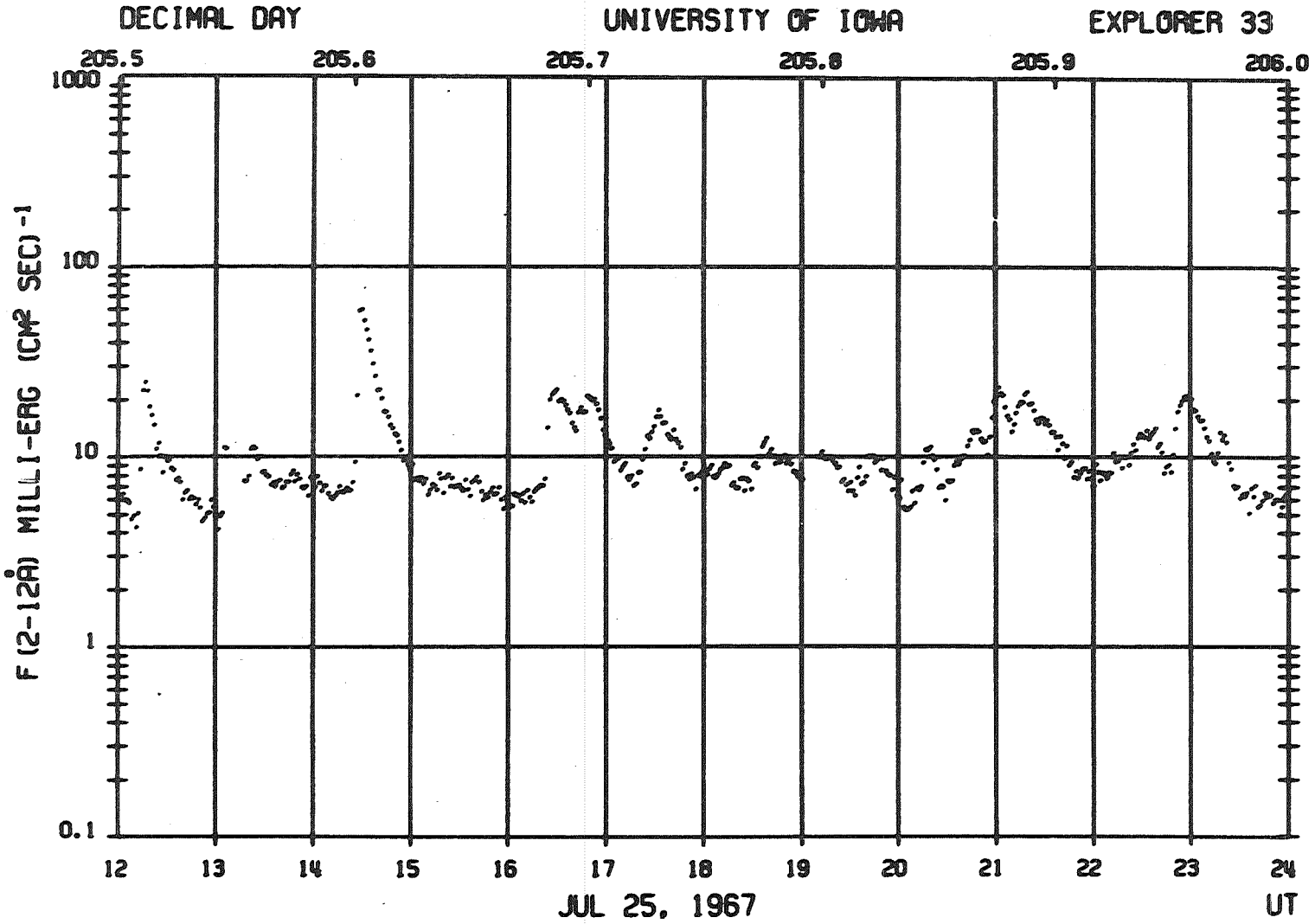
DECIMAL DAY
UNIVERSITY OF IOWA
EXPLORER 33
205.5
205.6
205.7
205.8
205.9
206.0
1000
100
10
1
0.1
F (2-12Å) MILLI-ERG (CM² SEC)⁻¹
12
13
14
15
16
17
18
19
20
21
22
23
24
JUL 25, 1967
UT
Figure 19

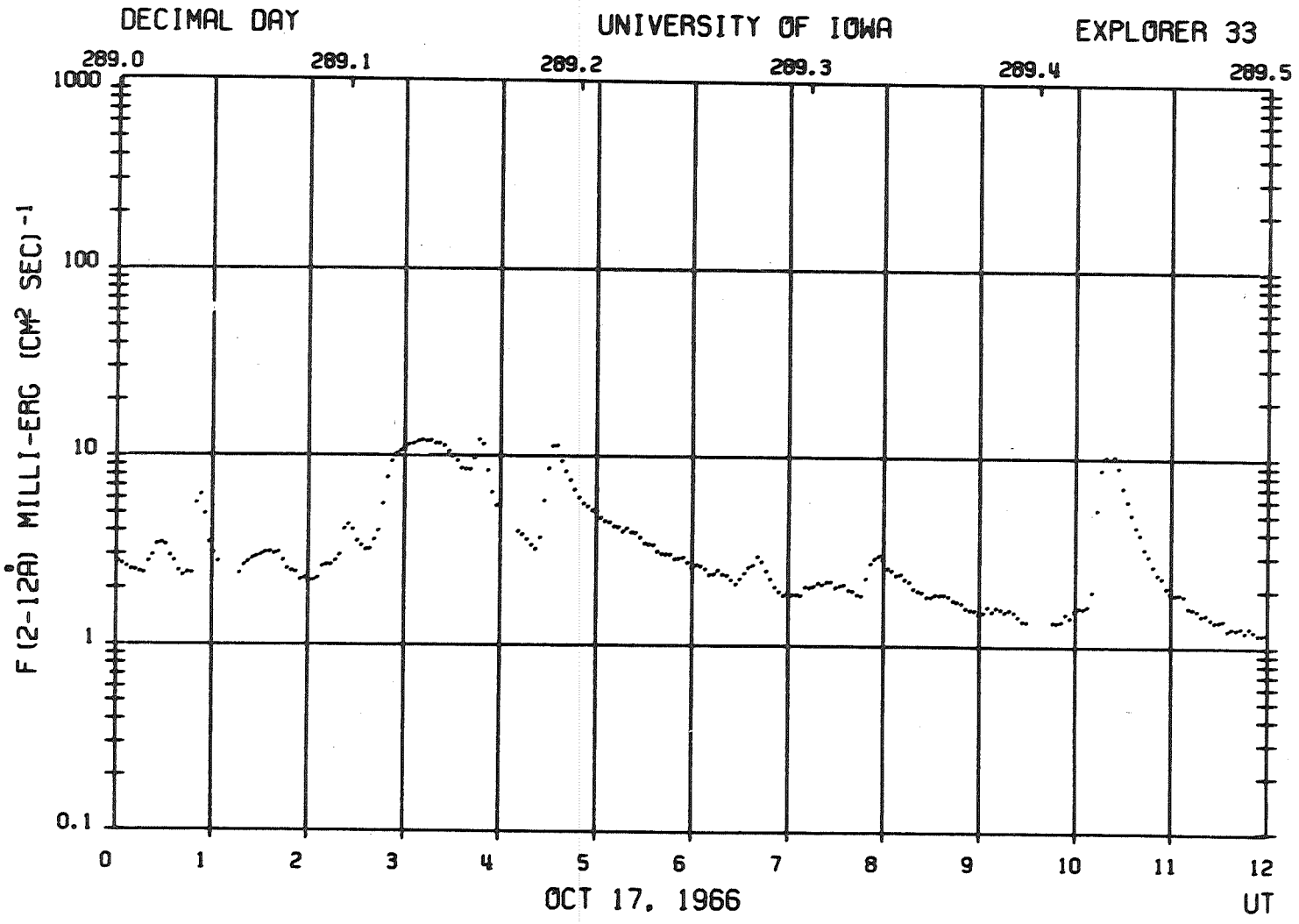
DECIMAL DAY
UNIVERSITY OF IOWA
EXPLORER 33
289.0
289.1
289.2
289.3
289.4
289.5
1000
100
10
1
0.1
F(2-12Å) MILLI-ERG (CM² SEC)⁻¹
0
1
2
3
4
5
6
7
8
9
10
11
12
OCT 17, 1966
UT

Figure 20

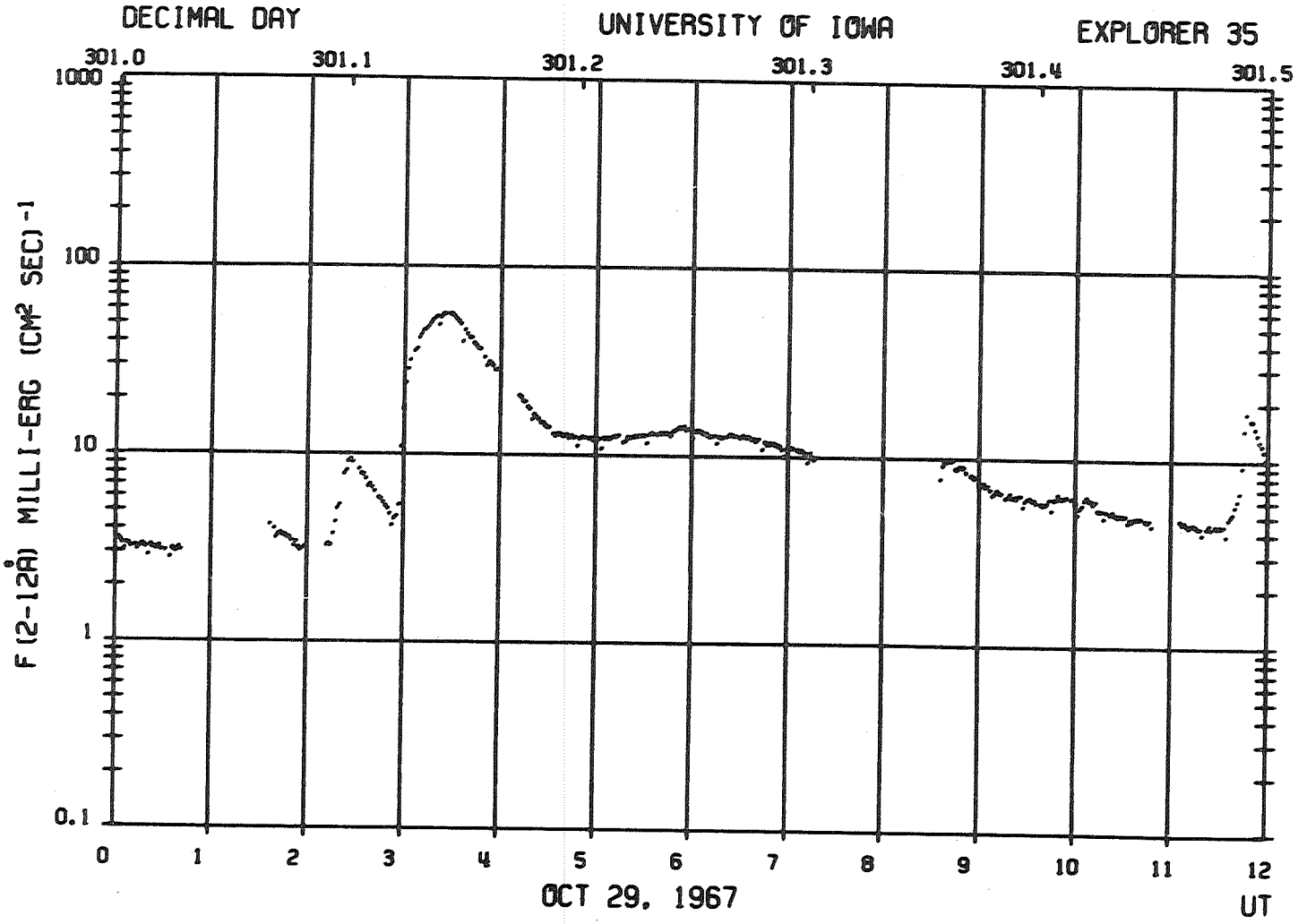
DECIMAL DAY
UNIVERSITY OF IOWA
EXPLORER 35
301.0
301.1
301.2
301.3
301.4
301.5
1000
100
10
1
0.1
F (2-12Å) MILLI-ERG (CM² SEC)⁻¹
0
1
2
3
4
5
6
7
8
9
10
11
12
OCT 29, 1967
UT

Figure 21

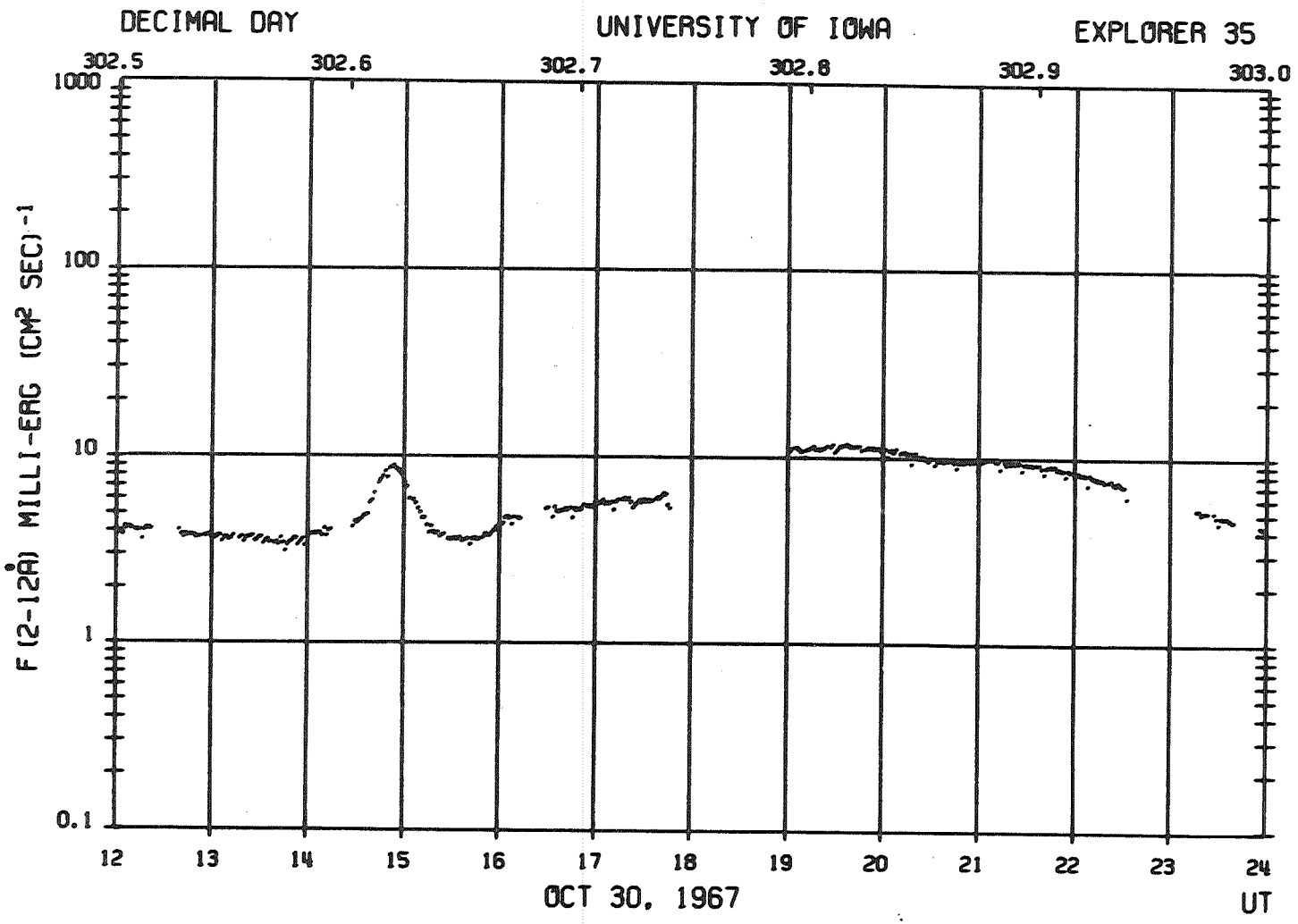
DECIMAL DAY
UNIVERSITY OF IOWA
EXPLORER 35
302.5
302.6
302.7
302.8
302.9
303.0
1000
100
10
1
0.1
F(2-12Å) MILLI-ERG (CM² SEC)⁻¹
12
13
14
15
16
17
18
19
20
21
22
23
24
OCT 30, 1967
UT

Figure 22

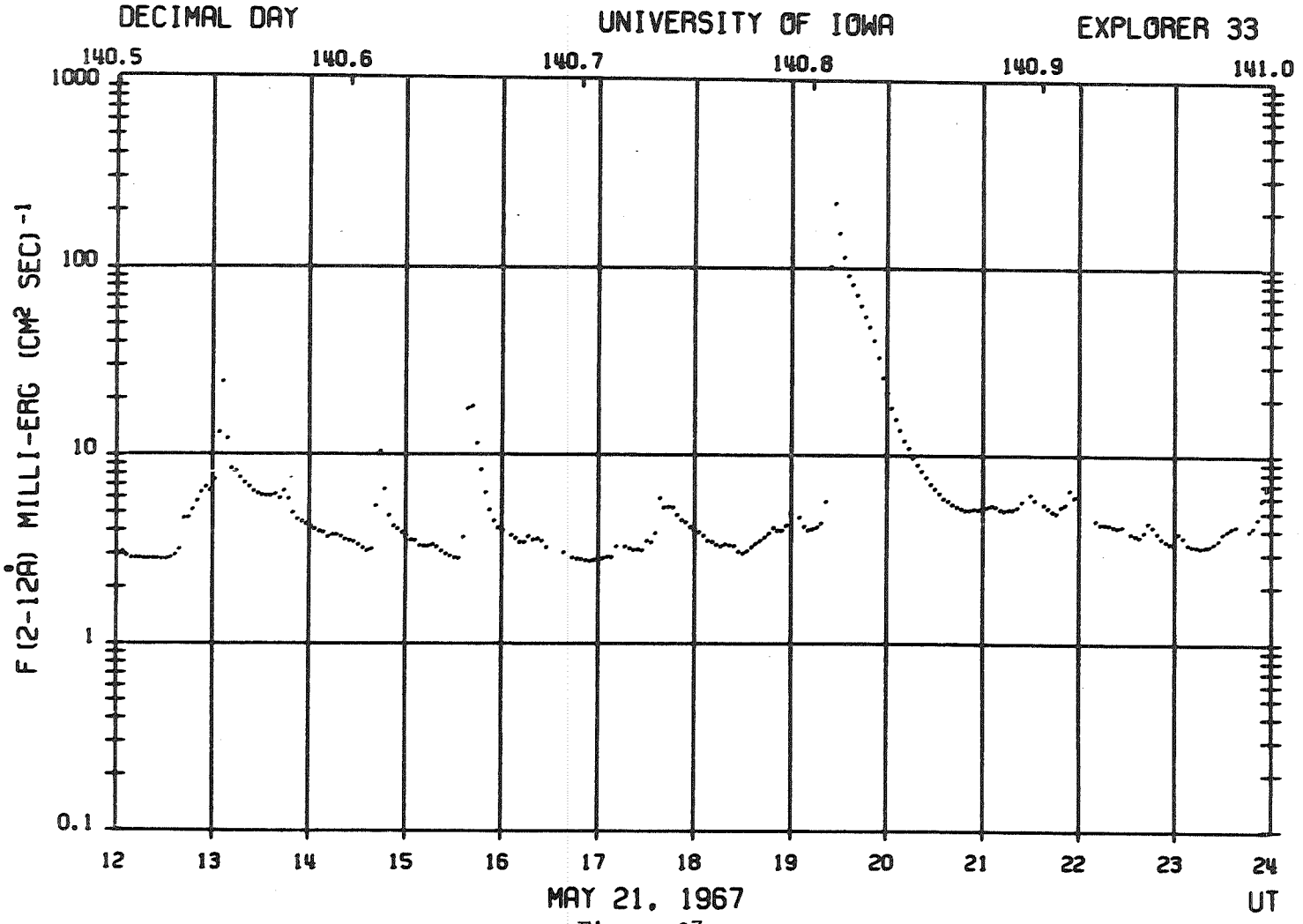
DECIMAL DAY
UNIVERSITY OF IOWA
EXPLORER 33
140.5
140.6
140.7
140.8
140.9
141.0
1000
100
10
1
0.1
F(2-12Å) MILLI-ERG (CM² SEC)⁻¹
12
13
14
15
16
17
18
19
20
21
22
23
24
MAY 21, 1967
UT

Figure 23

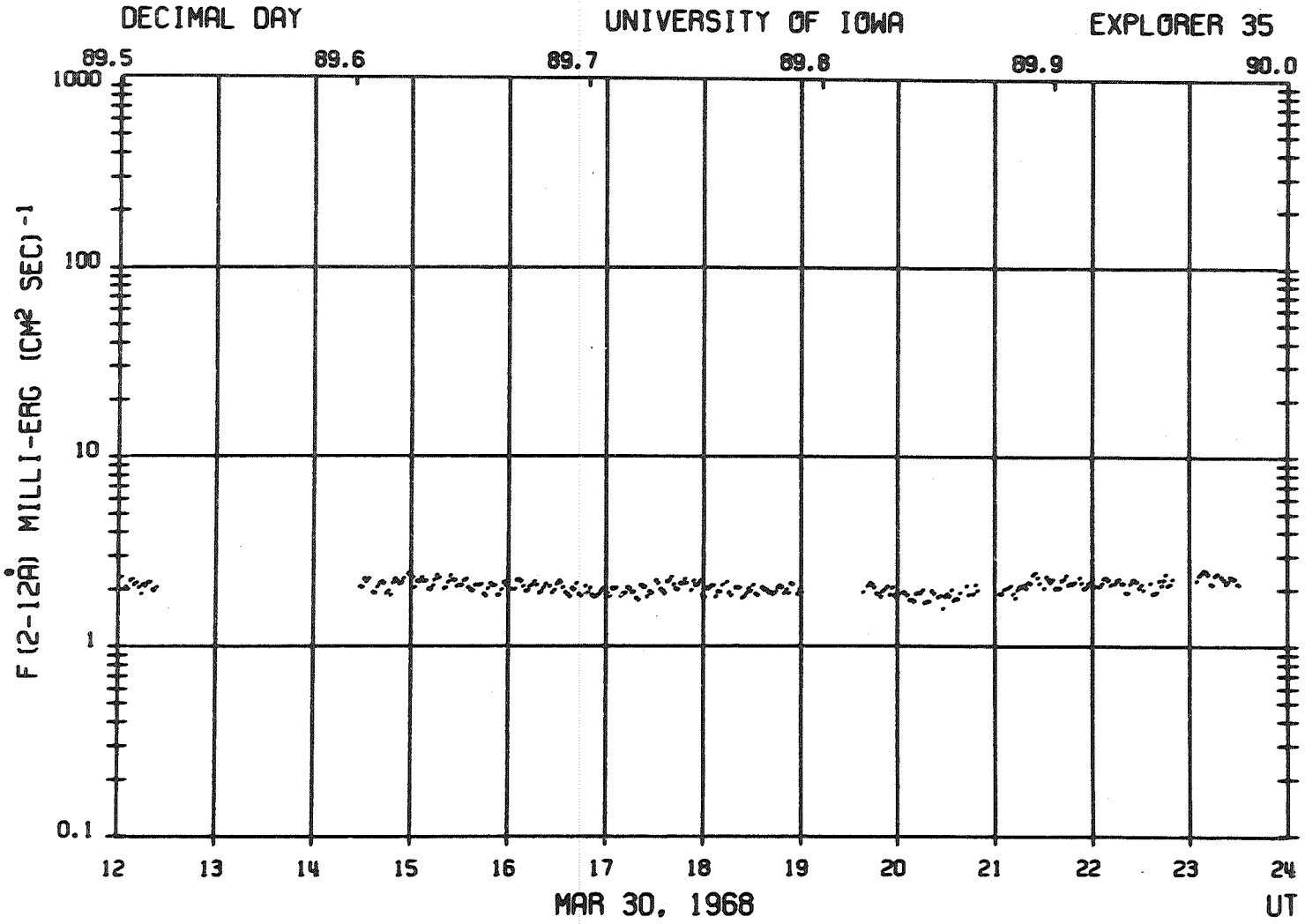
DECIMAL DAY
UNIVERSITY OF IOWA
EXPLORER 35
89.5
89.6
89.7
89.8
89.9
90.0
1000
100
10
1
0.1
F (2-12Å) MILLI-ERG (CM² SEC)⁻¹
12
13
14
15
16
17
18
19
20
21
22
23
24
MAR 30, 1968
UT

Figure 24

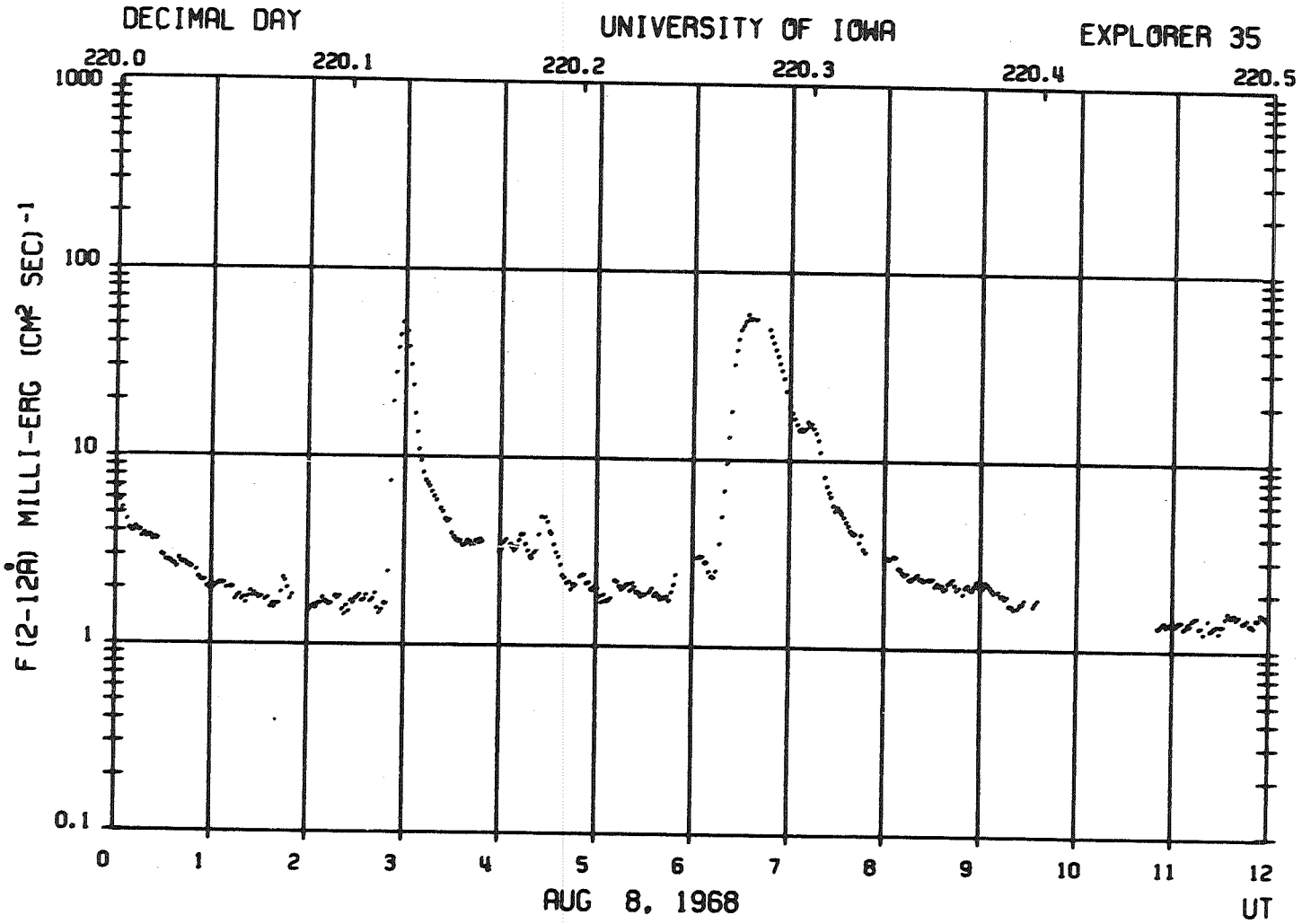
DECIMAL DAY
UNIVERSITY OF IOWA
EXPLORER 35
220.0
220.1
220.2
220.3
220.4
220.5
1000
100
10
1
0.1
F (2-12Å) MILLI-ERG (CM² SEC)⁻¹
0
1
2
3
4
5
6
7
8
9
10
11
12
AUG 8, 1968
UT

Figure 25

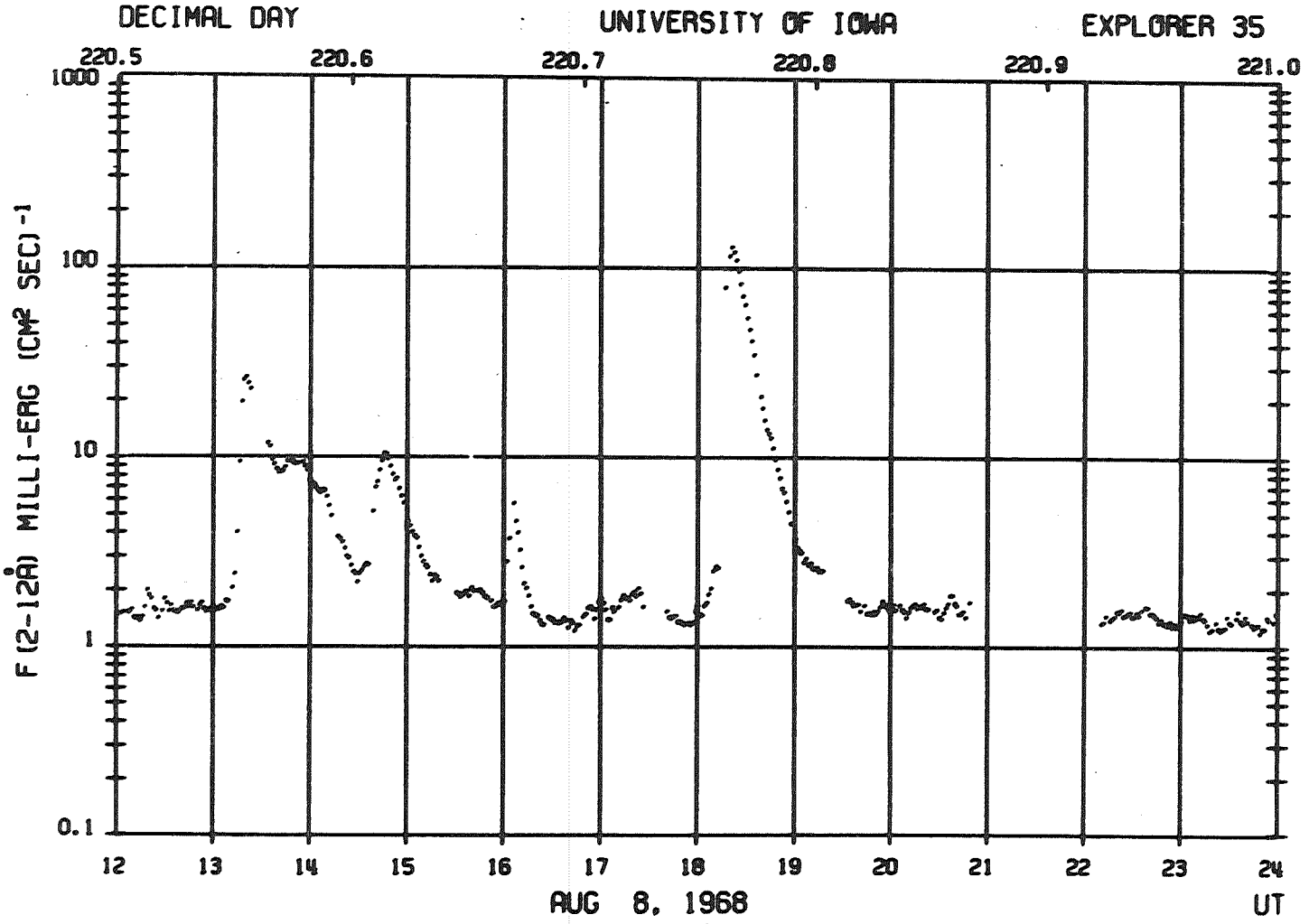
DECIMAL DAY
UNIVERSITY OF IOWA
EXPLORER 35
220.5
220.6
220.7
220.8
220.9
221.0
1000
100
10
1
0.1
F (2-12Å) MILLI-ERG (CM² SEC)⁻¹
12
13
14
15
16
17
18
19
20
21
22
23
24
AUG 8, 1968
UT
Figure 26

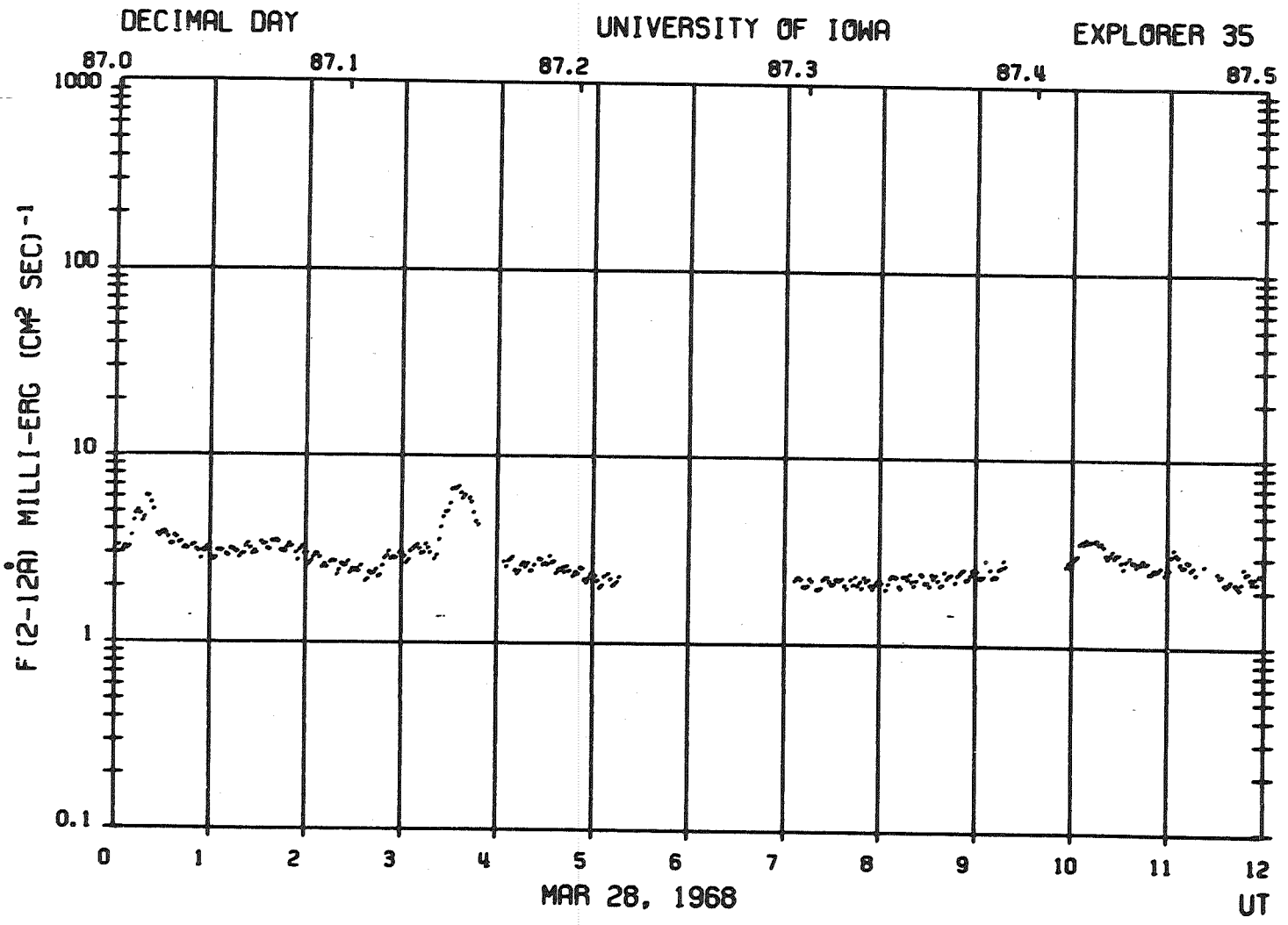
DECIMAL DAY
UNIVERSITY OF IOWA
EXPLORER 35
87.0
87.1
87.2
87.3
87.4
87.5
1000
100
10
1
0.1
F (2-12Å) MILLI-ERG (CM² SEC)⁻¹
0
1
2
3
4
5
6
7
8
9
10
11
12
MAR 28, 1968
UT

Figure 27

BEGIN			PEAK			END			PEAK		TIME									
YY	MON	DD	HH	MM	SS	HH	MM	SS	VALUE	RATIO	GAPS	RISE	DECAY	TOTAL	SUMF	R/D	R/T	D/T	TLOS
67	MAY	25	17	2	53#	17	8	21	17	29	28	2.05	1.589	0	0 5 27	0 21 7	0 26 35	1.782	0.26	0.21	0.79	0.000
67	MAY	25	19	28	34	19	46	31	20	4	42	5.30	2.511	0	0 17 57	0 18 11	0 36 9	6.311	0.99	0.50	0.50	0.000
67	MAY	25	20	47	11	20	54	41	21	20	52	3.67	2.040	0	0 7 30	0 26 11	0 33 41	4.768	0.29	0.22	0.78	0.000
67	MAY	25	22	22	7U	0	8	19U	2	14	24U	4.78	2.339	6D	1 46 12	1 30 38	3 52 17	11.418	1.17	0.46	0.39	0.904
						0	43	46				3.65	2.019									
67	MAY	26	12	35	51	12	40	58	12	52	29	8.94	3.401	0	0 5 7	0 11 31	0 16 38	5.937	0.44	0.31	0.69	0.000
67	MAY	26	13	37	15	14	30	3U	21	51	2U	6.55	2.783	14B	0 52 48	5 34 38	8 13 47	187.896	0.16	0.11	0.68	0.346
						16	16	24				12.53	4.453									
67	MAY	27	0	40	18U	1	57	15U	4	32	49U	8.85	3.723	4R	1 16 57	2 35 34	3 52 31	11.700	0.49	0.33	0.67	0.800
67	MAY	27	5	14	0U	5	43	35U	6	23	12	10.50	4.199	5D	0 29 35	0 39 37	1 9 13	10.387	0.75	0.43	0.57	0.821
67	MAY	27	11	53	48U	12	35	22	15	50	6	2.25	1.722	10B	0 41 34	0 25 40	3 56 18	13.986	1.62	0.18	0.11	0.273
						13	38	6				2.40	1.773									
						15	24	26				1.93	1.622									
67	MAY	27	23	3	49	23	16	13	23	30	54U	4.31	2.407	2D	0 12 25	0 14 40	0 27 5	3.617	0.85	0.46	0.54	0.334
67	MAY	28	0	27	51	0	38	2U	0	50	2	24.78	9.108	2D	0 10 11	0 12 0	0 22 11	17.606	0.85	0.46	0.54	0.445
67	MAY	28	5	40	5U	5	51	38	6	20	43U	333.70	110.632	3R	0 11 33	0 29 5	0 40 37	478.266	0.40	0.28	0.72	0.333
67	MAY	28	7	21	37#	7	57	4	9	44	58	11.57	4.697	6B	0 35 27	1 47 53	2 23 20	50.090	0.33	0.25	0.75	0.359
67	MAY	28	21	31	3	22	7	54	3	26	12	2.67	1.746	13B	0 36 51	3 7 24	5 55 9	21.333	0.20	0.10	0.53	0.282
						0	18	48				2.54	1.849									
67	MAY	29	4	16	58U	5	2	25U	5	31	27U	2.21	1.762	4	0 45 27	0 29 2	1 14 29	0.877	1.57	0.61	0.39	1.000
67	MAY	29	9	36	32	9	40	34U	9	53	6	1.62	1.576	1	0 4 2	0 12 33	0 16 35	0.480	0.32	0.24	0.76	0.571
67	MAY	29	14	19	36	14	29	38	14	49	29	1.38	1.549	0	0 10 2	0 19 51	0 29 54	1.480	0.51	0.34	0.66	0.000
67	MAY	29	14	59	54	15	2	21	15	9	50	1.73	1.688	0	0 2 27	0 7 29	0 9 56	0.643	0.33	0.25	0.75	0.000
67	MAY	29	18	51	53	19	7	47	19	45	19	3.50	2.389	1D	0 15 54	0 37 33	0 53 26	6.779	0.42	0.30	0.70	0.100
67	MAY	29	21	11	51	22	18	40	22	38	28	3.11	2.236	1R	1 6 49	0 19 48	1 26 37	5.981	3.37	0.77	0.23	0.152
67	MAY	29	22	45	43#	23	18	40	0	11	2	3.19	2.266	2B	0 32 56	0 52 22	1 25 18	6.626	0.63	0.39	0.61	0.152
67	MAY	30	2	24	35	2	29	34	2	38	57U	1.33	1.529	1	0 4 58	0 9 23	0 14 21	0.967	0.53	0.35	0.65	0.286
67	MAY	30	4	8	6	4	21	22	10	23	50	2.45	1.971	11D	0 13 16	1 37 57	6 15 44	22.804	0.14	0.04	0.26	0.275
						8	45	53				4.15	2.647									
67	MAY	30	17	27	56	17	34	55	17	53	53	6.14	3.313	0	0 6 59	0 18 58	0 25 57	5.892	0.37	0.27	0.73	0.000

Figure 28

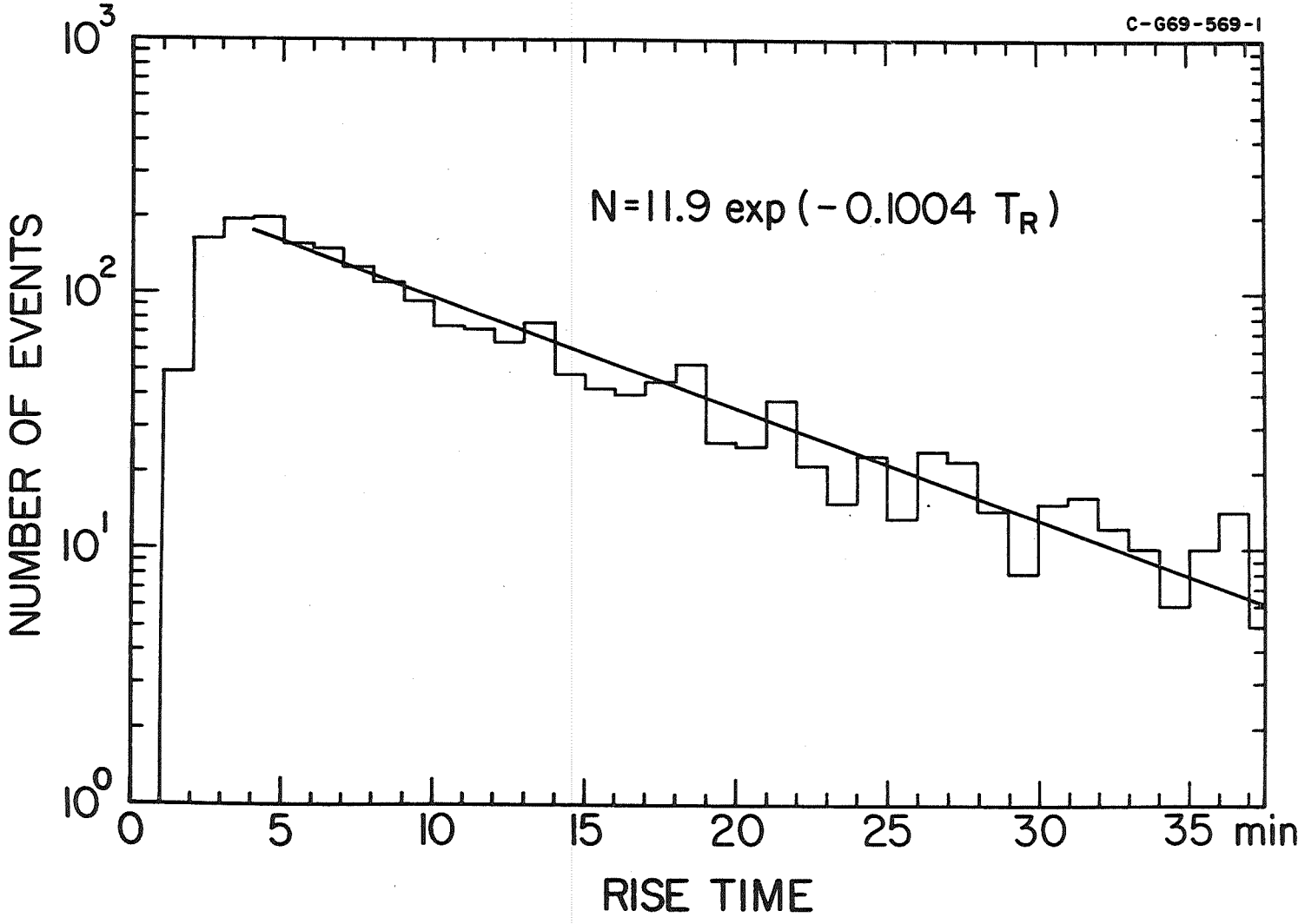
C-G69-569-1
10^3
10^2
10^1
10^0
NUMBER OF EVENTS
N=11.9 exp (-0.1004 T_R)
0
5
10
15
20
25
30
35 min
RISE TIME

Figure 29

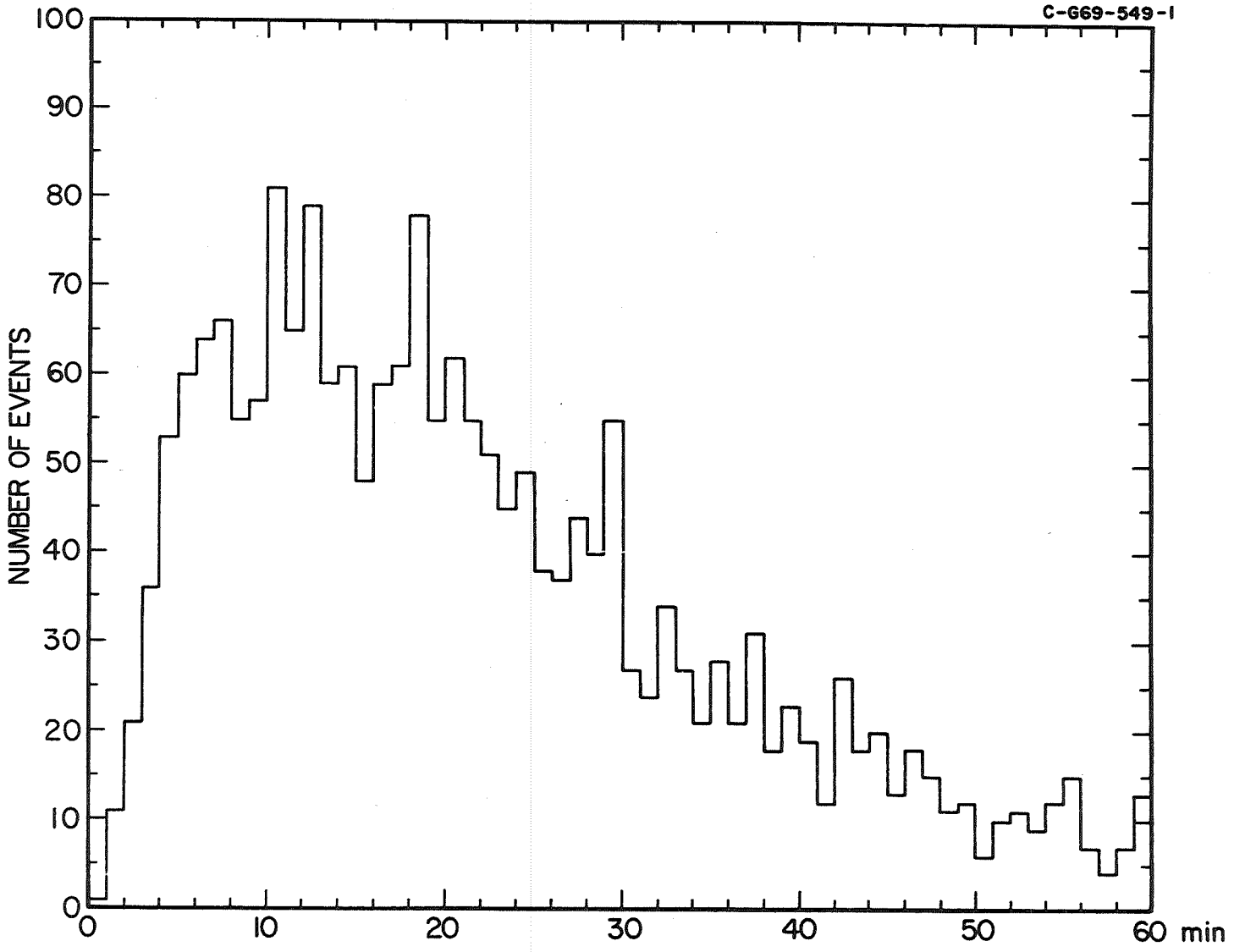
C-G69-549-1
NUMBER OF EVENTS
0
10
20
30
40
50
60
70
80
90
100
0
10
20
30
40
50
60 min
DECAY TIME
Figure 30

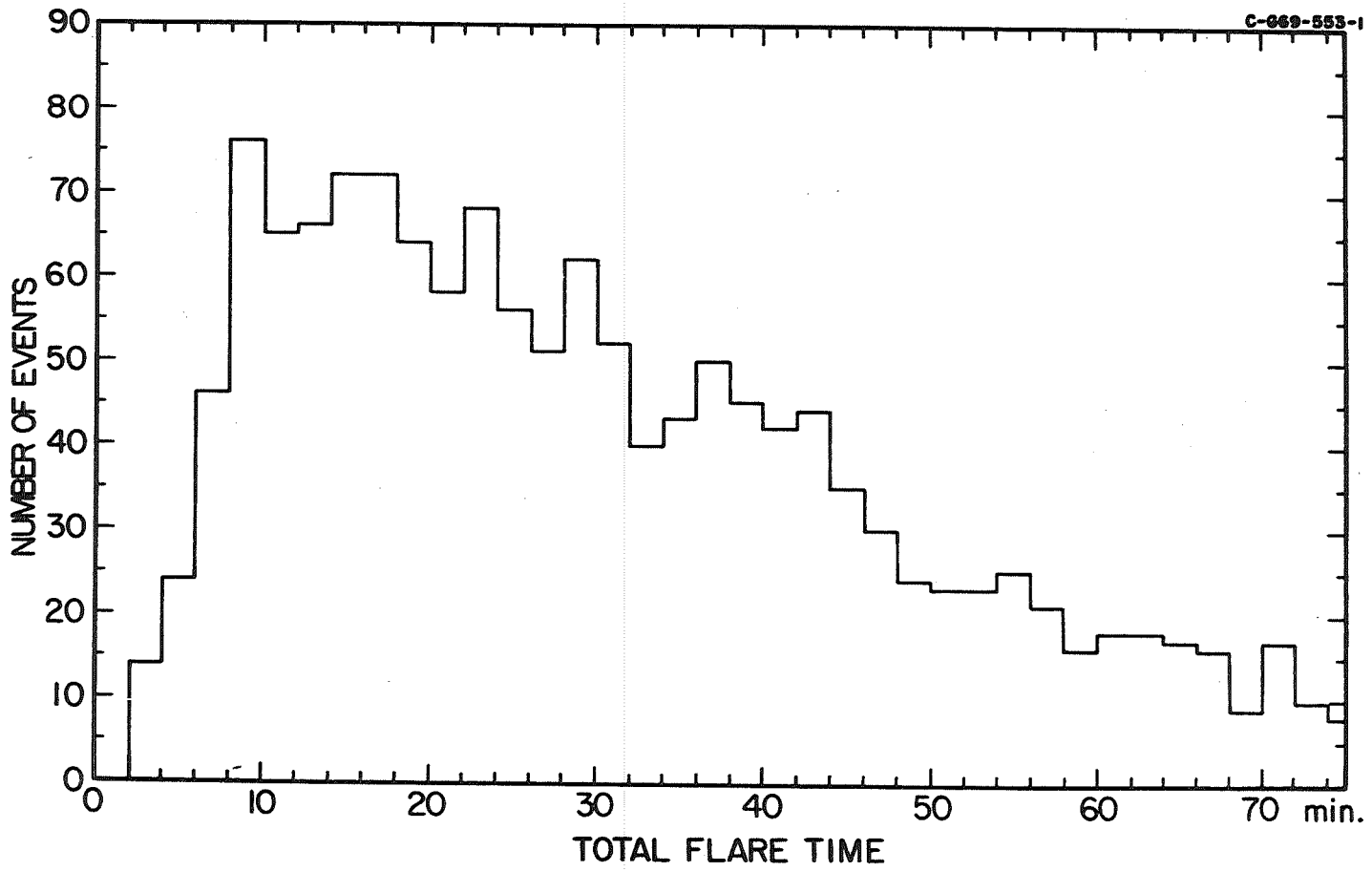
C-669-553-1
NUMBER OF EVENTS
0
10
20
30
40
50
60
70
80
90
0
10
20
30
40
50
60
70 min.
TOTAL FLARE TIME

Figure 31

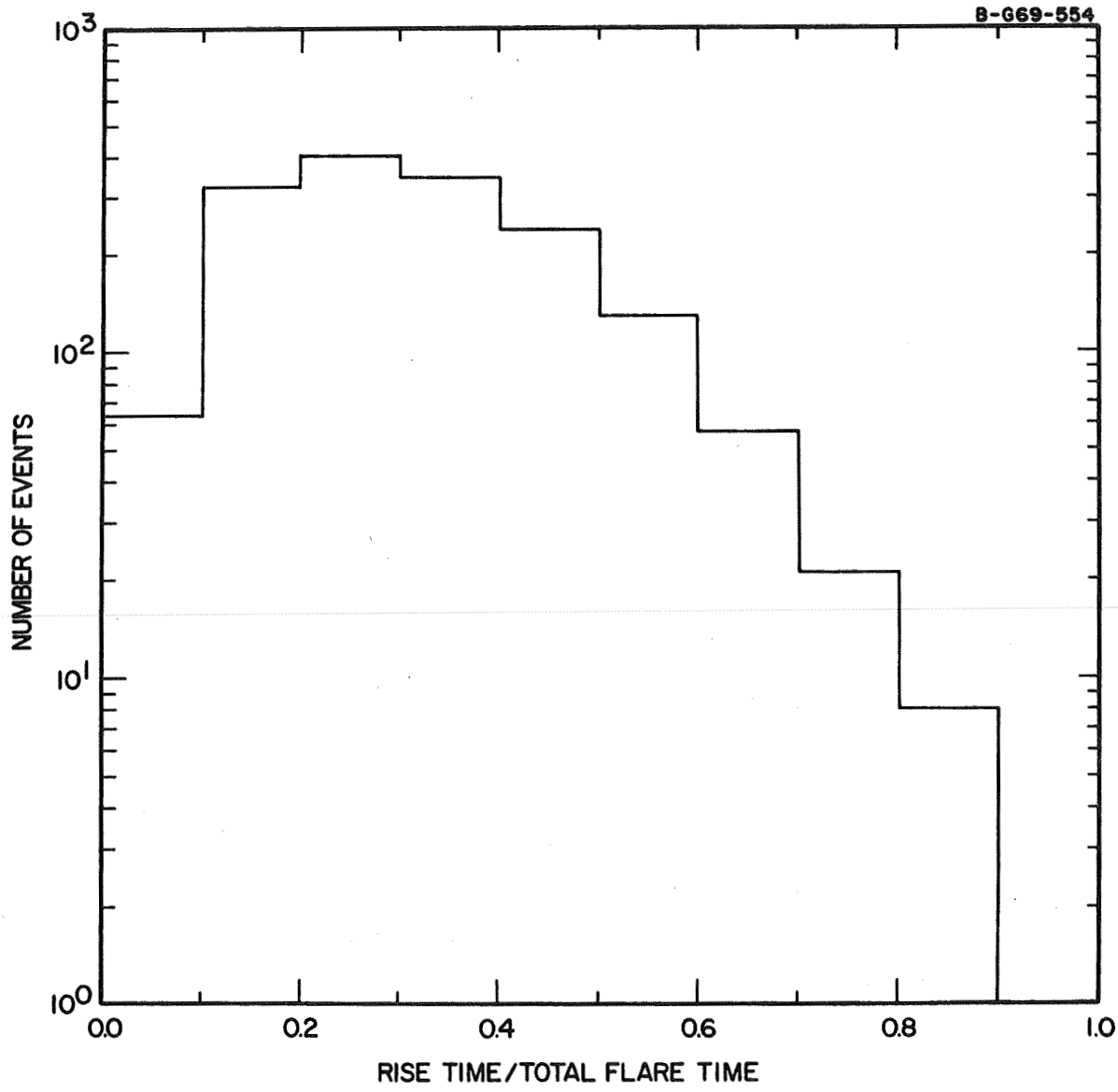
B-G69-554
10^3
10^2
10^1
10^0
NUMBER OF EVENTS
0.0
0.2
0.4
0.6
0.8
1.0
RISE TIME/TOTAL FLARE TIME

Figure 32

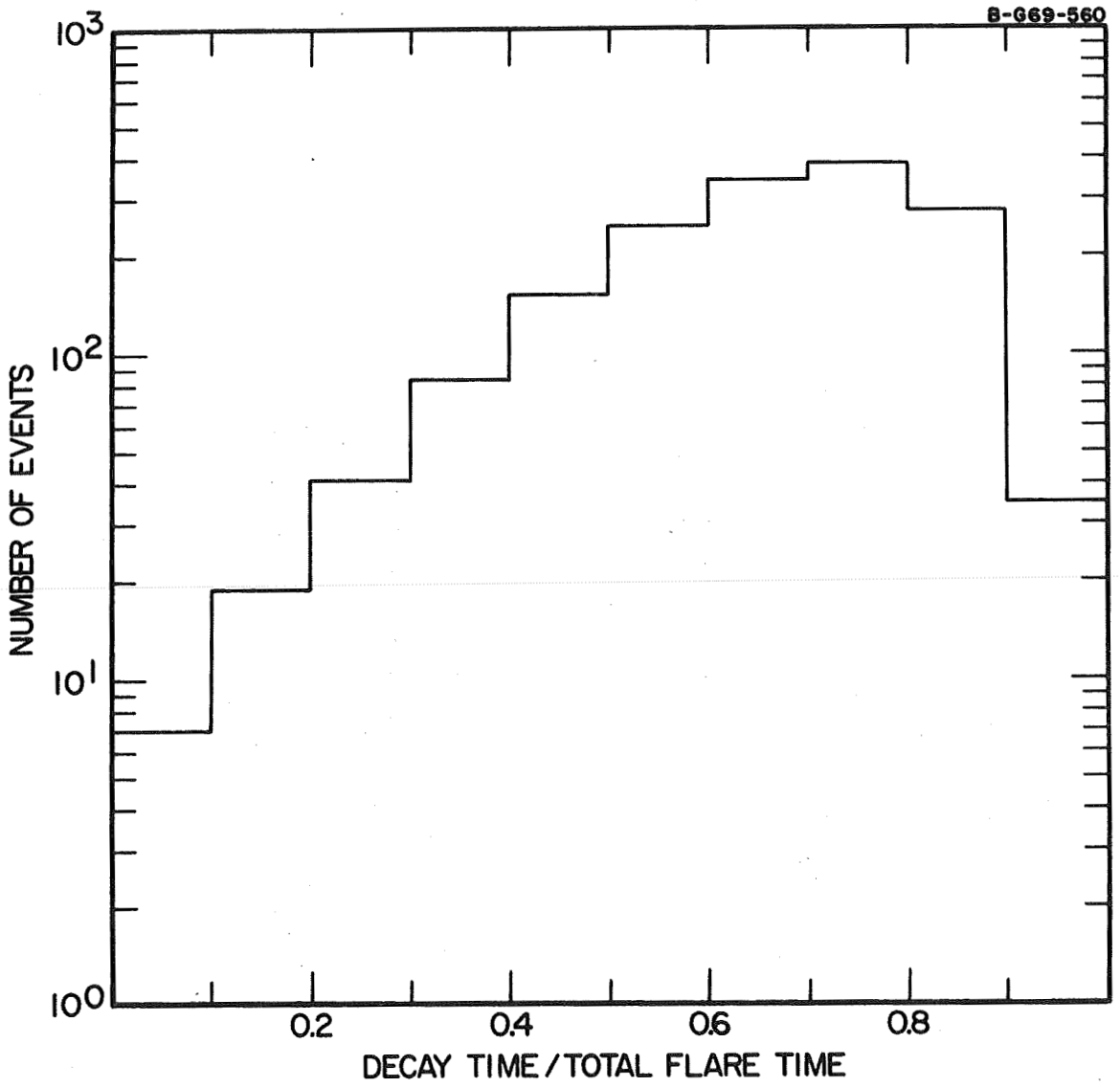
B-G69-560
10^3
10^2
10^1
10^0
NUMBER OF EVENTS
0.2
0.4
0.6
0.8
DECAY TIME / TOTAL FLARE TIME

Figure 33

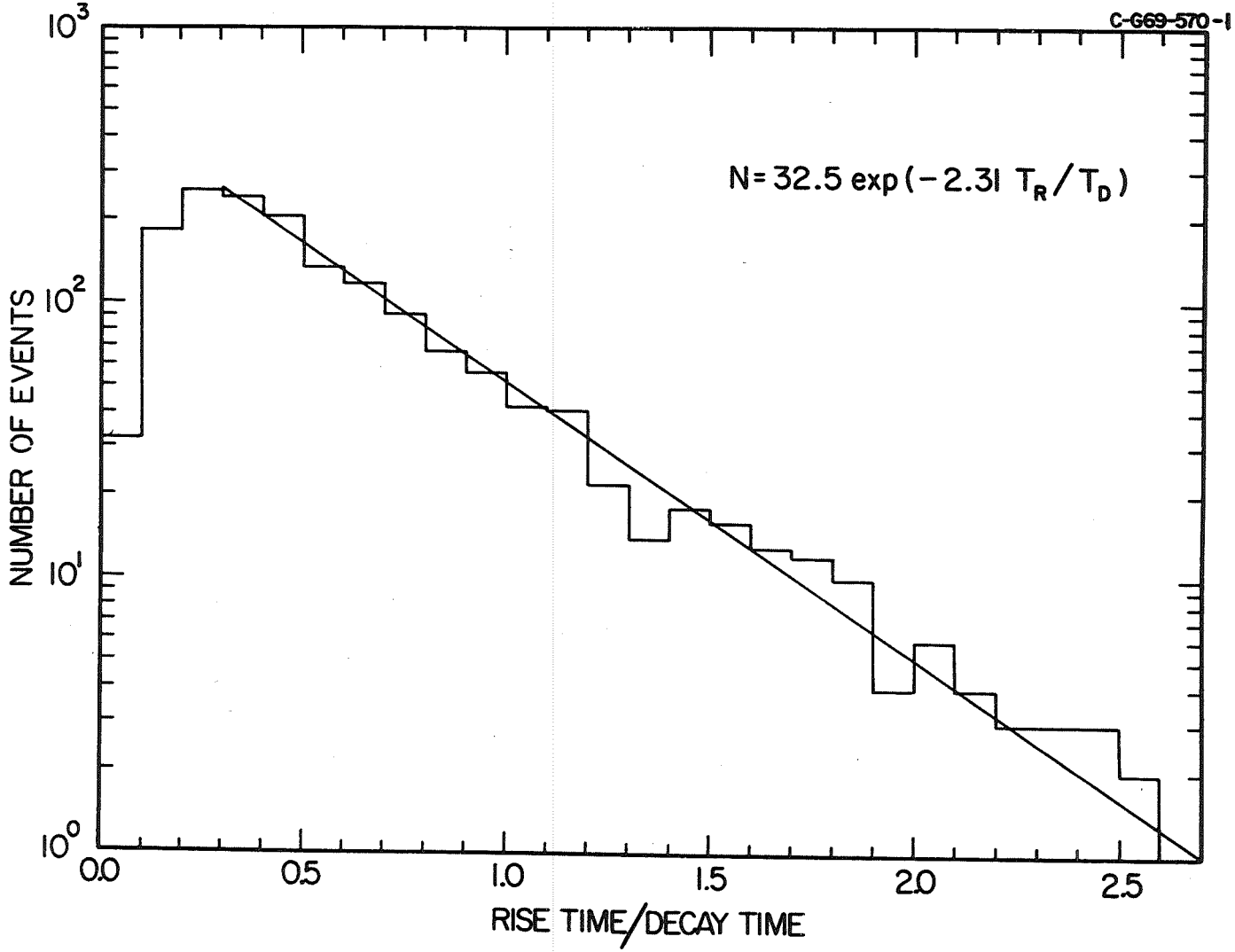
C-669-570-1
10^3
10^2
10^1
10^0
NUMBER OF EVENTS
N = 32.5 exp (−2.31 T_R / T_D)
0.0
0.5
1.0
1.5
2.0
2.5
RISE TIME/DECAY TIME

Figure 34

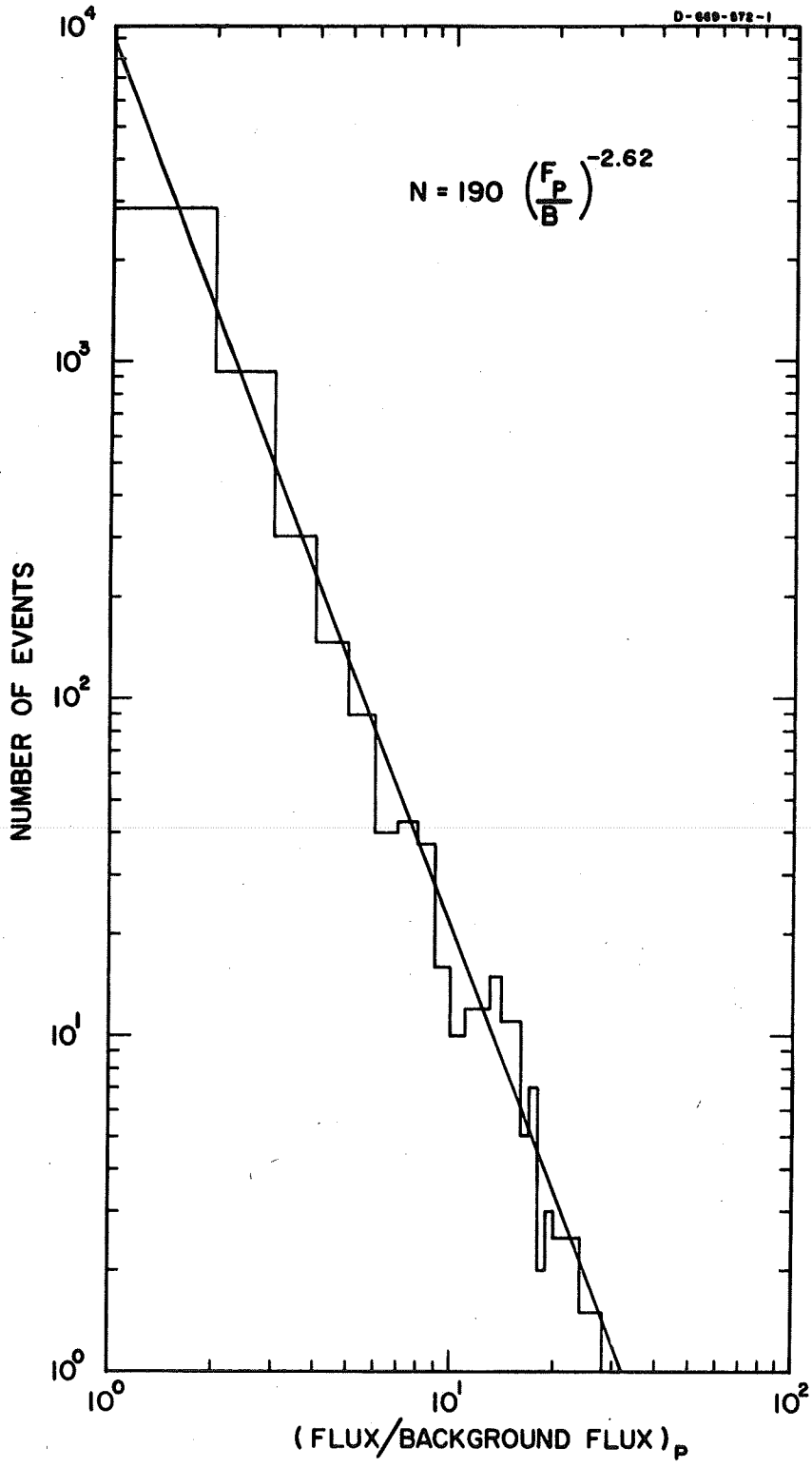
D-669-672-1
10^4
10^3
10^2
10^1
10^0
$N = 190 \left(\frac{F_P}{B}\right)^{-2.62}$
NUMBER OF EVENTS
10^0
10^1
10^2
(FLUX/BACKGROUND FLUX)$_P$

Figure 35

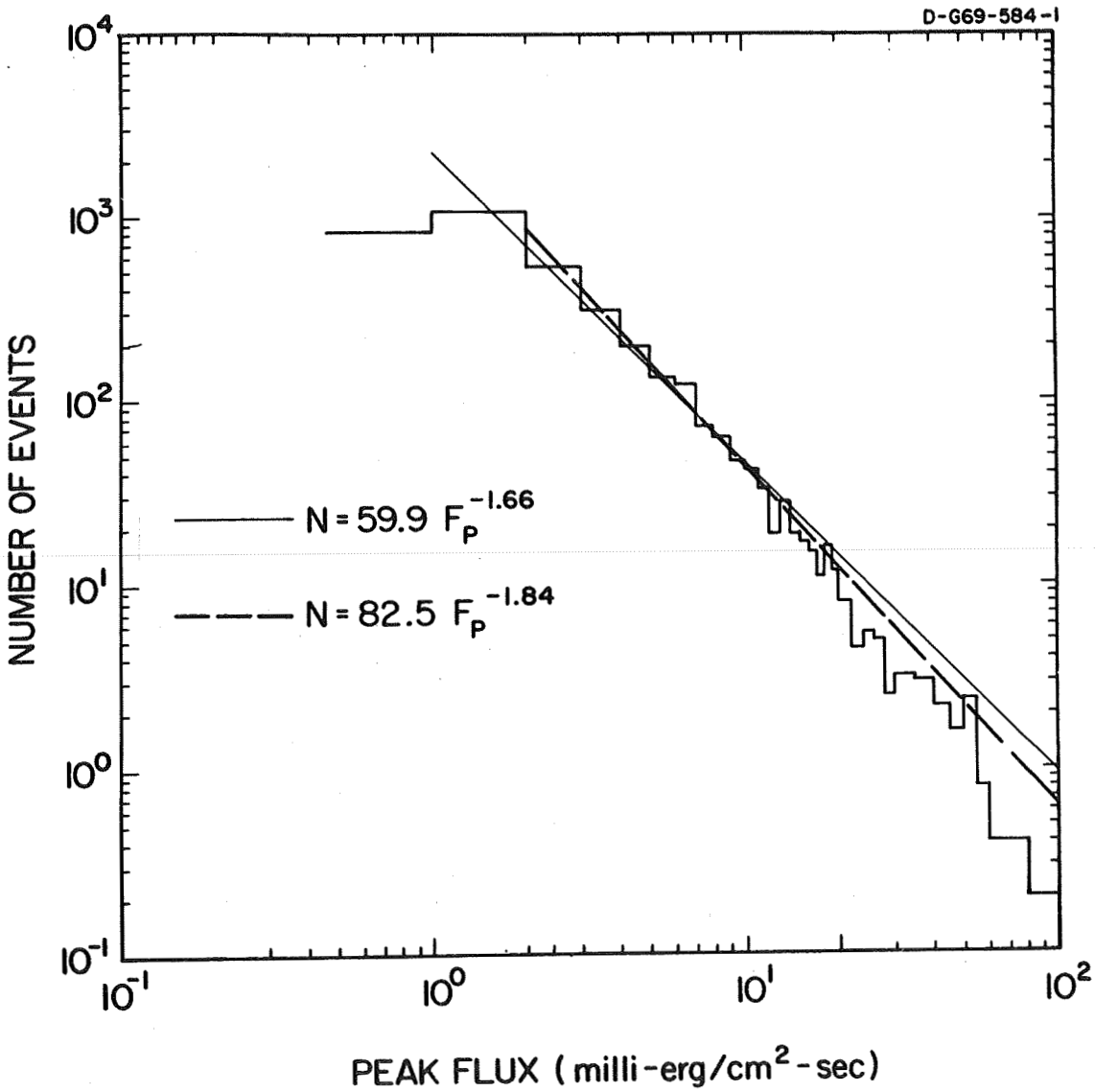
D-G69-584-1
NUMBER OF EVENTS
PEAK FLUX (milli-erg/cm^2-sec)
N = 59.9 $F_P^{-1.66}$
N = 82.5 $F_P^{-1.84}$
10^4
10^3
10^2
10^1
10^0
10^{-1}
10^{-1}
10^0
10^1
10^2

Figure 36

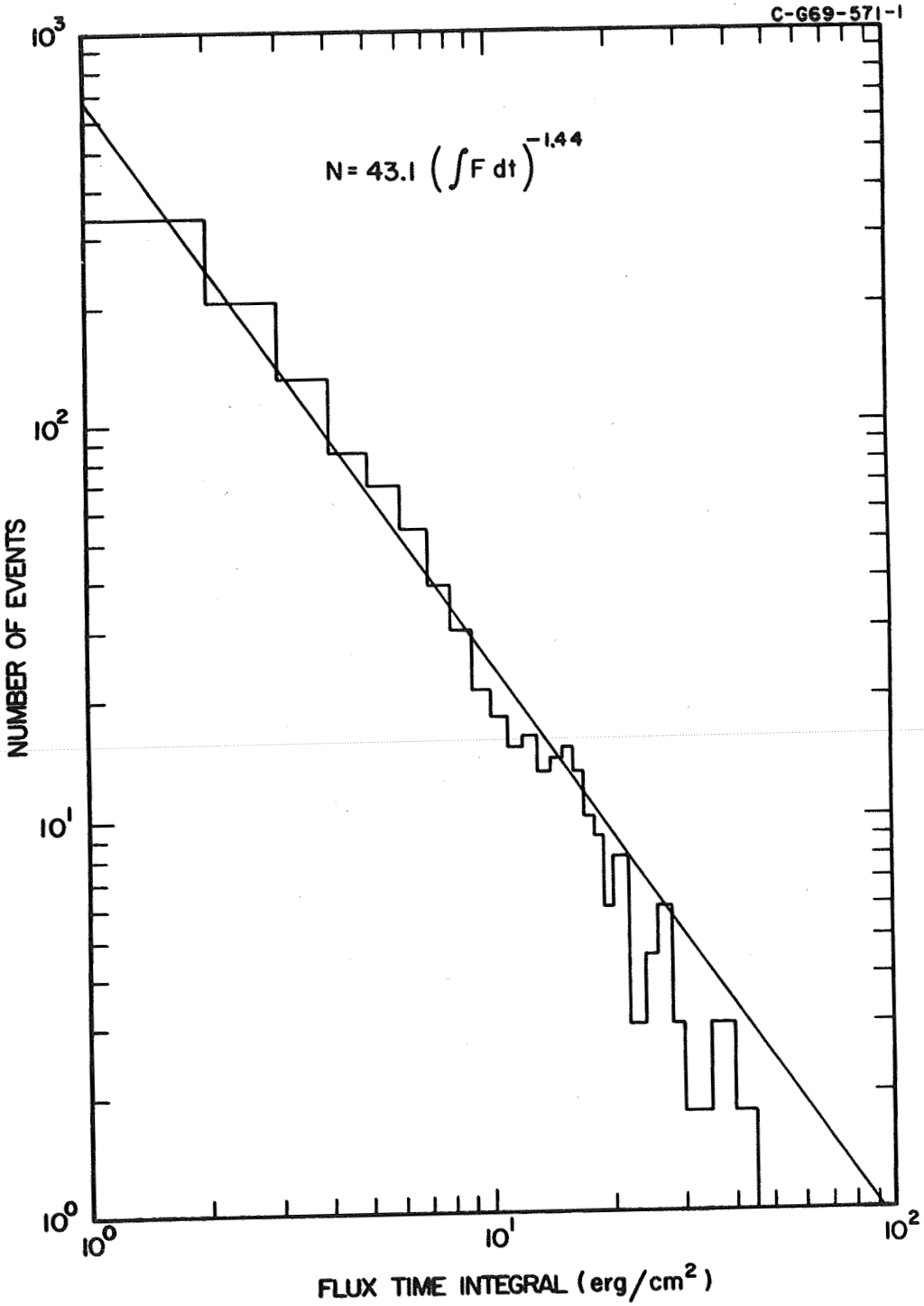
C-G69-571-1
10^3
10^2
10^1
10^0
$N = 43.1 \left(\int F\,dt\right)^{-1.44}$
NUMBER OF EVENTS
10^0
10^1
10^2
FLUX TIME INTEGRAL (erg/cm^2)

Figure 37

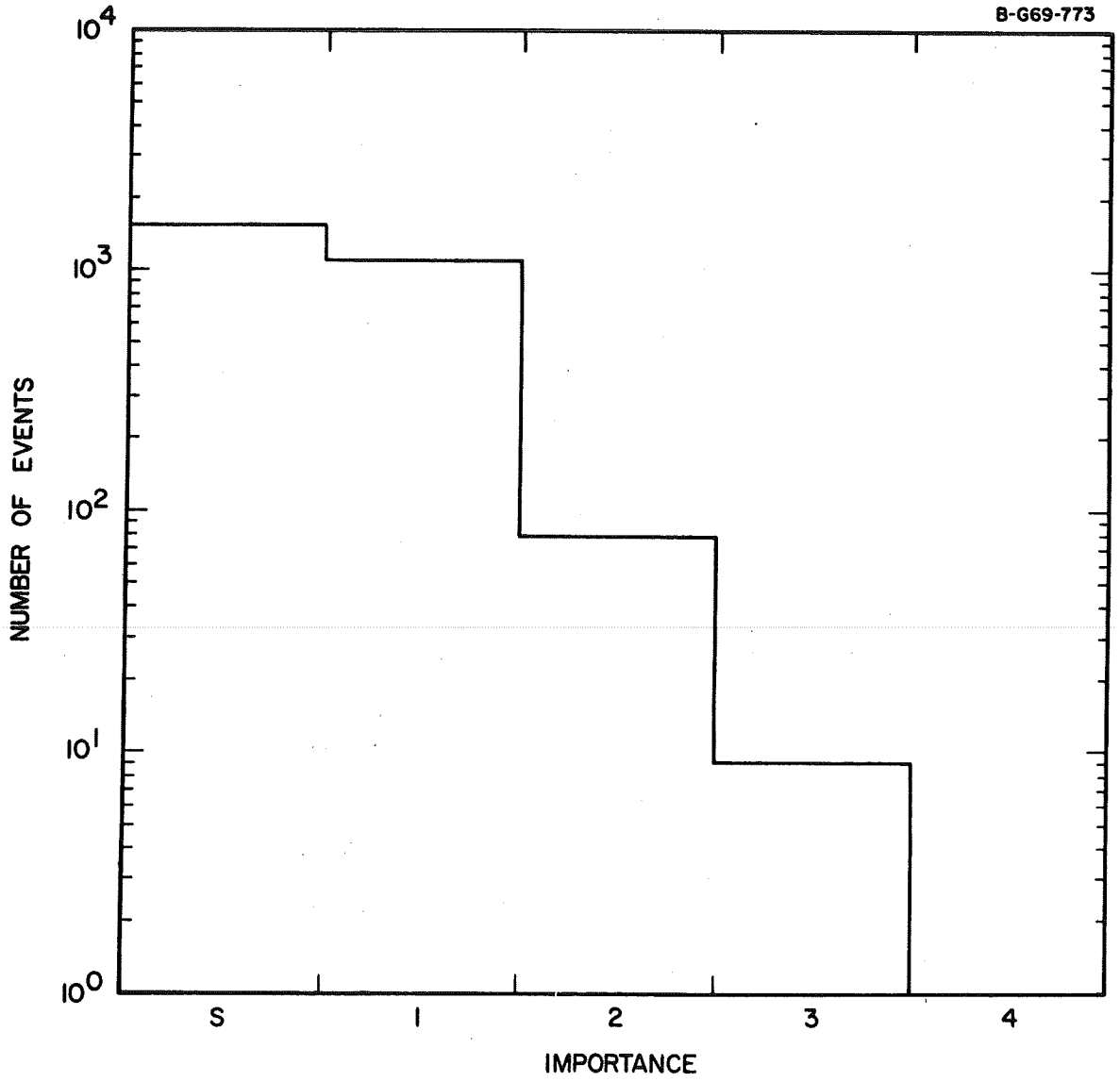
B-G69-773
10^4
10^3
10^2
10^1
10^0
NUMBER OF EVENTS
S
1
2
3
4
IMPORTANCE

Figure 38

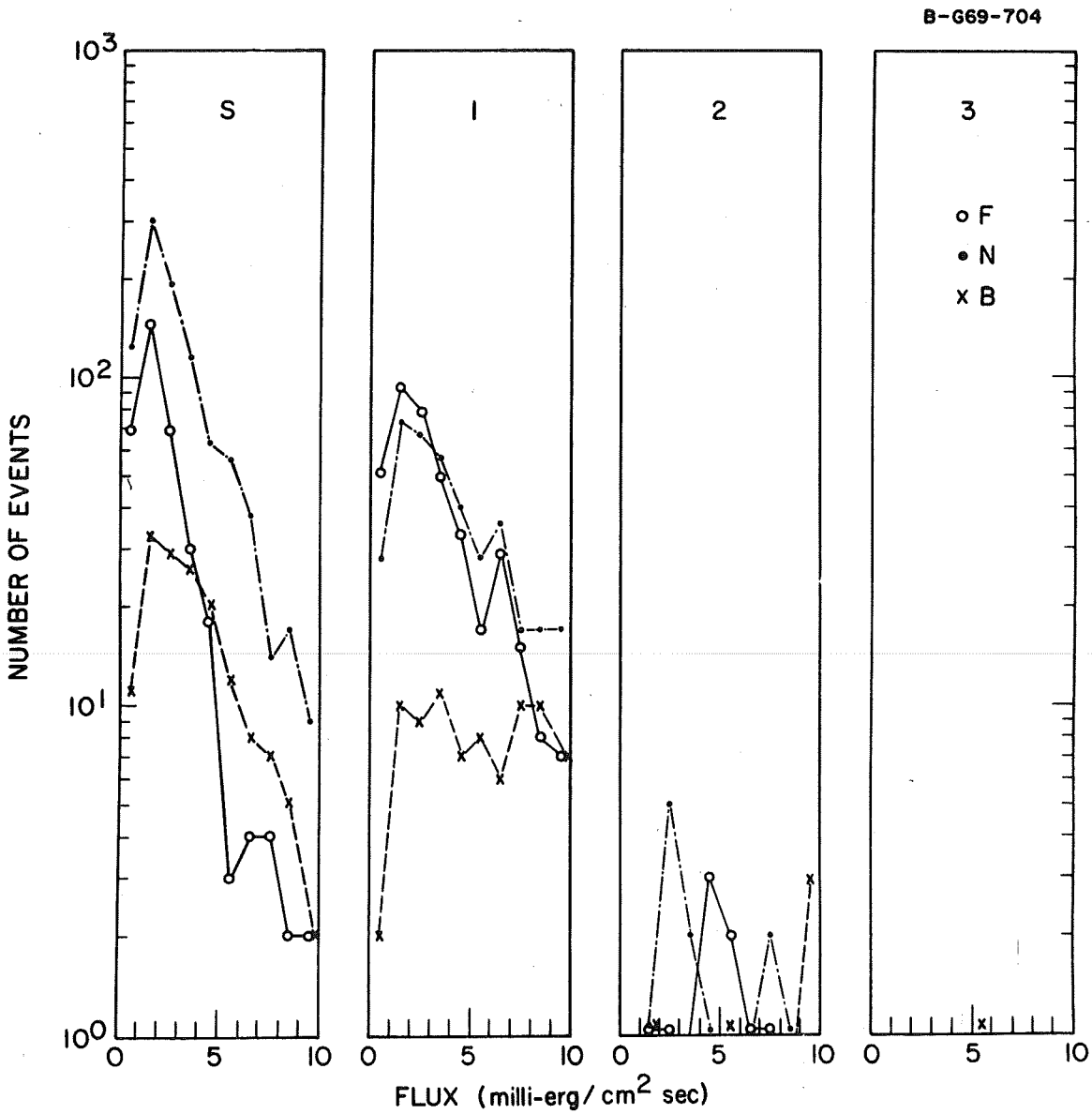
B-G69-704
S
1
2
3
o F
• N
x B
NUMBER OF EVENTS
10^3
10^2
10^1
10^0
0
5
10
FLUX (milli-erg/ cm^2 sec)

Figure 39

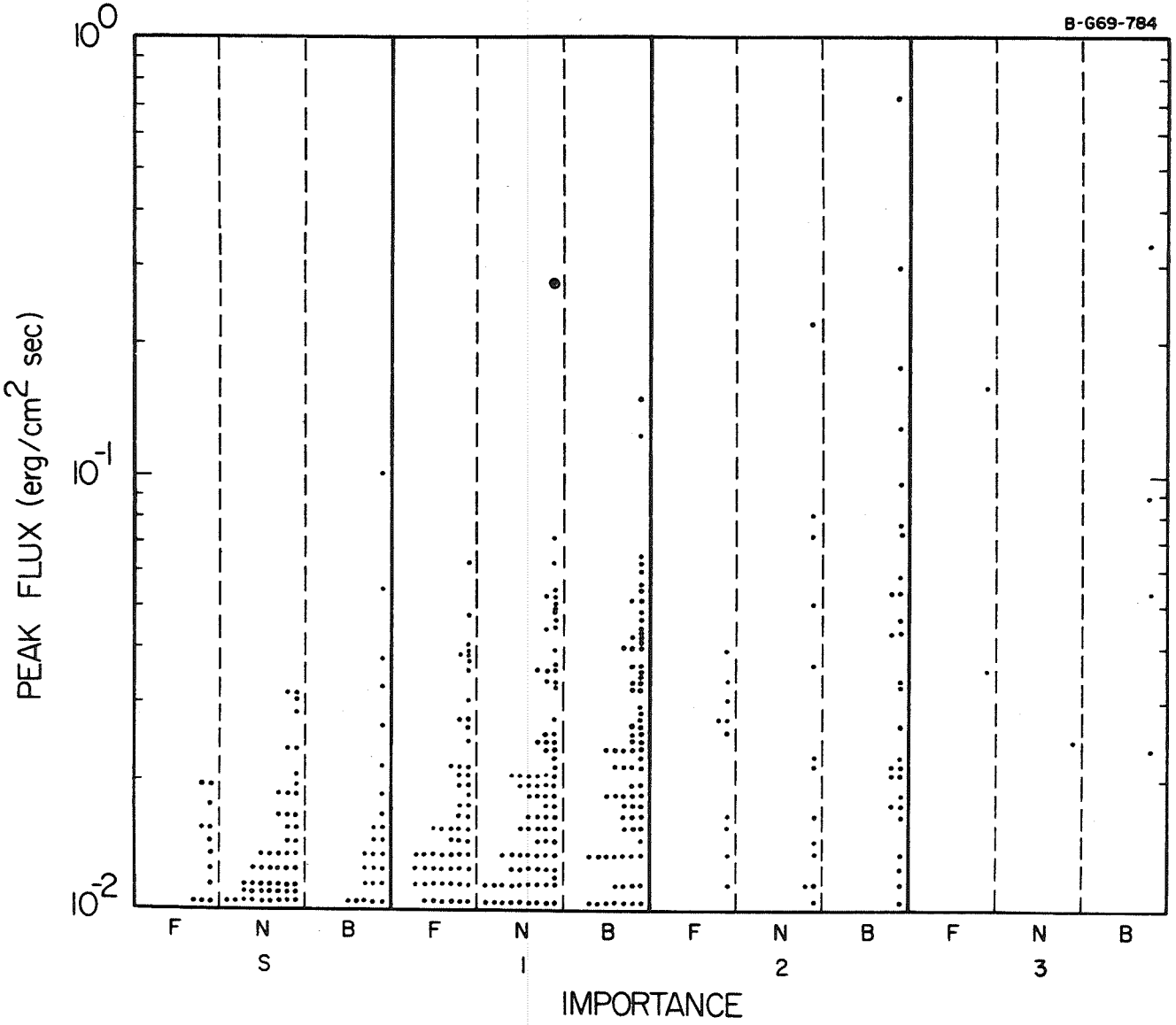
B-669-784
10^0
10^{-1}
10^{-2}
PEAK FLUX (erg/cm^2 sec)
F N B F N B F N B F N B
S 1 2 3
IMPORTANCE

Figure 40

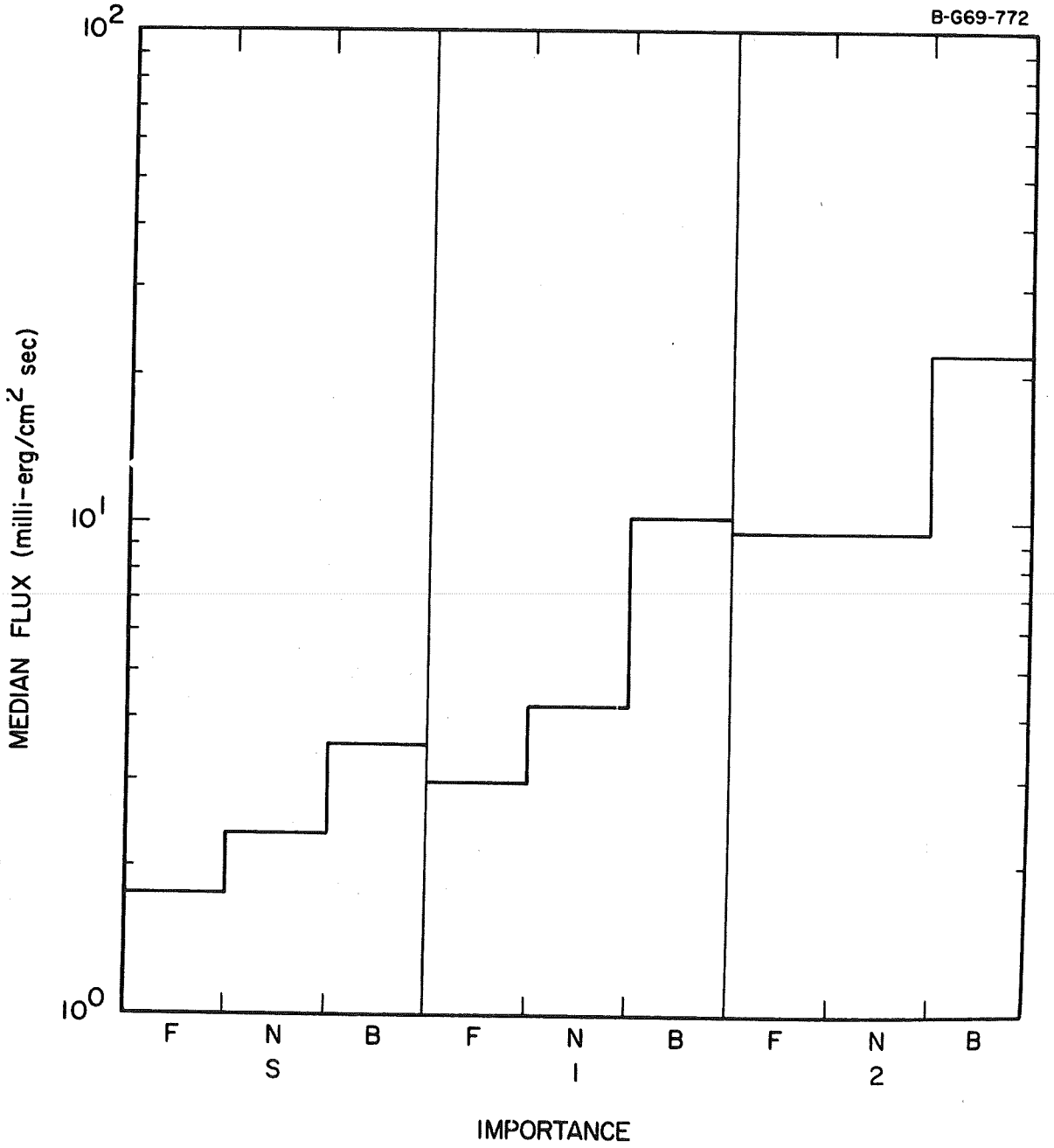
B-G69-772
10^2
10^1
10^0
MEDIAN FLUX (milli-erg/cm^2 sec)
F
N
S
B
F
N
I
B
F
N
2
B
IMPORTANCE

Figure 41

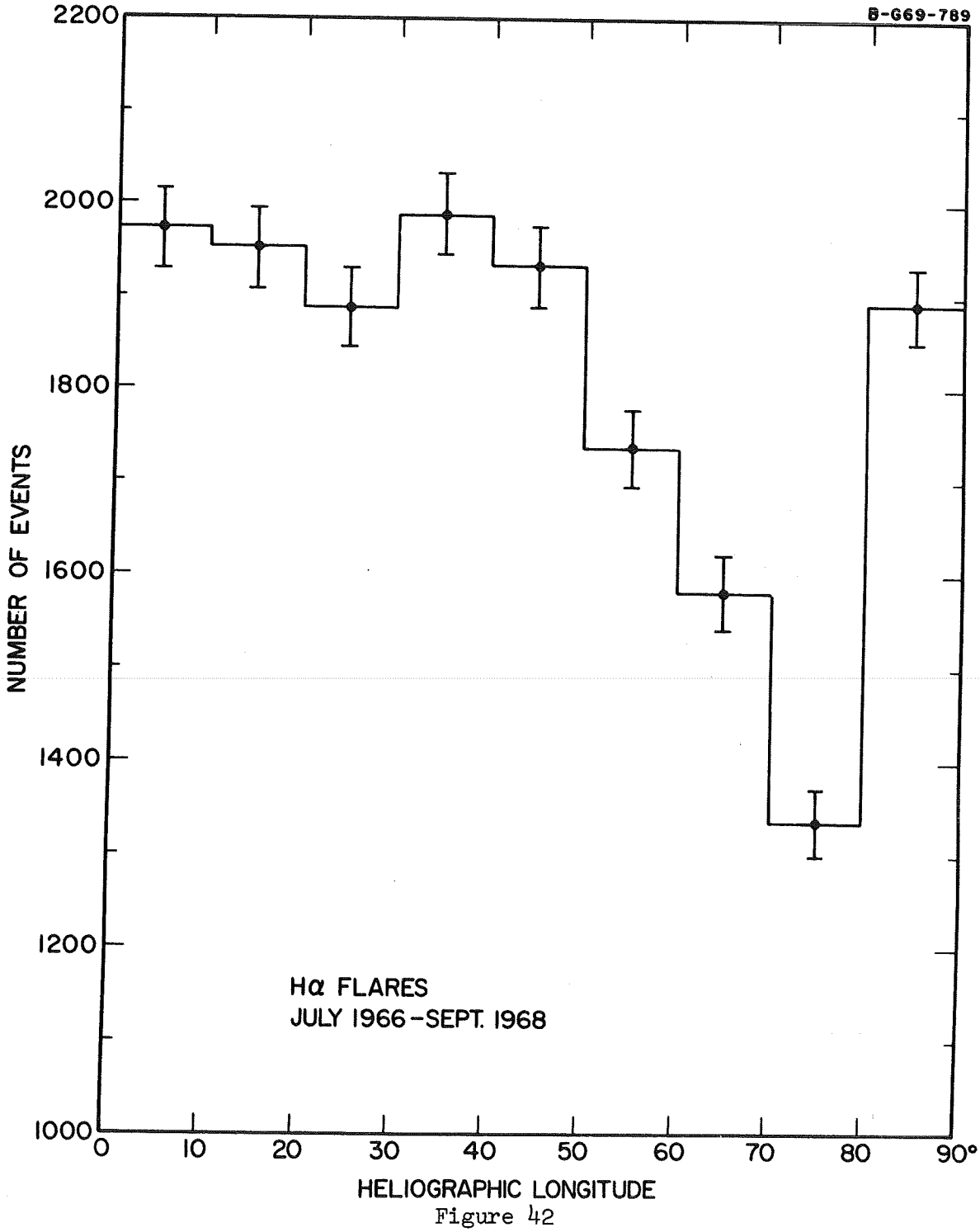
B-669-789
2200
2000
1800
1600
1400
1200
1000
NUMBER OF EVENTS
Hα FLARES
JULY 1966 - SEPT. 1968
0
10
20
30
40
50
60
70
80
90°
HELIOGRAPHIC LONGITUDE

Figure 42

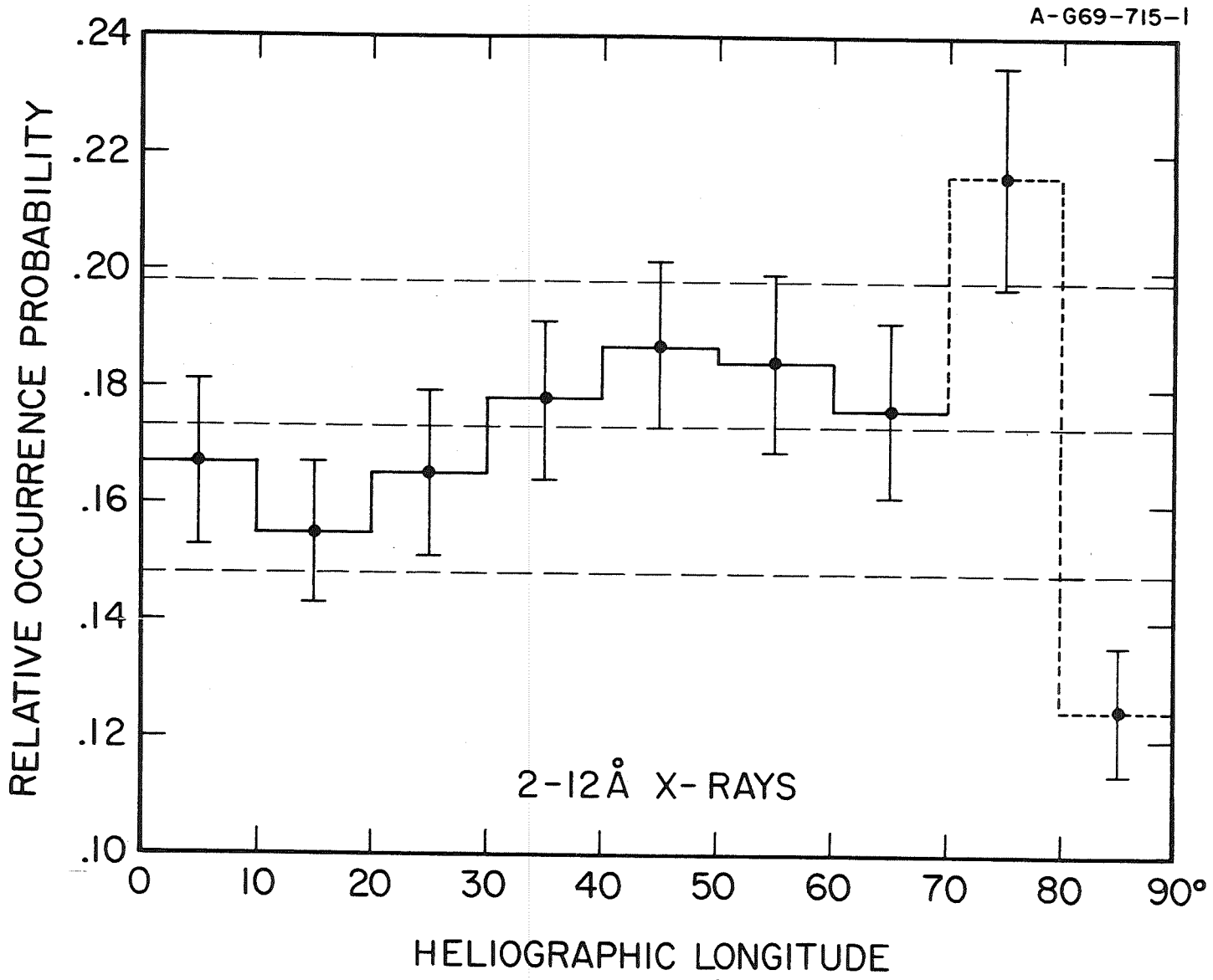
A-G69-715-1
.24
.22
.20
.18
.16
.14
.12
.10
RELATIVE OCCURRENCE PROBABILITY
2-12Å X-RAYS
0
10
20
30
40
50
60
70
80
90°
HELIOGRAPHIC LONGITUDE

Figure 43

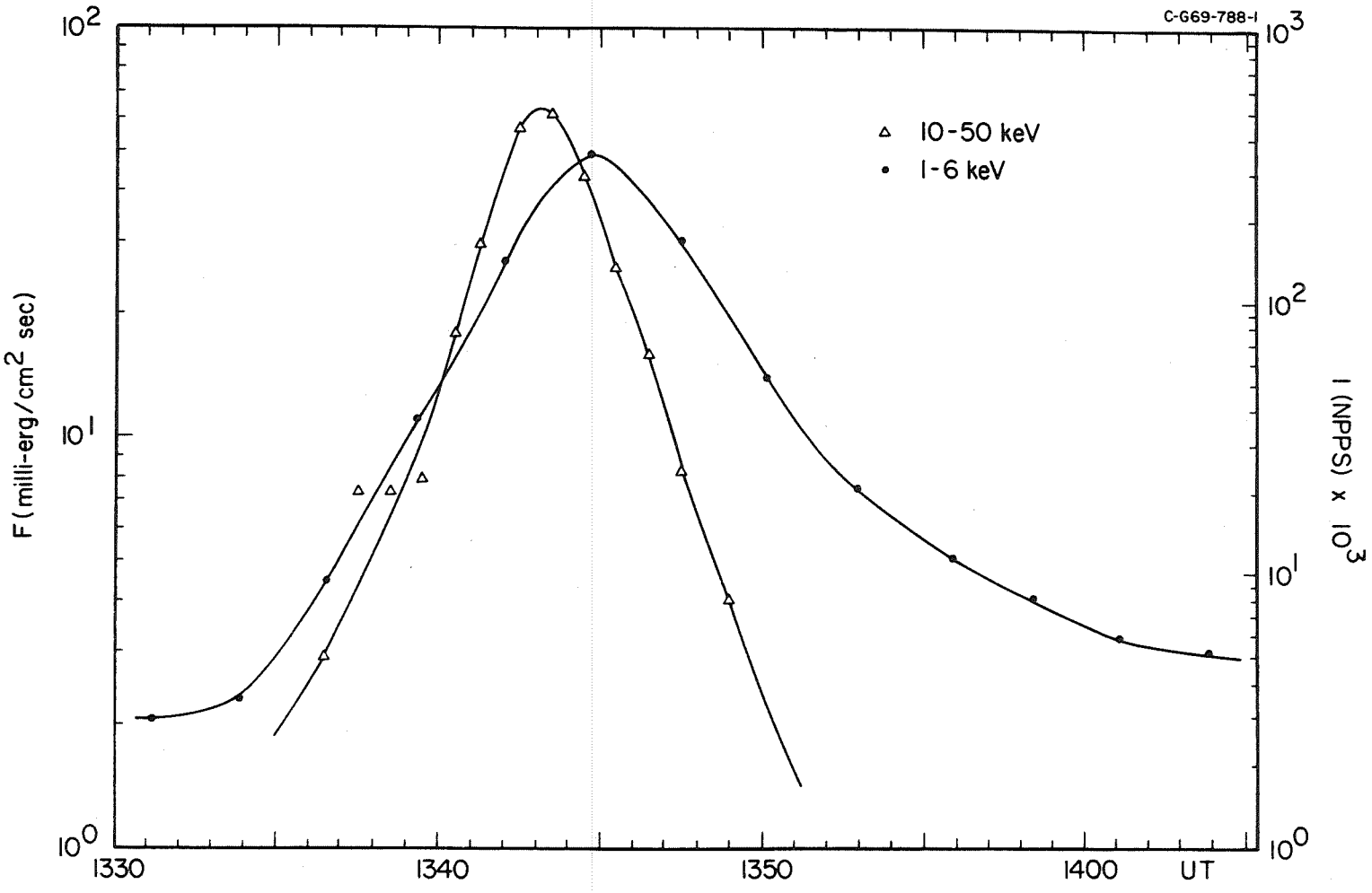
C-G69-788-I
10-50 keV
1-6 keV
F (milli-erg/cm2 sec)
I (NPPS) x 10^3
10^2
10^1
10^0
10^3
1330
1340
1350
1400
UT
13 OCTOBER 1966

Figure 44

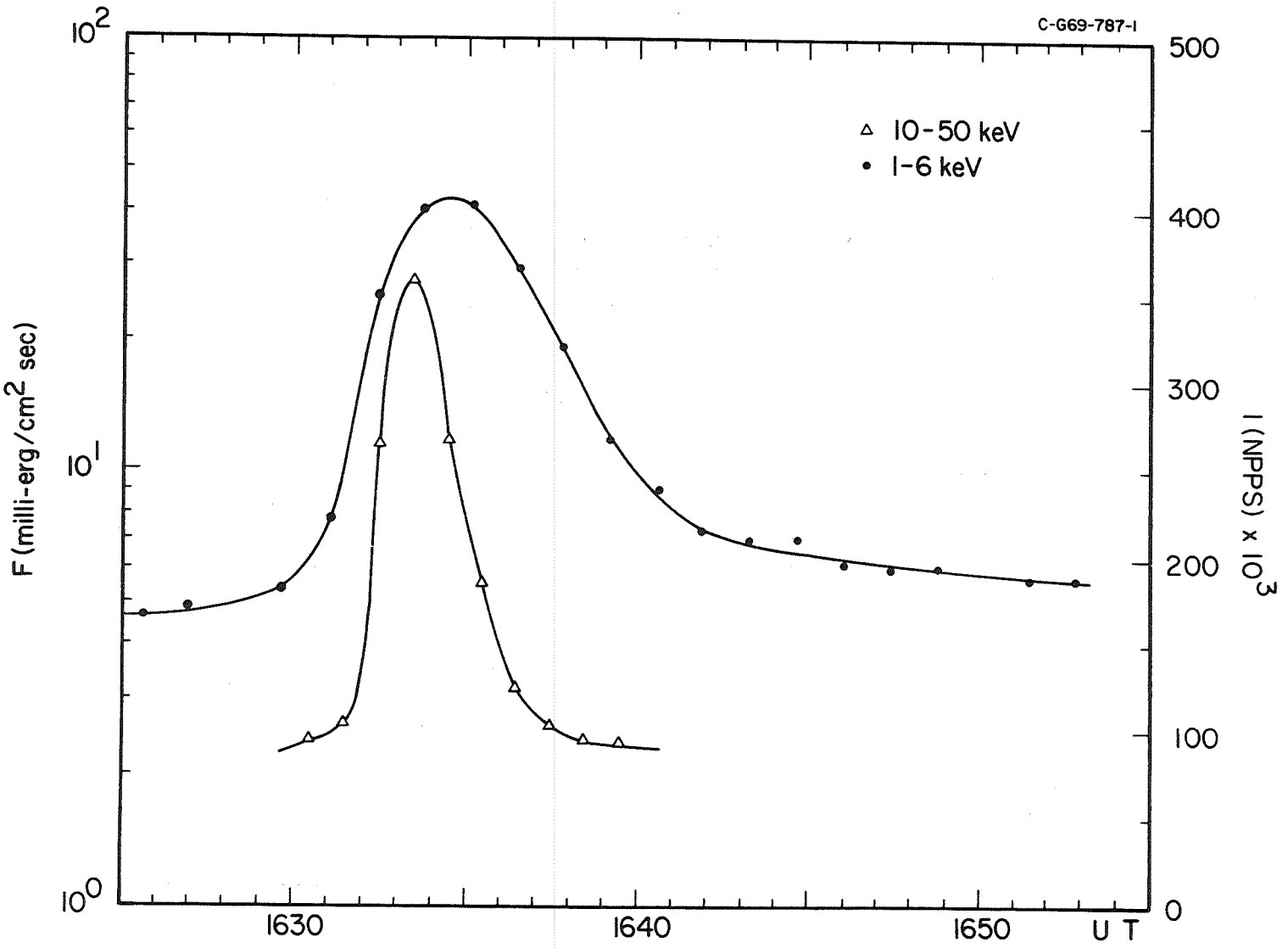

3 AUGUST 1967

Figure 45

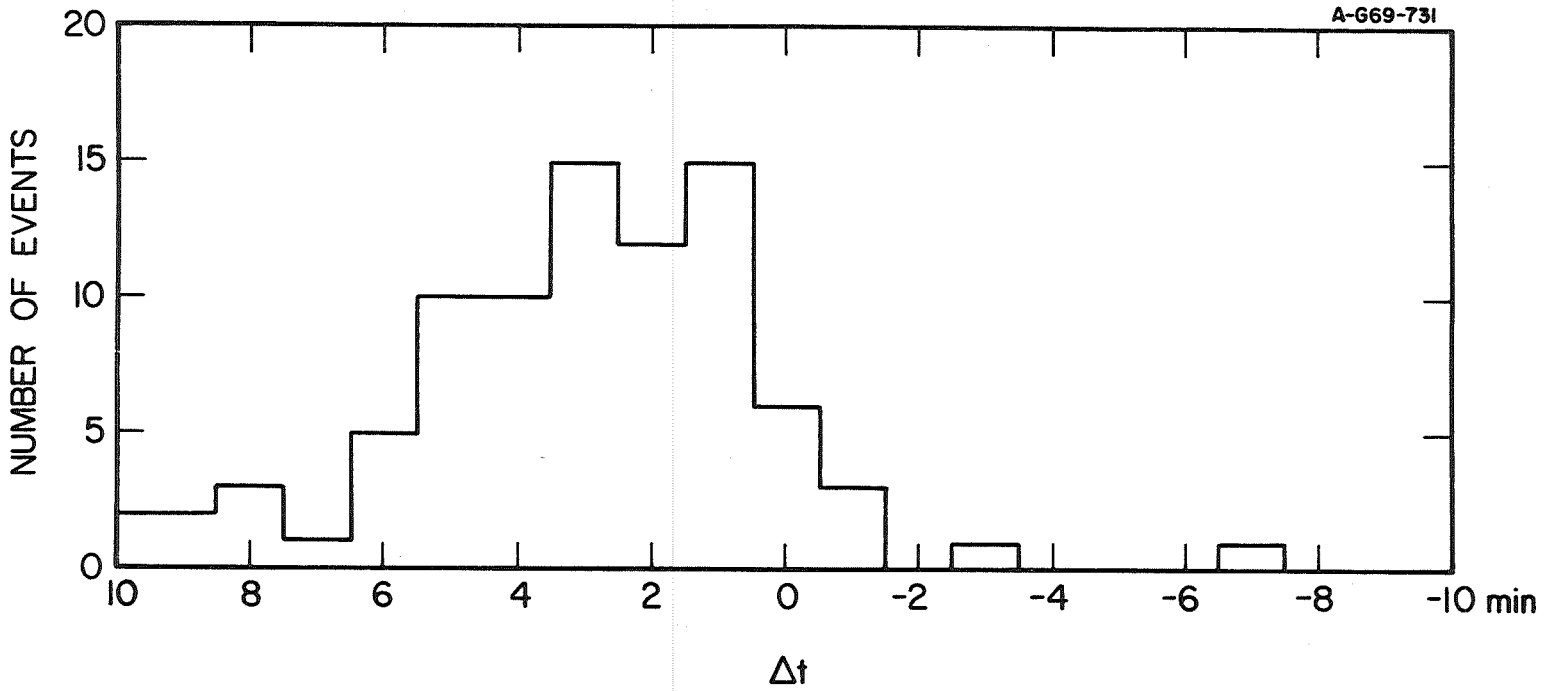

Figure 46

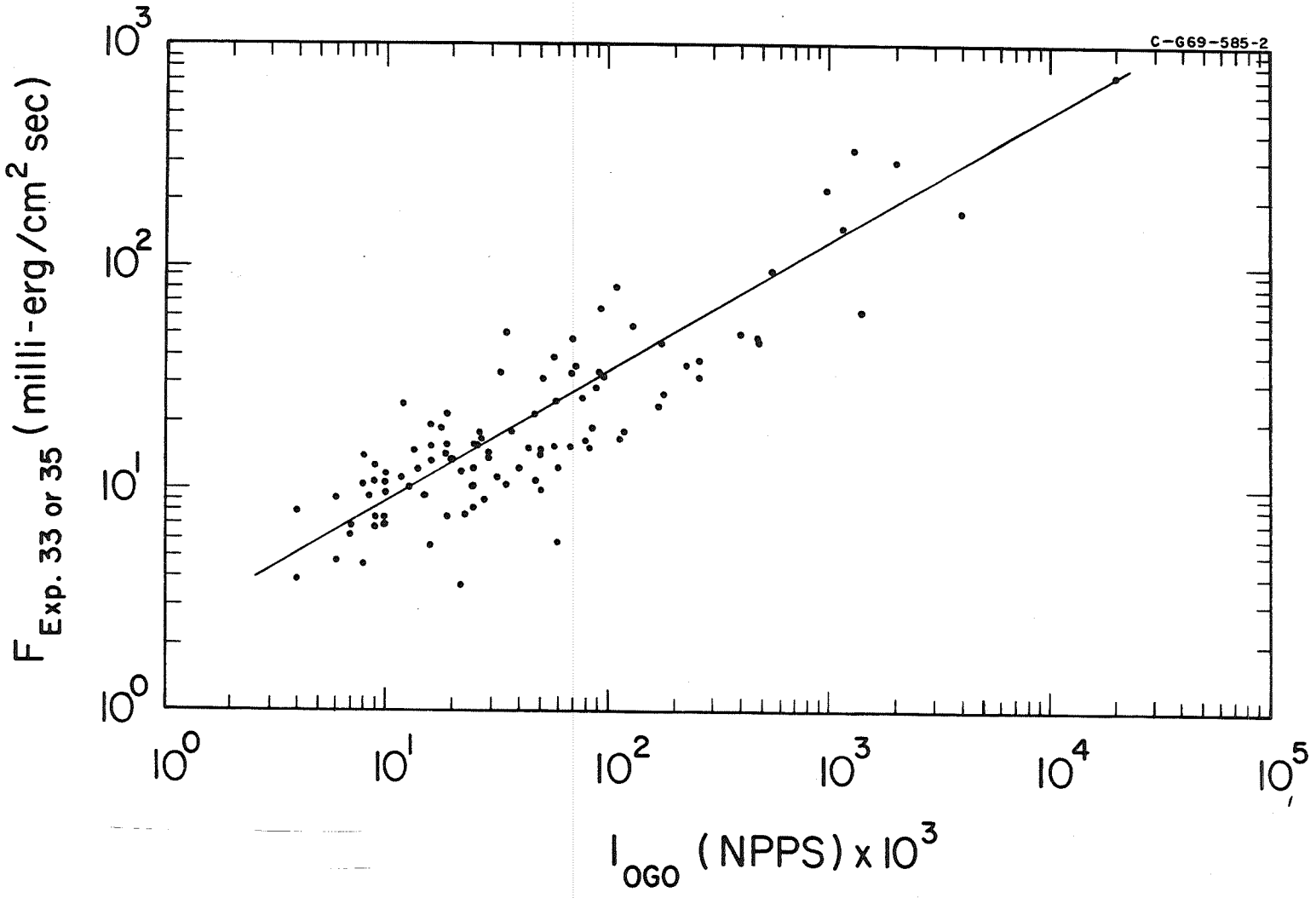
C-G69-585-2
$F_{Exp.\ 33\ or\ 35}$ (milli-erg/cm^2 sec)
10^3
10^2
10^0
10^0
10^1
10^2
10^3
10^4
10^5
I_{OGO} (NPPS) x 10^3

Figure 47

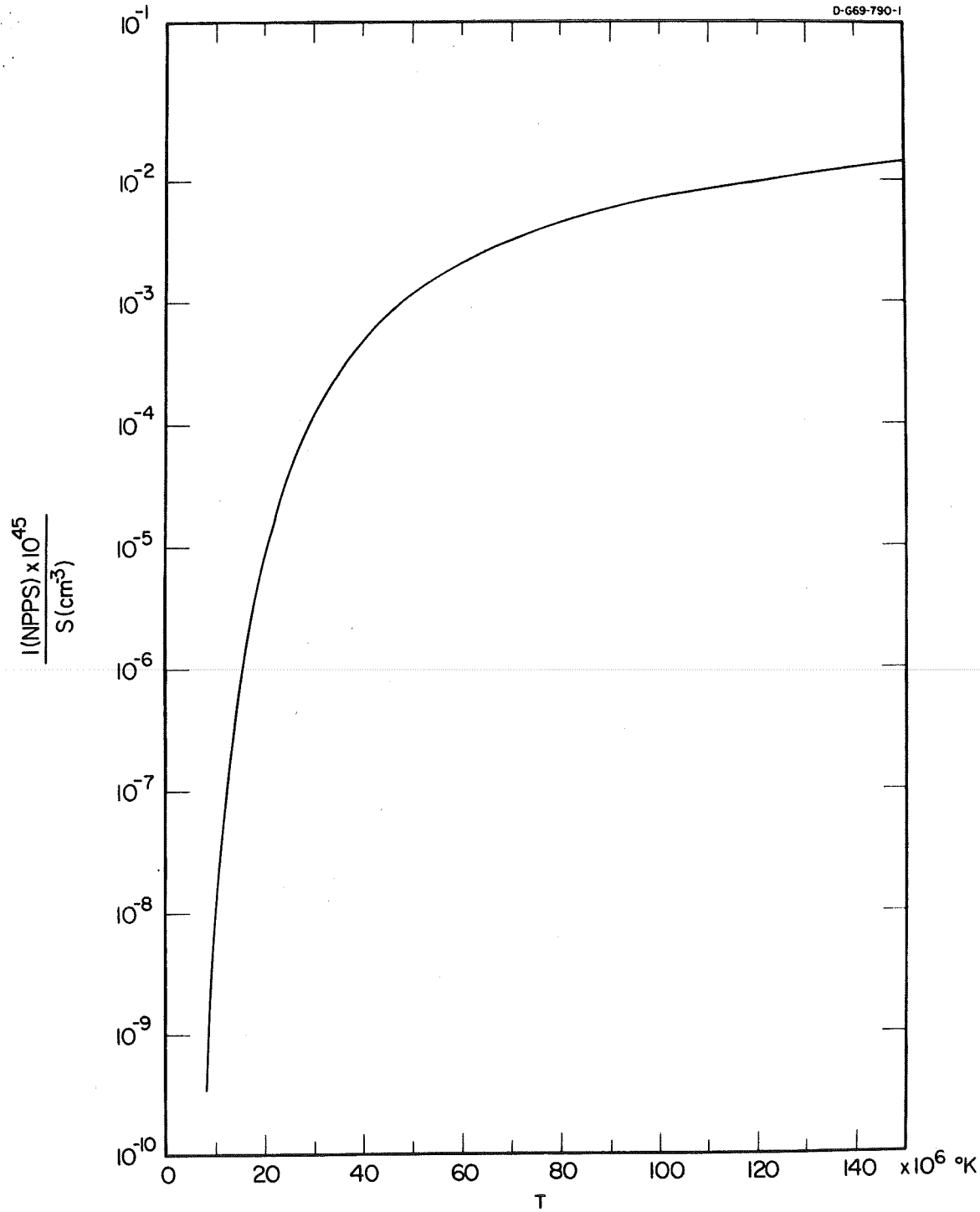
D-G69-790-1
10^{-1}
10^{-2}
10^{-3}
10^{-4}
10^{-5}
10^{-6}
10^{-7}
10^{-8}
10^{-9}
10^{-10}
$\frac{I(NPPS) \times 10^{45}}{S(cm^3)}$
0
20
40
60
80
100
120
140
$\times 10^6$ °K
T

Figure 48

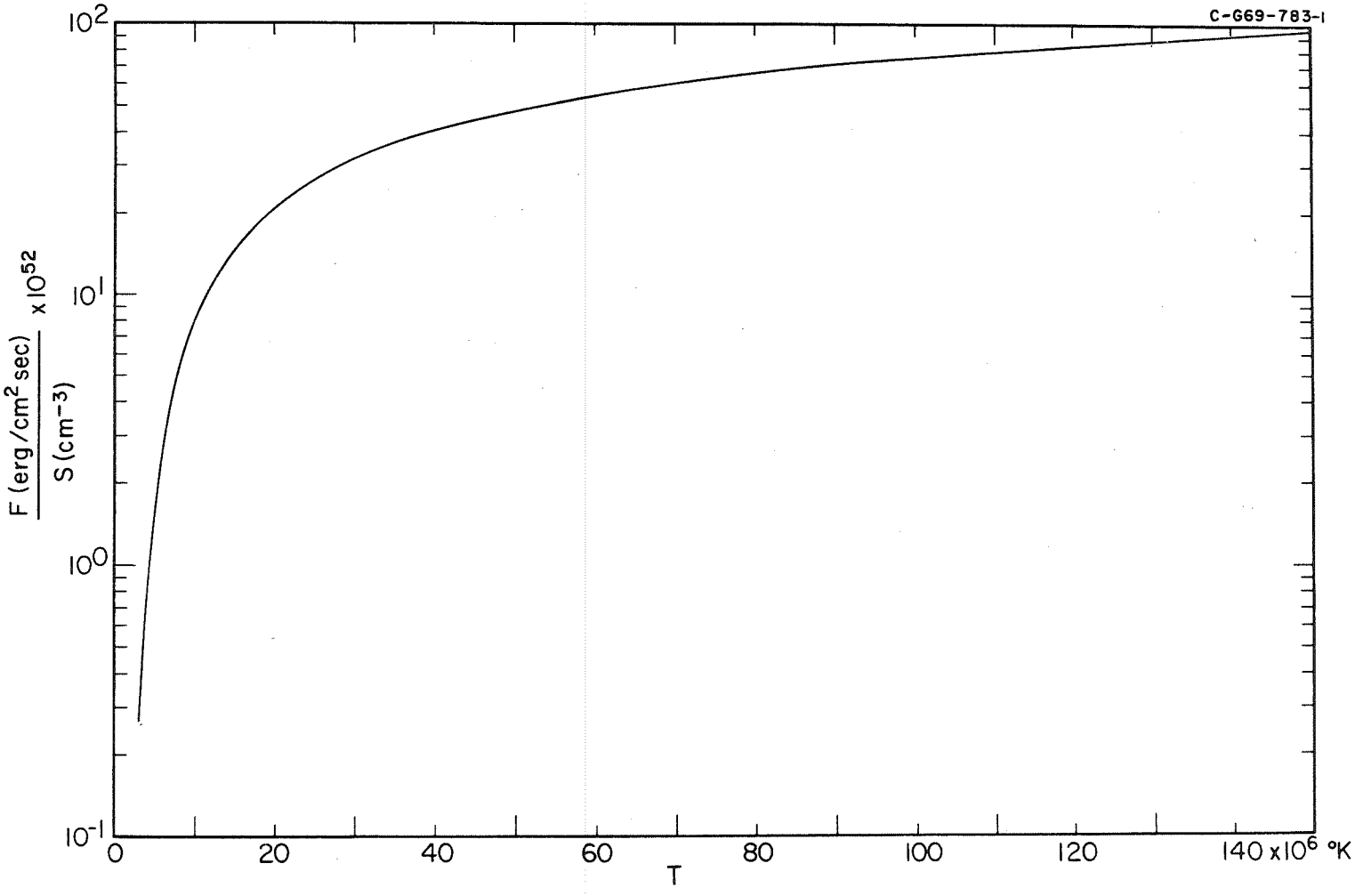
C-G69-783-1
10^2
10^1
10^0
10^{-1}
$\frac{F\,(erg/cm^2\,sec)}{S\,(cm^{-3})} \times 10^{52}$
0
20
40
60
80
100
120
140 x 10^6 °K
T

Figure 49

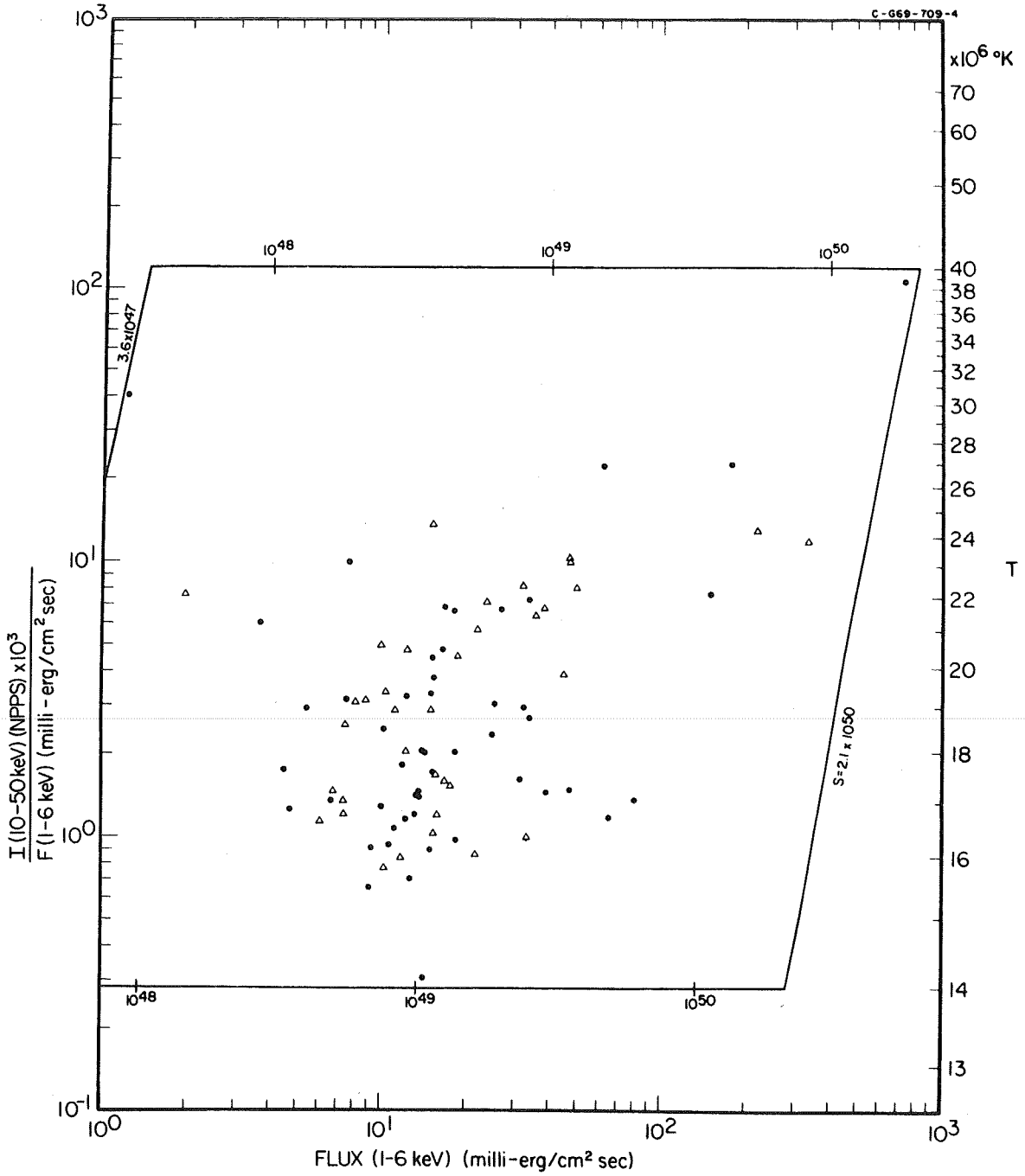
C-G69-709-4
10^3
10^2
10^1
10^0
10^{-1}
10^{48}
10^{49}
10^{50}
3.6x1047
S=2.1 x 1050
$\frac{I(10-50keV)(NPPS)\times10^3}{F(1-6\ keV)\ (milli-erg/cm^2\ sec)}$
FLUX (1-6 keV) (milli-erg/cm² sec)
10^0
10^1
10^2
10^3
x10⁶ °K
70
60
50
40
38
36
34
32
30
28
26
24
22
20
18
16
14
13
T

Figure 50

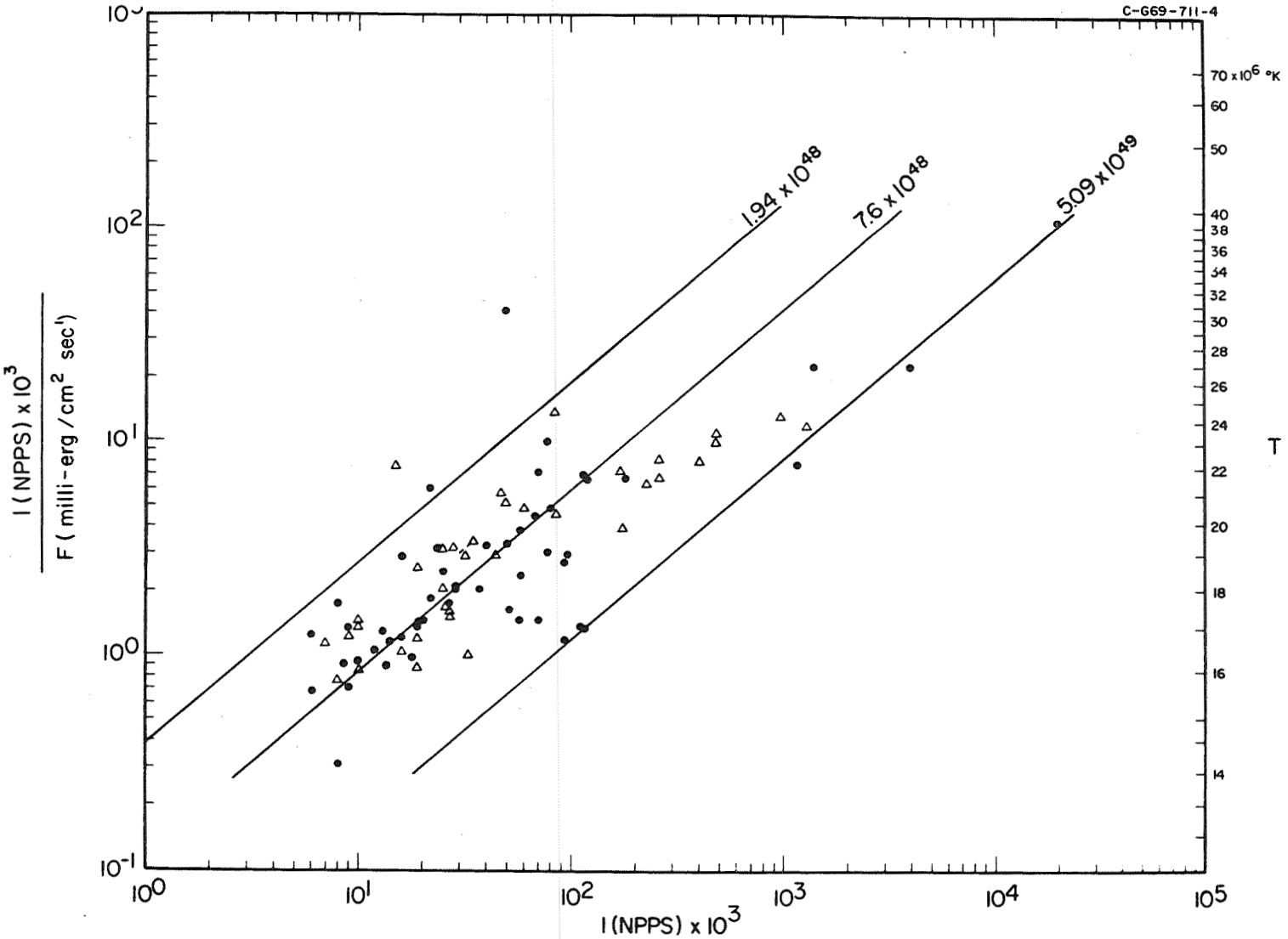
C-G69-711-4
$\frac{I\,(NPPS)\times 10^3}{F\,(milli\text{-}erg/cm^2\,sec^1)}$
$I\,(NPPS)\times 10^3$
10^{-1}
10^0
10^1
10^2
10^3
10^4
10^5
1.94 x 10^48
7.6 x 10^48
5.09 x 10^49
70 x 10^6 °K
60
50
40
38
36
34
32
30
28
26
24
22
20
18
16
14
T

Figure 51

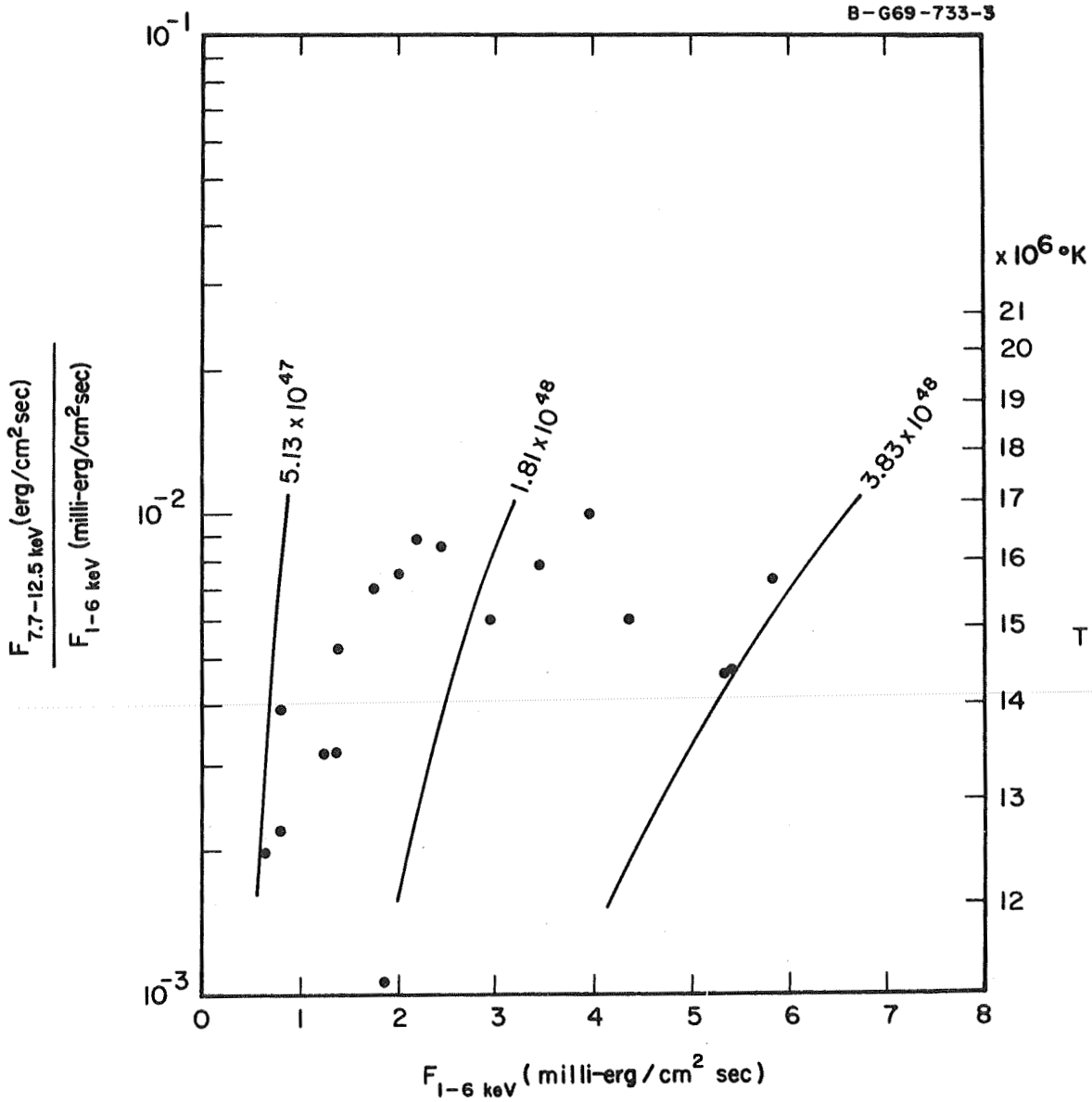
B-G69-733-3
10^{-1}
10^{-2}
10^{-3}
$\frac{F_{7.7-12.5\ keV}\ (erg/cm^2 sec)}{F_{1-6\ keV}\ (milli-erg/cm^2 sec)}$
5.13 x 10^{47}
1.81 x 10^{48}
3.83 x 10^{48}
x 10^6 °K
21
20
19
18
17
16
15
14
13
12
T
0
1
2
3
4
5
6
7
8
$F_{1-6\ keV}$ (milli-erg / cm^2 sec)

Figure 52

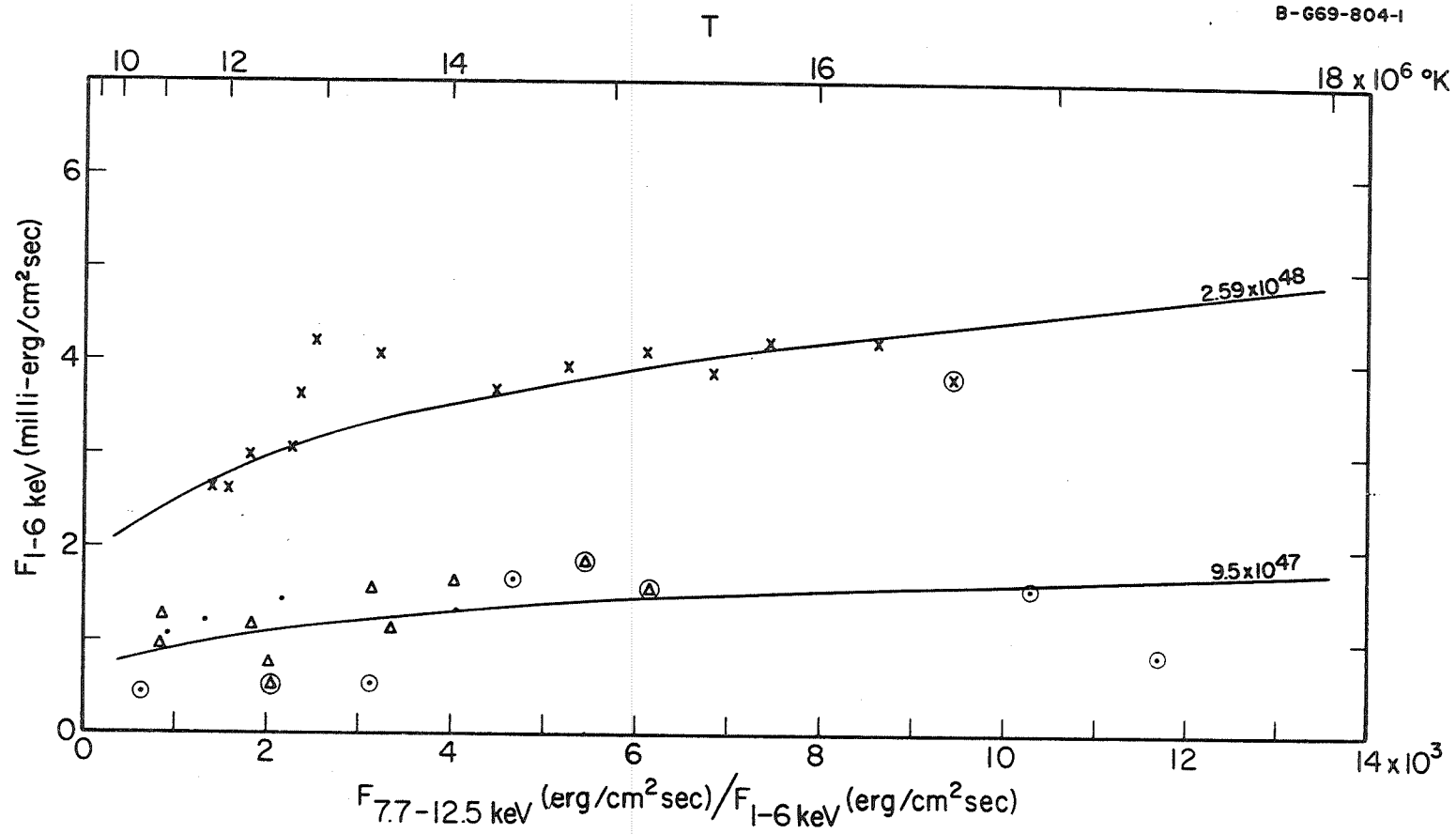
B-G69-804-1
T
10
12
14
16
18 x 10^6 °K
6
4
2
0
0
2
4
6
8
10
12
14 x 10^3
2.59x10^48
9.5x10^47
F1-6 keV (milli-erg/cm^2sec)
F7.7-12.5 keV (erg/cm^2sec)/F1-6 keV (erg/cm^2sec)

Figure 53

UNCLASSIFIED

Security Classification

DOCUMENT CONTROL DATA - R&D

(Security classification of title, body of abstract and indexing annotation must be entered when the overall report is classified)

1. ORIGINATING ACTIVITY (Corporate author)	2a. REPORT SECURITY CLASSIFICATION
The University of Iowa Department of Physics and Astronomy	UNCLASSIFIED
	2b GROUP

3. REPORT TITLE

Soft Solar X-Ray Burst Characteristics

4. DESCRIPTIVE NOTES (Type of report and inclusive dates)

Progress January 1970

5. AUTHOR(S) (Last name, first name, initial)

Drake, Jerry F.

6. REPORT DATE	7a. TOTAL NO. OF PAGES	7b. NO. OF REFS
January 1970	169	48

8a. CONTRACT OR GRANT NO. Nonr 1509(06)	9a. ORIGINATOR'S REPORT NUMBER(S)
b. PROJECT NO.	U. of Iowa 70-1
c.	9b. OTHER REPORT NO(S) (Any other numbers that may be assigned this report)
d.	

10. AVAILABILITY/LIMITATION NOTICES

Distribution of this document is unlimited.

11. SUPPLEMENTARY NOTES	12. SPONSORING MILITARY ACTIVITY

13. ABSTRACT

[See pages following]

DD FORM 1 JAN 64 1473

UNCLASSIFIED

Security Classification

14. KEY WORDS	LINK A		LINK B		LINK C	
	ROLE	WT	ROLE	WT	ROLE	WT
Solar X-Ray Bursts (2 - 12 Å)						
Solar Flares						
Thermal Bremsstrahlung						

INSTRUCTIONS

1. ORIGINATING ACTIVITY: Enter the name and address of the contractor, subcontractor, grantee, Department of Defense activity or other organization *(corporate author)* issuing the report.

2a. REPORT SECURITY CLASSIFICATION: Enter the overall security classification of the report. Indicate whether "Restricted Data" is included. Marking is to be in accordance with appropriate security regulations.

2b. GROUP: Automatic downgrading is specified in DoD Directive 5200.10 and Armed Forces Industrial Manual. Enter the group number. Also, when applicable, show that optional markings have been used for Group 3 and Group 4 as authorized.

3. REPORT TITLE: Enter the complete report title in all capital letters. Titles in all cases should be unclassified. If a meaningful title cannot be selected without classification, show title classification in all capitals in parenthesis immediately following the title.

4. DESCRIPTIVE NOTES: If appropriate, enter the type of report, e.g., interim, progress, summary, annual, or final. Give the inclusive dates when a specific reporting period is covered.

5. AUTHOR(S): Enter the name(s) of author(s) as shown on or in the report. Enter last name, first name, middle initial. If military, show rank and branch of service. The name of the principal author is an absolute minimum requirement.

6. REPORT DATE: Enter the date of the report as day, month, year; or month, year. If more than one date appears on the report, use date of publication.

7a. TOTAL NUMBER OF PAGES: The total page count should follow normal pagination procedures, i.e., enter the number of pages containing information.

7b. NUMBER OF REFERENCES: Enter the total number of references cited in the report.

8a. CONTRACT OR GRANT NUMBER: If appropriate, enter the applicable number of the contract or grant under which the report was written.

8b, 8c, & 8d. PROJECT NUMBER: Enter the appropriate military department identification, such as project number, subproject number, system numbers, task number, etc.

9a. ORIGINATOR'S REPORT NUMBER(S): Enter the official report number by which the document will be identified and controlled by the originating activity. This number must be unique to this report.

9b. OTHER REPORT NUMBER(S): If the report has been assigned any other report numbers *(either by the originator or by the sponsor)*, also enter this number(s).

10. AVAILABILITY/LIMITATION NOTICES: Enter any limitations on further dissemination of the report, other than those imposed by security classification, using standard statements such as:

(1) "Qualified requesters may obtain copies of this report from DDC."

(2) "Foreign announcement and dissemination of this report by DDC is not authorized."

(3) "U. S. Government agencies may obtain copies of this report directly from DDC. Other qualified DDC users shall request through _____."

(4) "U. S. military agencies may obtain copies of this report directly from DDC. Other qualified users shall request through _____."

(5) "All distribution of this report is controlled. Qualified DDC users shall request through _____."

If the report has been furnished to the Office of Technical Services, Department of Commerce, for sale to the public, indicate this fact and enter the price, if known.

11. SUPPLEMENTARY NOTES: Use for additional explanatory notes.

12. SPONSORING MILITARY ACTIVITY: Enter the name of the departmental project office or laboratory sponsoring *(paying for)* the research and development. Include address.

13. ABSTRACT: Enter an abstract giving a brief and factual summary of the document indicative of the report, even though it may also appear elsewhere in the body of the technical report. If additional space is required, a continuation sheet shall be attached.

It is highly desirable that the abstract of classified reports be unclassified. Each paragraph of the abstract shall end with an indication of the military security classification of the information in the paragraph, represented as *(TS)*, *(S)*, *(C)*, or *(U)*.

There is no limitation on the length of the abstract. However, the suggested length is from 150 to 225 words.

14. KEY WORDS: Key words are technically meaningful terms or short phrases that characterize a report and may be used as index entries for cataloging the report. Key words must be selected so that no security classification is required. Identifiers, such as equipment model designation, trade name, military project code name, geographic location, may be used as key words but will be followed by an indication of technical context. The assignment of links, roles, and weights is optional.

ABSTRACT

The burst component of the solar x-ray flux in the soft wavelength range 2 Å $< \lambda <$ 12 Å observed from Explorer 33 and Explorer 35 from July 1966 to September 1968 were analyzed. In this period 4028 burst peaks were observed.

The differential distributions of the temporal and intensity parameters of the bursts revealed no separation into more than one class of bursts. The most frequently observed value for rise time was 4 minutes and for decay time was 12 minutes. The distribution of the ratio of rise-to-decay time can be represented by an exponential with exponent -2.31 from a ratio of 0.3 to 2.7; the maximum in this distribution occurred at a ratio of 0.3. The values of the total observed flux, divided by the background flux, at burst maximum, can be represented by a power law with exponent -2.62 for ratios between 1.5 and 32. The distribution of peak burst fluxes can be represented by a power law with exponent -1.75 over the range 1 - 100 milli-erg $(cm^2\ sec)^{-1}$. The flux time integral values are given by a power law with exponent -1.44 over the range 1 - 50 erg cm^{-2}.

The distribution of peak burst flux as a function of Hα importance revealed a general trend for larger peak x-ray fluxes to occur

with both larger Hα flare areas and with brighter Hα flares. The heliographic longitude dependence of soft x-ray bursts indicated no significant dependence of x-ray burst occurrence on heliographic longitude; the emission thus lacks directivity.

The theory of free-free emission by a thermal electron distribution was applied to a quantitative explanation of both hard x-ray fluxes (data from Arnoldy, Kane, and Winckler [1968]; Kane and Winckler [1969]; and Hudson, Peterson, and Schwartz [1969]) and soft x-ray fluxes during solar x-ray bursts. Using bursts in three different energy intervals, covering a total range of 1 - 50 keV, temperatures of 12 - 39 x 10^6 °K and emission measures of 3.6 x 10^{47} to 2.1 x 10^{50} cm^{-3} were derived. The emission measure was found to vary from event to event. The peak time of hard x-ray events was found to occur an average of 3 minutes before the peak time of the corresponding soft x-ray bursts. Thus a changing emission measure during the event is also required. A free-free emission process with temperatures of 12 - 39 x 10^6 °K and with an emission measure in the range 3.6 x 10^{47} to 2.1 x 10^{50} cm^{-3} which varies both from event to event and within an individual event is required by the data examined.